AD-A101 144   AIR FORCE INST OF TECH WRIGHT-PATTERSON AFB OH SCHOO--ETC F/G 12/1
THE FINITE ELEMENT METHOD APPLIED TO THE SYSTEM-GENERATED ELECT--ETC(U)
FEB 81 J A GAUDET
UNCLASSIFIED   AFIT/DS/PH/81-1   NL

1 OF 2
AD
A101144

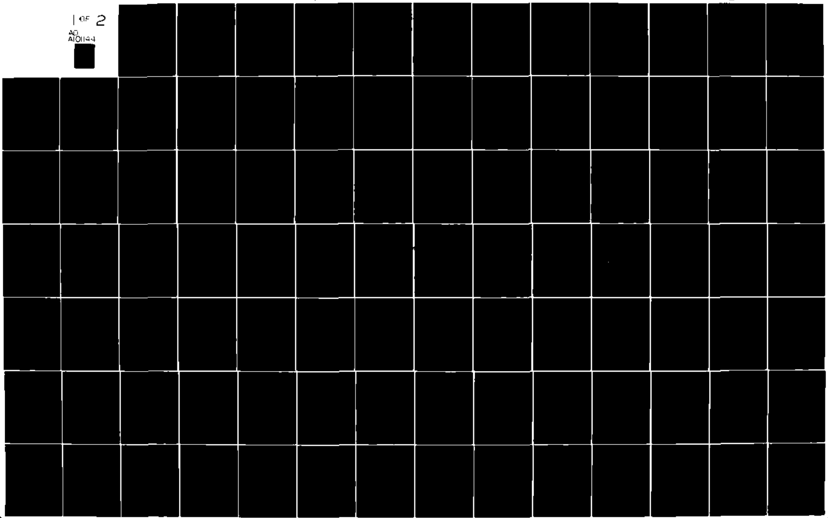

AD A101144

THE FINITE ELEMENT METHOD APPLIED

TO THE SYSTEM-GENERATED ELECTROMAGNETIC PULSE

BOUNDARY LAYER

DISSERTATION

AFIT/DS/PH/81-1

John A. Gaudet
Capt USAF

Approved for public release; distribution unlimited

UNCLASSIFIED

SECURITY CLASSIFICATION OF THIS PAGE (When Data Entered)

REPORT DOCUMENTATION PAGE		READ INSTRUCTIONS BEFORE COMPLETING FORM
1. REPORT NUMBER AFIT/DS/PH/81-1	2. GOVT ACCESSION NO. AD-A101144	3. RECIPIENT'S CATALOG NUMBER
4. TITLE (and Subtitle) THE FINITE ELEMENT METHOD APPLIED TO THE SYSTEM-GENERATED ELECTROMAGNETIC PULSE BOUNDARY LAYER		5. TYPE OF REPORT & PERIOD COVERED PhD Dissertation 6. PERFORMING ORG. REPORT NUMBER
7. AUTHOR(s)		8. CONTRACT OR GRANT NUMBER(s)
9. PERFORMING ORGANIZATION NAME AND ADDRESS Air Force Institute of Technology (AFIT-EN) Wright-Patterson AFB, Ohio 45433		10. PROGRAM ELEMENT, PROJECT, TASK AREA & WORK UNIT NUMBERS WDNE0713
11. CONTROLLING OFFICE NAME AND ADDRESS Air Force Weapons Laboratory (AFWL) Kirtland AFB, New Mexico 87117		12. REPORT DATE February, 1981 13. NUMBER OF PAGES 135
14. MONITORING AGENCY NAME & ADDRESS(if different from Controlling Office)		15. SECURITY CLASS. (of this report) 15a. DECLASSIFICATION/DOWNGRADING SCHEDULE

16. DISTRIBUTION STATEMENT (of this Report)

Approved for public release; distribution unlimited

Fredric C. Lynch

17. DISTRIBUTION STATEMENT (of the abstract entered in Block 20, if different from Report)

FREDRIC C. LYNCH, Major, USAF
Director of Public Affairs
Air Force Institute of Technology (ATC)
Wright-Patterson AFB, OH 45433

18. SUPPLEMENTARY NOTES

Approved for public release; IAW AFR 190-17

25 MAR 1981

19. KEY WORDS (Continue on reverse side if necessary and identify by block number)

Finite elements
System-Generated Electromagnetic Pulse
Nuclear Weapons Effects
Plasma

20. ABSTRACT (Continue on reverse side if necessary and identify by block number)

The Finite Element Methods was used to solve the nonlinear electron plasma equations for the System-Generated Electromagnetic Pulse boundary layer in one spatial dimension. These equations were solved in distance-velocity phase space using a rectangular finite element mesh. Linear approximations were used for both the trial and weight functions for each element. The advection terms in the Vlasov plasma equation were treated with the Heinrich upwinding technique.

DD FORM 1 JAN 73 1473 EDITION OF 1 NOV 65 IS OBSOLETE

UNCLASSIFIED

SECURITY CLASSIFICATION OF THIS PAGE (When Data Entered)

The time integration was performed using an explicit two-step Lax-Wendroff procedure. The system of algebraic equations were solved with a fully-packed Gauss-Seidel iteration scheme.

A value of 2/3 for the upwinding parameter was found to provide the best compromise between dispersion of the pulse, and computer storage requirements. The savings in computer memory results in increased execution speed for the algorithm. Also, it is shown that the numerical scheme does not permit spurious pulse reflections from the edges of the mesh.

Results for several test cases are presented. Comparsions are given which show favorable agreement for the finite element technique with other solution methods.

Empirical relationships for the mesh parameters are given which must be followed in order to produce valid results witn the numerical scheme developed.

AFIT/DS/PH/81-1

THE FINITE ELEMENT METHOD APPLIED TO THE SYSTEM-GENERATED ELECTROMAGNETIC PULSE BOUNDARY LAYER

DISSERTATION

Presented to the Faculty of the School of Engineering

of the Air Force Institute of Technology

Air University

in Partial Fulfillmnet of the

Requirements for the Degree of

Doctor of Philosophy

by

John A. Gaudet, A.B., M.S.

Captain USAF

AFIT/DS/PH/81-1

THE FINITE ELEMENT METHOD APPLIED TO THE SYSTEM-GENERATED ELECTROMAGNETIC PULSE BOUNDARY LAYER

by

John A. Gaudet, A.B., M.S.

Captain USAF

Approved:

David D. Hardin Chairman	23 Feb 81
John H. Ehlich	23 Feb 81
David A. Lee	23 Feb 81
Charles J. Bridgman	24 Feb 81
Bernard Kaplan	24 Feb 81
John Jones Jr	24 Feb 81
Donn G. Shankland	24 Feb 81

Accepted:

J S Przemieniecki Dean, School of Engineering	24 Feb 81

ACKNOWLEDGEMENTS

This dissertation would not have been completed without the support of several individuals to whom I am forever grateful.

First of all, I want to express my appreciation to the Chairman of my doctoral committee, Capt David Hardin. His expertise with the Finite Element Method greatly contributed to my understanding of the technique. His patience endured over many hours of long-distance phone conversations, providing me with excellent advice. I am aslo grateful to my former advisor, Dr. James Bridgman, who guided me early in this program, and has always remained highly suportive.

I would like to thank Dr. Jones in the Mathematics Department at AFIT for introducing me to numerical analysis in general, and finite elements in particular.

I received much support form the Air Force Weapons Laboratory. Dr. Bill Page provided me with many fruitful hours of discussion about SGEMP. All of my co-workers were equally supportive, giving me the opportunity to pursue this degree.

Lastly, I owe my biggest debt of gratitude to my family. I wish to thank my mother and father for making many sacrifices to educate me. And, my wife, Sandy, and children, Brian, Keith and Steven, gave me constant encouragement while I spent many nights and weekends completing this task.

TABLE OF CONTENTS

TABLE OF CONTENTS

LIST OF FIGURES

LIST OF FIGURES

LIST OF TABLES

Abstract

The Finite Element Method was used to solve the nonlinear electron plasma equations for the System-Generated Electromagnetic Pulse boundary layer in one spatial dimension. These equations were solved in distance-velocity phase space using a rectangular finite element mesh. Linear approximations were used for both the trial and weight functions for each element. The advection terms in the Vlasov plasma equation were treated with the Heinrich upwinding technique.

The time integration was performed using an explicit two-step Lax-Wendroff procedure. The system of algebraic equations was solved with a fully-packed Gauss-Seidel iteration scheme.

A value of 2/3 for the upwinding parameter was found to provide the best compromise between dispersion of the pulse and computer storage requirements. The savings in computer memory results in increased execution speed for the algorithm. Also, it is shown that the numerical scheme does not permit spurious pulse reflections from the edges of the mesh.

Results for several test cases are presented. Comparisons are given which show favorable agreement for the finite element technique with other solution methods.

Empirical relationships for the mesh parameters are given which must be followed in order to produce valid results with the numerical scheme developed.

THE FINITE ELEMENT METHOD APPLIED TO THE SYSTEM-GENERATED ELECTROMAGNETIC PULSE BOUNDARY LAYER

I. Introduction

DEFINITION OF SGEMP. System-Generated Electromagnetic Pulse (SGEMP) is an effect of a nuclear weapon detonation. It will occur whenever the ionizing radiations (X-rays, gamma rays, and neutrons) from a nuclear event are incident upon an object in a low pressure (high altitude) environment. The radiation interacts with the object via the Compton and photoelectric processes. These mechanisms produce free electrons inside the object and in the region surrounding it. The electromagnetic field created by the electrons in motion about the object is called SGEMP.

A nuclear burst in space is of particular interest to the Air Force. Line-of-sight radiation from such a burst will be received by a satellite unattenuated by atmospheric interactions. The line-of-sight radiation arrives at the satellite affected only by the spherical divergence factor of $1/4\pi r^2$, where r = distance from the burst point to the satellite.

The depth of interaction into the material of the satellite depends on the energy and type of radiation. High energy X-rays, gamma rays and neutrons will penetrate a few, to tens of centimeters, into the material before interactions take place. These interactions lead to direct injection of current into the satellite's circuitry.

However, the penetrating radiations are only a minor fraction of a nuclear weapon's energy output. Approximately 80% of the energy released from a nuclear burst is in the form of X-rays (Ref 1, Chapter 7). A fraction of these X-rays are in the energy range of 1 keV. These relatively low-energy photons will primarily interact with the surface atoms of the satellite (usually a metal such as Aluminum). About half of all the electrons generated by the photoelectric effect (the major interaction mechanism at these photon energies) are back-scattered into space off of the satellite (Ref 2, Chapters 23-25). Consequently, electromagnetic fields will surround the satellite, generating surface currents in the process. These surface currents may also find their way into the circuitry of the satellite, creating a potential hazard to electronic components. The creation of surface currents via this process is known as the external (or outside) System-Generated Electromagnetic Pulse problem, or simply SGEMP, and is the phenomenon analyzed here.

IMPORTANCE OF UNDERSTANDING SGEMP. The ability of a satellite to withstand a nuclear environment is critical to our national defense. Therefore, a quantitative knowledge of the nuclear threat to these systems is necessary. The SGEMP effect is an important consideration for space systems. Realistic testing is one of the best methods to measure the impact of SGEMP on space vehicles. Unfortunately, the creation of the right kind of radiation with the proper energy, flux, and time history is difficult to produce in the laboratory. Underground nuclear testing can be done, but the cost, and large size of some systems makes such experiments difficult to accomplish, at best.

As a result, the Air Force has instituted a technical program for the theoretical understanding of SGEMP. This program encompasses both analytical and computational methods. Researchers have studied several important properties of the SGEMP process since the institution of this program. One of these is the boundary layer.

THE BOUNDARY LAYER. The electron boundary layer is created near the surface of the satellite. This effect is due to the large, normal electric field created by the removal of charge from the material of the satellite. Since this electric field is directed away from the surface, electrons experience a force directed back towards the satellite. In fact, the electric field can get so strong that subsequently ejected electrons of lower energy will not be able to penetrate this small region near the satellite. This region will contain a high density of electrons, some which have been slowed down considerably, others which have actually turned around. It is even possible for electrons to exist in this area under quasi-static equilibrium conditions.

This region of dense electrons which retards the progress of other emitted electrons is known as the boundary layer. The dimensions of this layer cannot be defined precisely. However, a generally accepted practice is to consider the boundary layer to be a few Debye lengths thick. The Debye length is the characteristic distance of a plasma defined by the relaxation length of exponential screening. That is, it is the distance that is required for the electric potential to drop by a factor of 1/e. The significance of the Debye length lies in the fact that the electrostatic potential felt by an electron at a distance much greater than a few Debye lengths from a charge distribution will be very small. Because the Debye length is the characteristic distance of a plasma, it is natural to use it as the defining parameter for the boundary layer.

The boundary layer sets up a potential screen between the electrons leaving the surface and those which are beyond the boundary layer. This screen reduces the energies of electrons. It also determines electron flow on the surface of the satellite by affecting the electromagnetic fields at the surface. Some of the surface current may get into the satellite's interior. This is the important physical quantity of design interest. Therefore, a detailed knowledge of the surface currents, hence boundary layer, is an important step to the understanding of the SGEMP.

PRIOR RELATED WORK. Serious technical effort to understand the fundamental physical processes of SGEMP, including the boundary layer and surface currents, began in the mid 1960's. The Air Force Weapons Laboratory and the Defense Nuclear Agency sponsored large SGEMP programs to develop theoretical knowledge and computational techniques. Conrad Longmire, Neal Carron and others analyzed the composition of the electron boundary layer via theoretical and semi-analytical means (Ref 3,4,5, and 6). Others concentrated on the development of one-, two-, and three-dimensional computer codes (Ref 7,8,9, and 10). An excellent article by Higgins et al (Ref 11) reviews the progress made in SGEMP analysis up to 1978.

As Higgins points out, the majority of numerical approaches used to date are particle simulation codes. This technique, also called "particle pushing", relies upon a statistical model of macro-charges. That is, one makes the assumption that a given amount of charge can be modelled as one large macro-particle. This allows the force on each particle to determine its movement about the satellite. Each individual particle represents millions of electrons. The greater the number of macro-particles used, the better the accuracy.

Only a few researchers have approached transient SGEMP using a continuum model for the electron distribution (Ref 12 and 13). This approach is very common in plasma studies, where the electrons exhibit periodic motion (Ref 14 and 15). In this method, a distribution function is defined which depends upon the position, x, and velocity, v, of the electrons. This distribution function then describes the density of the electrons in the (x,v) phase space.

The major difficulties associated with the particle-pushing codes are noise fluctuations produced by the statistical nature of the algorithms, and the computer memory requirements. The distribution function approach also has storage problems. Additionally, the dominant advection terms in the equations are difficult to treat numerically. However, as Holland points out (Ref 12), for cases that require tracking of many particles which do not leave the numerical mesh, the distribution function approach will become more efficient than particle pushing after relatively few time cycles. Holland roughly estimates that, for a particular two-dimensional problem he considered, 80,000 storage locations would be required by a particle-pushing method to achieve results of comparable accuracy to those obtained by a distribution function approach with 35,000 locations. Thus, the distribution function method may be more efficient for long running problems with large boundary layer effects. But the advective nature of the equation remains a problem.

THE FINITE ELEMENT METHOD (FEM). The FEM is a numerical technique which has been used extensively by engineers to perform complex structural analyses in the aircraft industry. It was first introduced for this purpose twenty years ago (Ref 16). Since that time, researchers in other disciplines have recognized that for some problems the FEM has certain desirable qualities. As a result, the technical literature has become filled with finite element applications for such diverse fields as nuclear reactor technology, electromagnetic field scattering and oceanic water wave behavior. This widespread interest in the FEM prompted mathematicians to study the technique in great detail. Consequently, there are now many texts which describe the FEM from both the engineering and mathematical points-of-view. References 16,17, and 18 are just a few examples of these texts.

The success of the method was clouded by one fact: although finite elements worked well for elliptic and parabolic equations, there was some doubt as to the usefulness of the technique on hyperbolic equations (Ref 17, Chapter 7) and advective-dominated transport equations. The equations of SGEMP formulated with a continuous distribution function for the electrons' behavior are dominated by advection terms. Recently, several authors have shown that the FEM can be effective for hyperbolic equations and for advective-dominated propagation such as found in SGEMP (Ref 19, Chapters 2 and 19).

There has also been a continuing debate over the accuracy of the FEM versus a finite difference solution to the same equations. However, Gresho et al (Ref 19, Chapter 19) have reported improvements over finite difference results for pure advection in one dimension when using finite elements. Also, Demerdash and Nehl (Ref 20) claim to have achieved more accurate results for static and sinusoidally varying nonlinear electromagnetic field problems using less computer time and memory with the FEM. These last achievements are important for SGEMP research because it, too, is a nonlinear electromagnetic problem.

PURPOSE OF DISSERTATION. The major goal for this dissertation is to investigate the FEM as a new approach for the one-dimensional SGEMP problem. The weight and trial functions for the FEM will be developed with attention given to the strongly-advective equations of SGEMP. The elements which reduce implementation difficulties will be used. Parameters introduced when using advective methods will be analyzed to determine which values to use. The nonlinear SGEMP equations will be integrated using methods proven to work for other finite element equations.

The impact of the FEM on the solutions to specific SGEMP problems will be examined. The sensitivity of the finite element solutions to the space, velocity and time intervals shall be analyzed. Additionally, results using this different technique will be compared with the more traditional methods of analysis; namely, theoretical solutions and finite difference methods. Thus, another set of results will be produced to describe the effects of the nonlinear boundary layer.

OVERVIEW. The finite element solution to the one-dimensional SGEMP equations was done on a Control Data CYBER 176 series computer using a FORTRAN IV program called FEMNEP (Finite Element Method for a Nonlinear Electromagnetic Problem). This program was written by the author as a research tool, not specifically designed for large-scale, production running.

Chapter II of this dissertation presents the equations and physics of SGEMP. Prior solution techniques, as well as the inherent difficulties built into the equations are discussed. Chapter III contains the basic numerical prescriptions used in this dissertation to solve the equations of Chapter II. The FEM itself, the time integration, and the special numerical treatments are included in this chapter. Chapter IV presents the results of the FEM when applied to the one-dimensional SGEMP boundary layer. Finally, Chapter V summarizes the results and lists the conclusions of this dissertation.

Many of the derivations, and other discussions not directly related to the development of the subject matter being presented, are relegated to the appendices.

II. System Generated Electromagnetic Pulse

THE EQUATIONS. For the purpose of this study, only SGEMP produced by X-rays will be considered. Thus, consider an object illuminated by a pulse of X-rays of short duration (~ 1 μsec) in a vacuum. Through nuclear interaction processes with the object, primarily the photoelectric effect for Aluminum (Ref 2 Chapter 25), electrons will be ejected off its surface. The behavior of these electrons in their own self fields is determined by the Vlasov Equation, a form of the Boltzmann Equation (Ref 12 and Ref 22, p. 260):

$$\frac{\partial f}{\partial t}(\vec{x},\vec{v},t) + \vec{v}\cdot\nabla f(\vec{x},\vec{v},t) + \vec{a}\cdot\nabla_v f(\vec{x},\vec{v},t) = S(\vec{x},\vec{v},t) \qquad (1)$$

where $\vec{x}$ = position of electron

$\vec{v}$ = velocity of electron

t = time

$f(\vec{x},\vec{v},t)$ = distribution function for electrons
= number of electrons per $d\vec{v}$ per $d\vec{x}$ at time, t

$\vec{a}$ = acceleration of electrons

$S(\vec{x},\vec{v},t)$ = source of electrons
= rate of electrons produced per $d\vec{x}$ per $d\vec{v}$ at time, t.

Since the electrons of interest will be traveling at less than 1%

of the speed of light, the acceleration, $\vec{a}$, is given by the Lorentz Force,

$$\vec{a}(\vec{x},\vec{v},t) = -\frac{e}{m}[\vec{E}(\vec{x},t) + \vec{v} \times \vec{B}(\vec{x},t)] \qquad (2)$$

for rationalized MKS units. In this equation,

e = charge of electron = 1.6×10^{-19} Coulomb

m = mass of electron = 9.11×10^{-31} Kgm

$\vec{E}(\vec{x},t)$ = electric field in Volts/m

$\vec{v}$ = velocity of electron in m/sec

$\vec{B}(\vec{x},t)$ = magnetic induction field in Weber/m^2

In order to complete the solution of Eqn (1), Maxwell's Equations in free space are needed:

$$\nabla\cdot\vec{E}(\vec{x},t) = \frac{\rho(\vec{x},t)}{\varepsilon_o} \quad (3a); \qquad \nabla\cdot\vec{B}(\vec{x},t) = 0 \quad (3b)$$

$$\nabla \times \vec{E}(\vec{x},t) = -\frac{\partial\vec{B}}{\partial t}(\vec{x},t) \qquad (3c)$$

$$\nabla \times \vec{B}(\vec{x},t) = \mu_o\vec{J}(\vec{x},t) + \mu_o\varepsilon_o\frac{\partial\vec{E}}{\partial t}(\vec{x},t) \qquad (3d)$$

$\rho(\vec{x},t)$ = charge density in Coul/m^3

$\vec{J}(\vec{x},t)$ = current density in Amp/m^2

μ_o = permeability of free space
= $4\pi \times 10^{-7}$ Henry/m

ε_o = permittivity of free space
= 8.85×10^{-12} Farad/m

The solution to Eqns (3a) and (3b) is facilitated by the fact that if $\vec{E}$ and $\vec{B}$ fields are found which satisfy these equations at any time, then the advancement of these solutions in time via Eqns (3c) and (3d) will produce fields which always satisfy them (Ref 23 Sec. 1.2).

One other auxiliary equation is required to complete the physical description of the SGEMP process; that is, the connection between the distribution function, $f(\vec{x},\vec{v},t)$, and the driving term of Maxwell's Equations, $\vec{J}(\vec{x},t)$, the current density. This is really a matter of definition, and is:

$$\vec{J}(\vec{x},t) = -e \int_{-\infty}^{+\infty} \vec{v} f(\vec{x},\vec{v},t)\, d\vec{v} \qquad (4)$$

Its more recognizable form is $\vec{J}=-ne\vec{v}$, where n = number of electrons per cubic meter. An actual integration can be performed by using upper and lower limits which are chosen so that $f(\vec{x},\vec{v},t)$ is negligible outside these limits. In principle, then, Eqns (1), (2), (3c), (3d), and (4) provide the physics of SGEMP. All that is needed to complete the solution are initial conditions, boundary conditions, the specification of the source characteristics and a technique to solve the equations.

One numerical method of solution would proceed the following way: assume all electromagnetic fields are zero to start with; then, with a knowledge of $S(\vec{x},\vec{v},0+\Delta t)$, the distribution function, $f(\vec{x},\vec{v},0)$ is advanced to $f(\vec{x},\vec{v},0+\Delta t)$ by Eqn (1). From this information, the source term for Maxwell's Equations, $\vec{J}(\vec{x},0+\Delta t)$, is specified through Eqn (4). Then, Eqns (3c) and (3d) are solved for $\vec{B}(\vec{x},0+\Delta t)$ and $\vec{E}(\vec{x},0+\Delta t)$ in some leap-frog fashion. Once E and B are determined, the acceleration, $\vec{a}$, is known at advanced time, $t=\Delta t$, from Eqn (2). The procedure now can be repeated for $t=t+2\Delta t$, and so on.

Of course, there are many subtleties in this prescription which make an actual numerical solution extremely difficult. The numerical solution to Maxwell's Equations, alone, is a challenging task (Ref 24).

ONE-DIMENSIONAL APPROXIMATION. In order to study the properties of the highly space-charge-limited region, or boundary layer, of the SGEMP problem, it is usually only necessary to consider the motion of the electrons in one spatial dimension. That is, a one-dimensional approximation is valid for an infinite flat emitting surface. And, the surface may be considered flat if the boundary layer thickness is small compared to the linear dimensions and radii of curvature for the region of interest. Now, a typical boundary layer for an aluminum surface and typical incident 1 keV blackbody X-ray spectrum with a 0.001 cal/(cm^2-nanosec) flux has a boundary layer thickness of about 1 millimeter. Therefore, it is reasonable to make a one-dimensional model in order to study the boundary layer since satellites have many exterior linear dimensions which are much larger than millimeter size.

In one dimension, several simplifications to Eqns (1) thru (4) can be made since all dependent variables are functions of one spatial direction and one velocity direction only. Let these variables be z and $v_z=v$. It is easy to show from both physical and mathematical principles that no magnetic fields can exist in these equations when the problem is limited to one spatial dimension (see Appendix A). Letting $E_z = E$, Eqns (1) and (2) can be combined to give:

$$\frac{\partial f}{\partial t}(z,v,t) + v\frac{\partial f}{\partial z}(z,v,t) - \frac{e}{m}E(z,t)\frac{\partial f}{\partial v}(z,v,t) = S(z,v,t) \qquad (5)$$

Likewise, if $J_z = J$, Eqns (3d) and (4) yield:

$$\frac{\partial E}{\partial t}(z,t) = \frac{e}{\varepsilon_o}\int_{\text{all } v} vf(z,v,t)\, dv \qquad (6)$$

Equation (5) is the one-dimensional Vlasov Equation and Eqn (6) says that the Maxwell displacement current is proportional to the ordinary current when no magnetic field exists (Ampere's Law minus a magnetic field but with displacement current). The Vlasov Equation can be thought of as a statement of particle conservation in a two-dimensional phase space. The simplified Ampere's Law describes the build-up of the electric field as a function of the electron current.

There is an alternative to using Ampere's Law in the one-dimensional approximation. Gauss' Law, Eqn (3a), can be used to determine the electric field. That is, a complete description for E can be obtained from:

$$\frac{\partial E}{\partial z}(z,t) = \frac{1}{\varepsilon_o}\rho(z,t) \qquad (7)$$

This is possible because E responds only to changes in the charge properties of density and current, not magnetic fields, in one dimension. The charge density $\rho(z,t)$ can be determined from $f(z,v,t)$

through the relationship,

$$\rho(z,t) = -e \int_{\text{all } v} f(z,v,t)\, dv \qquad (8)$$

Therefore, an equivalent approach is to use Eqn (5) with Eqns (7) and (8) to solve the one dimensional SGEMP problem. For higher two-dimensional and three-dimensional situations, Ampere's Law, Eqn (3d), must be used because magnetic fields are present.

SOLUTION TECHNIQUES FOR ONE-DIMENSIONAL SGEMP. There are two basic approaches that can be used to attack SGEMP, numerical simulation and numerical solution. A third possible technique, exact analytic solutions, is only feasible for very restricted, idealized cases. This is true because even in one dimension, the equations are a set of coupled, nonlinear, integro-differential equations which have no closed-form, analytic solution for an arbitrary source. Nonetheless, there are some interesting cases which do have analytic or semi-analytic answers (Ref 4).

Numerical simulation is, by far, the most common approach taken to solve the SGEMP problem. This technique is equivalent to the solution of Eqn (5) by the method of characteristics (Ref 25, Chapter 8). The characteristic lines for the Vlasov Equation, by itself, are those which exist in (t,z,v) space such that their directions are determined by dt = k, dz = kv, and dv = ka, where k is a constant and a = acceleration. Thus, if numerical solutions are sought such that v = dz/dt and a = dv/dt, the characteristics of the Vlasov Equation are being followed. Note that:

$$a = \frac{dv}{dt} = \frac{d^2 z}{dt^2} = \frac{F}{m} = -\frac{e}{m}E(z,t) \qquad (9)$$

is a representation of Newton's Second Law. The idea in numerical simulation is that the particles (electrons) move in accordance with Eqn (9) and the definition of the particles position as a function of its velocity, $v = dz/dt$. Therefore, "particles" representing a large amount of charge can be moved about with Eqn (9), and the electric field found with Gauss' Law or Ampere's Law. This is called "particle pushing".

There are several documented computer codes that employ particle pushing (Refs 7, 8, 10 and 15). The major drawback of this method is that the smoothness of the solution depends upon the statistical number of "particles" which are tracked at one time. This is why it is truly numerical simulation. Electrons are simulated by a given amount of charge in a numerical mesh. They are injected into the mesh, moved about using prescribed physical laws, and "killed" when they leave the system, return to the emitting surface, or are reduced in energy below some pre-determined value. The primary concern in actually implementing such a procedure is the particle weighting scheme; that is, proper treatment of the particle density within each cell. The actual solution of the equations of motion and Gauss' Law (or Ampere's Law) is done through conventional finite difference techniques. Elaborate computer programs have been written which solve the SGEMP problem in one, two, and even three spatial dimensions using particle pushing algorithms.

An alternative to particle simulation for the general problem is to solve the equations numerically. There has been one documented finite difference solution to the plasma equations (Ref 12). The solution was done in two spatial dimensions, primarily to study secondary electron effects, not highly space-charge-limited regions, although it clearly could be used for such a purpose. There does not appear to be a well-documented finite difference study of a one-dimensional SGEMP model using the Vlasov Equation to analyze the transient behavior of the boundary layer.

The subject of this dissertation is the application of a third numerical technique, the Finite Element Method, on the highly space-charge-limited SGEMP problem in one dimension.

MATHEMATICAL CONSIDERATIONS. Equation (5) with Eqn (6) is a system of nonlinear integro-differential equations. Certain features of these equations must be kept in mind before any attempt is made to solve them. The Vlasov Equation describes convective transport and contains the advection term, $v\frac{\partial f}{\partial z}$. It is well known that the numerical treatment of such a term requires care. For example, Richtmyer and Morton show that the standard, centered, second order finite difference approximation of this term is not satisfactory (Ref 26, Sec. 12.3).

Also, if an explicit finite difference scheme is used on the time variable, t, then it is likely that some type of restriction must apply to the relative size of the z-step versus t-step, such as the Courant-Friedrichs-Lewy condition (Ref 26 Sec. 10.2):

$$\left|\frac{v\Delta t}{\Delta z}\right| \leq 1 \qquad (10)$$

This condition ensures that the propagating pulse is not allowed to traverse more than one z-cell in one time step when an explicit scheme is used. It seems reasonable to assume that a similar condition should exist in the velocity direction, such as:

$$\left|\frac{a\Delta t}{\Delta v}\right| \leq 1 \qquad (11)$$

where a is the acceleration. However, there is no guarantee that any of these criteria will preserve stability for the finite element equations needed in SGEMP calculations. In Chapter IV, data will be presented which demonstrate the usefulness of these Courant conditions for the present problem. There are some cases for which these conditions are unimportant. This will also be discussed in further detail in Chapter IV.

PHYSICAL CONSIDERATIONS. Besides the purely mathematical concerns mentioned above, there are physical restrictions which need to be considered. Since the distribution function, f(z,v,t), represents a particle density, physically it must always be positive. However, when numerical techniques are used to propagate a pulse through a mesh, oscillations in front of, and behind the pulse often occur (Ref 27). Consequently, the distribution function may become negative. However, this is due to the numerical behavior of the algorithms rather than some actual physical effect. It has been reported that in nonlinear problems such as this one, the negative oscillations can very quickly become intolerable (Ref 22, p. 369). Therefore, steps must be taken to mitigate this potential hazard.

The second physical requirement on the solution to the SGEMP equations is due to the concept of the plasma Debye length. In rationalized MKS units, the Debye length for the electrons of a plasma is defined as (Ref 28, Chapter 8):

$$\lambda_D = \sqrt{\frac{\varepsilon_o kT}{en}} \qquad (12)$$

where k = Boltzmann constant = 1.38×10^{-23} Joule/^oK

T = temperature of electrons in ^oK

n = number density of electrons in m^{-3}

This definition is based upon the plasma being in Maxwell-Boltzmann equilibrium, and represents the distance within which the electrons are able to interact individually. The number of electrons within a Debye length of each other are just those contained within a sphere of radius $= \lambda_D$. Using Eqn (12), this turns out to be N_λ , where,

$$N_\lambda = \frac{4\pi}{3} \frac{(\varepsilon_o kT/e)^{3/2}}{\sqrt{n}} \qquad (13)$$

The charge at the center of this sphere is screened from those which lie outside the sphere.

This collective behavior of a plasma has important implications to the numerical solution of Vlasov's Equation. If the spatial grid is chosen so that it is larger than the Debye length, the numerical scheme will not be able to handle the steep gradients in particle density which would occur for every cell width. Therefore, the mesh spacing of the spatial variable, Δz, must be sufficiently fine to resolve the plasma Debye length.

BOUNDARY AND INITIAL CONDITIONS. In order to complete the solution to Eqns (5) and (6), boundary conditions and initial conditions must be presribed for the system of equations. The initial conditions for the problem specify that the following variables are zero at t = 0:

$$f(z,v,0) = E(z,0) = S(z,v,0) = 0, \quad \text{for all } v,z \geq 0 \qquad (14)$$

The boundary conditions on the Vlasov Equation can be treated in the same manner that any transport phenomenon is handled. In the (z,v) mesh for the one-dimensional problem of Fig. 1, there is only one physical boundary that represents the division between the infinite sheet of material and space, the boundary at z=0, v ≥ 0. However, all four boundaries must be considered. Basically, free surface boundaries exist for this equation on all sides of the mesh, similar to the conditions described by Bell and Glasstone (Ref 29, Sec. 1.1d). The difference is that for the Vlasov Equation, particles are restricted to move in only one direction for any given part of the mesh. Therefore, particles which are allowed to enter (exit) the mesh at z=0 ($z=z_{max}$) cannot exit (enter) from that same part of the boundary. This makes the free surface boundary conditions exactly correct at these locations, not the idealization referred to by Bell and Glasstone. Using the free surface boundary conditions at $z=\pm v_{max}$ is an idealization, however, for the assumption must be made that no electrons can return after leaving the mesh from either of these interfaces. Specifically, the free surface boundary conditions require that electrons which leave the mesh cannot return. Therefore, the following conditions must be met along the boundaries of the mesh, as depicted in Fig. 1:

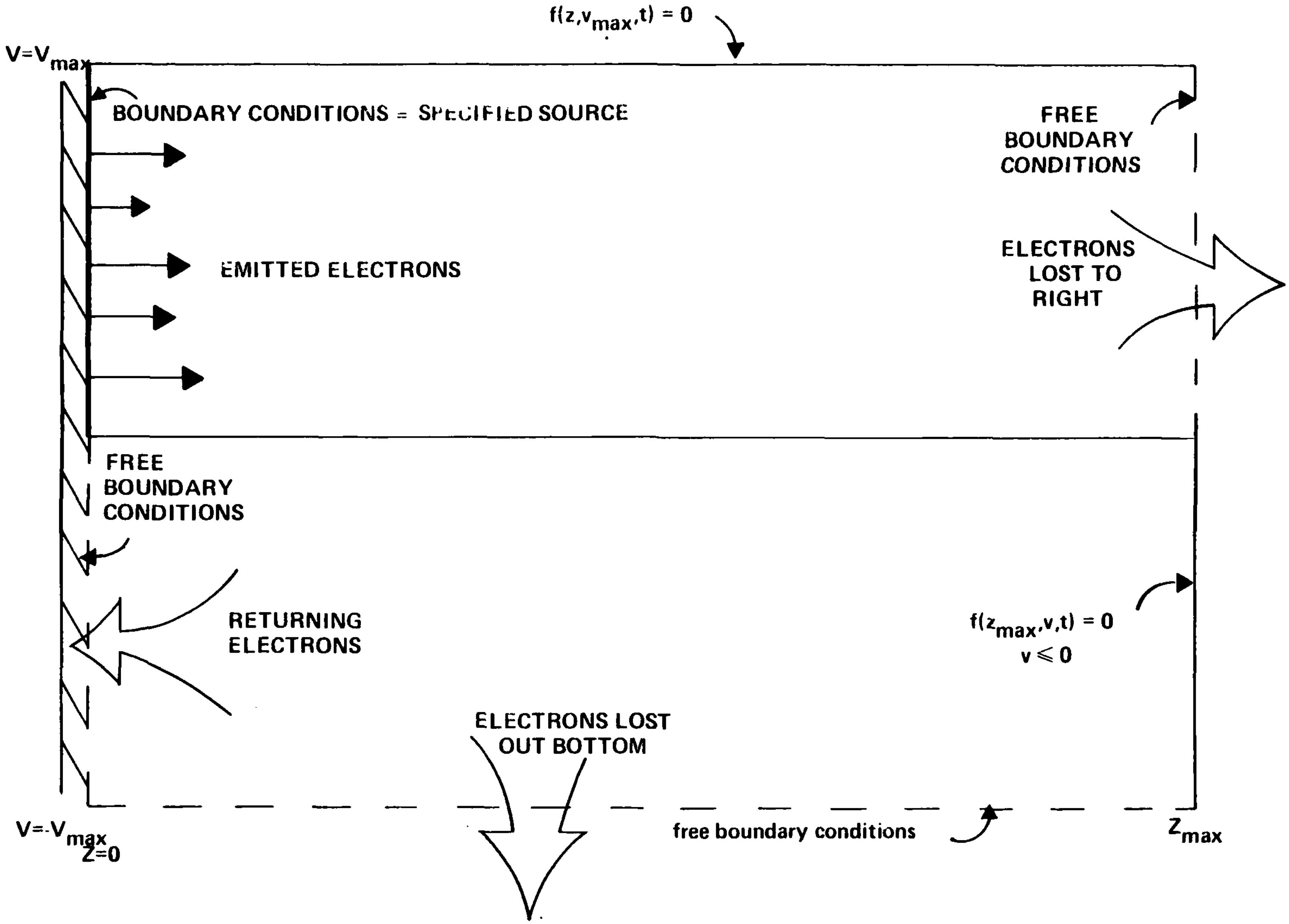

Fig. 1 Boundary Conditions for 1D SGEMP

$$f(z,+v_{max},t) = 0, \text{ for all } z,t \qquad (15a)$$

$$f(z_{max},v,t) = \begin{cases} 0, & v<0 \\ \text{free}, & v>0 \end{cases} \qquad (15b)$$

$$f(0,v,t) = \begin{cases} \text{source}, & v>0 \\ \text{free}. & v<0 \end{cases} \qquad (15c)$$

$$f(z,-v_{max},t) = \text{free, for all } z,t \qquad (15d)$$

Equation (15a) is true because it is assumed that no electrons can accelerate out the top of the mesh. Therefore, the only flow possible is into the mesh, which is set to zero. The distribution function is allowed to be whatever it wants to be at z_{max}, $v > 0$, and, $z=0$, $v < 0$; that is a free boundary.

Special note must be made about the conditions that exist at $z=0$, $v>0$, Eqn (15c). Because the source of electrons is assumed to be only at the surface, the boundary condition at this interface is the true requirement to get electrons into the mesh. That is, there is no volume source, $S(z,v,t)$, which is spread throughout the region of interest. Rather, the source only exists at the boundary, and, therefore, actual insertion of electrons into the mesh will be done through a boundary specification.

The boundary condition for the electric field is taken care of automatically by having the correct distribution function. There are only two boundaries for $E(z,t)$: $z=0$ and $z=\infty$. At the interface of a near perfect conductor (like Aluminum) the boundary conditions for Maxwell's Equations require that only the normal component of E exist near the surface. Inside the conductor, E is zero (Ref 30, Sec. 8.1).

Therefore, the E field on the surface is determined by having the correct charge density on the surface. Since it is reasonable to assume a perfect conductor for the SGEMP problem, the distribution function, $f(0,v,t)$, a surface charge density, will determine the correct electric field on the surface. At the other boundary, $z=z_{max}$, the electric field is allowed to take on whatever value $f(z_{max},v,t)$ forces it to be.

SOURCE DESCRIPTION. The final remaining topic of discussion to conclude this chapter on SGEMP is the way that the source of electrons can be described. The determination of the electron emission properties is a very complicated process in itself. There are elaborate computer programs which perform these calculations (Ref 31). They take into account such factors as: the thickness, shape and composition of the target; the angle of incidence, energy spectrum, time history and total fluence of the photon radiation; and the individual nuclear processes which release electrons (Compton scattering, photoelectric effect and pair production). This is a difficult problem to solve in itself. Fortunately, however, it is possible to separate the electron emission problem from the SGEMP problem. That is, the electrons which are emitted into space from initial arriving radiation do not interact appreciably with the late arriving radiation. The probability of a photon interacting with an electron in free space via Compton or Thomson scattering is extremely small due to the very low density of electrons. For example, the electron number density for a typical SGEMP plasma is $n \sim 10^{12}\ cm^{-3}$. For Thomson scattering, the cross section for interaction is $6.0 \times 10^{-25}\ cm^2/e^-$, which is larger than for Compton scattering (Ref 2, Chapter 23). Therefore, the linear attenuation coefficient is about 1.0×10^{-13} cm at most. This is to be contrasted with photon scattering probabilities in a solid material with densities of 10^{24} cm^{-3}, and linear attenuation coefficients of approximately 0.1 cm^{-1}. As a result, all treatments of SGEMP in existence rely on pre-determined emission properties.

As was just noted in the previous section, the SGEMP problem has a unique condition on the source of electrons. Because there is no actual volume source, but only a source defined at an interface, the emission of electrons is really a boundary condition. Thus, from now on, Eqn (5) will be considered to have no driving term on the right-hand-side. Rather, the boundary conditions on Eqn (5) will act as the electron driver.

An assumption that is very frequently made about the electron source is that the energy, hence velocity, dependence and time dependence are separable. That is, one assumes,

$$f(0,v,t) = T(t)\, f_v(v), \quad v>0 \qquad (16)$$

This separation is for convenience only, and is approximately true. Should some variation of the velocity spectrum as a function of time be supplied, there are no unique difficulties which would arise in the solution.

VELOCITY DEPENDENCE OF ELECTRON SOURCE. Numerical calculations of the photomission properties for X-ray radiation show that the electron energy spectrum is represented well by an exponential function when the X-rays are treated as blackbody radiation. The results also show that a a $\cos\theta$ angular distribution is a good approximation (Ref 5). If the X-rays are normally incident on a flat surface, then the electron velocity spectrum is reduced to the following expression in one dimension (see Appendix B):

$$f_v(v) = \frac{m}{w_1} Y \phi_o E_1\left(\frac{mv^2}{2w_1}\right) \quad [\mathrm{sec}^2/\mathrm{m}^4] \qquad (17)$$

where Y_1 = material yield (electrons/Joule)

w_1 = exponentiation energy (Joules), which is property of material and photon spectrum

ϕ_o = X-ray fluence (Joule/m^2)

$E_1(x)$ = exponential integral (Ref 32, Chapter 5)

$$= \int_x^\infty \frac{e^{-t}}{t}\, dt$$

It should be noted that variations other than the above type of exponential dependence of the velocity spectrum are possible, depending on the exact nature of the source.

TIME DEPENDENCE OF ELECTRON SOURCE. The choice of the time dependence of the source function, T(t), is a crucial one since it is this parameter which determines whether or not scaling of the SCEMP problem is possible. Carron and Longmire (Ref 6) have shown that if the X-ray pulse rises as a integer power of time, the one-dimensional, normal incidence SGEMP boundary layer scales. This means that the problem can be solved once, with all variables scaled to this one solution. If the scaled variables are represented by t', z', v', f', a', and S', then these similarity variables are defined by: t=Tt', z=Lz', v=$\langle v \rangle$v', f=Nf'/$\langle v \rangle$, a=$\langle v \rangle$a'/T, and S=NS'. The variables, t, z, v, f, a and S are defined in Eqns (2) and (5). The parameters, T, L, $\langle v \rangle$ and N are the plasma period, characteristic length, average velocity and a reference number density of the electrons, respectively. If the time dependence is slowly varying enough, then the equations may be reduced to a quasi-static case for which closed-form or quadrature solutions exist (Ref 4).

Although these cases are of general interest for their simplicity and for certain laboratory sources, SGEMP caused by a nuclear detonation and some pulsed electron beam sources are driven by an approximately exponentially rising and falling pulse. One analytic form of this dependence frequently used is:

$$T(t) = c_3 \frac{e^{c_1 t}}{1 + e^{c_2 (t-c_4)}} \qquad (18)$$

where c_3 = normalization constant ($\sec^{-1}$)

c_1 = approximate rise rate ($\sec^{-1}$)

c_2 = approximate fall rate ($\sec^{-1}$)

c_4 = approximate peak time (sec)

The following condition is used as a normalization requirement:

$$\int_{-\infty}^{+\infty} T(t)\, dt = 1$$

When this integral is carried out, c_3 is determined to be,

$$c_3 = \frac{c_2 \sin(\pi c_1 / c_2)}{\pi e^{c_1 c_4}} \qquad (20)$$

If the source is represented by Eqns (16), (17) and (18), only a general numerical solution is possible using either direct techniques or particle simulation.

SUMMARY OF NUMERICAL PROBLEM. The next chapter begins the discussion of the finite element techniques for the SGEMP boundary layer in one-dimension. For ease of reference, the mathematical problem is restated here. The distribution function for the electrons, f(z,v,t), satisfies the Vlasov Equation:

$$\frac{\partial f}{\partial t}(z,v,t) + v\frac{\partial f}{\partial z}(z,v,t) - \frac{e}{m}E(z,t)\frac{\partial f}{\partial v}(z,v,t) = 0 \qquad (5)$$

The electric field, E(z,t), is related to f(z,v,t) via:

$$\frac{\partial E}{\partial t}(z,t) = \frac{e}{\varepsilon_o}\int_{\text{all } v} v f(z,v,t)\, dv \qquad (6)$$

The initial conditions for this system of equations are that:

$$f(z,v,0) = E(z,0) = 0, \quad \text{for all } v,z > 0 \qquad (14)$$

The boundary conditions needed are:

$$f(z,+v_{max},t) = 0, \quad \text{for all } z,t \qquad (15a)$$

$$f(z_{max},v,t) = \begin{cases} 0, & v < 0 \\ \text{free}, & v > 0 \end{cases} \qquad (15b)$$

$$f(0,v,t) = \begin{cases} T(t)f\ (v), & v > 0 \\ \text{free}. & v < 0 \end{cases} \qquad (15c)$$

$$f(z,-v_{max},t) = \text{free}, \quad \text{for all } z,t \qquad (15d)$$

The behavior of the distribution function at the boundary can be approximated by:

$$f_v(v) = \frac{m}{w_1} Y\phi_o E_1\left(\frac{mv^2}{2w_1}\right) \qquad (17)$$

Finally, the time history of the electron source, T(t), is assumed to be of the form:

$$T(t) = c_3 \frac{e^{c_1 t}}{1 + e^{c_2(t-c_4)}} \qquad (18)$$

III. The Numerical Techniques

This chapter will present all the numerical approaches used for the solution to the SGEMP one-dimensional boundary layer problem discussed in Chapter II. Primarily, this consists of the application of the finite element method (FEM) to Eqns (5) and (6). But there are several other considerations. The time integration is a vital part to the solution of this problem. Also, the boundary conditions must be handled with care. Finally, the resulting set of algebraic equations requires an efficient solution technique, which is closely coupled to the computer requirements (storage and processing time) for the entire method. First of all, a discussion of the FEM, itself, is in order.

THE FINITE ELEMENT METHOD. The FEM is a numerical technique which provides a systematic method for solving physical problems in an arbitrary global mesh. The mesh can be nonuniform and irregular, composed of "elements" of any shape, but usually they are chosen as simple polygons (rectangles, triangles, tetrahedrons, etc.). Another important feature of the technique is that it allows controlled application of virtually any reasonable order polynomial approximation in the mesh. Mathematically, the FEM is an extension of the Rayleigh-Ritz-Galerkin technique (Ref 17, Chapter 1). The global region is subdivided into smaller regions called "elements". The unknown function, $g(x)$, is expanded into a set of piecewise polynomials, $\phi_i(x)$. That is,

$$g(x) = \sum_{j=1}^{N} \phi_j(x) g_j \qquad (21)$$

The FEM prescibes the way that the trial functions are to be chosen. For Lagrangian elements, they are built so that for every node, k, $\phi_j(x_k) = \delta_{jk}$. This gives the expansion coefficients, g_j, physical significance. In this dissertation, the expansion coefficients are the distribution function values, and the the electric field values, at the nodes.

METHOD OF WEIGHTED RESIDUALS. There are, in general, two different ways that the solution via the FEM for any problem may be set up (Ref 18, Sec. 3.4). The first approach is to solve a variational problem. That is, the physical situation is stated as an integral relationship for an entire set of functions —— a functional. Then, the correct solution is that function which minimizes the functional. This method is very common when there exists some physical variable which must be a minimum as some parameter is varied throughout its range, such as the Lagrangian (kinetic energy - potential energy) of a conservative system. The FEM is an integral (global) solution technique, as opposed to a discrete (local) method such as finite difference methods. The latter approach numerically solves the differential equations for the physical situation.

Of course, both the differential and integral equations represent the same physical reality. However, it is not always possible to determine the correct functional for a particular problem. When this happens, a different approach must be taken. The FEM can still be used by developing global, integral expressions from the differential equations. The Method of Weighted Residuals (MWR) is such a process. The residual is the difference between the true solution and the approximate one. The differential equation is multiplied by a set of functions, called weights, and the new equation is integrated over the entire solution domain. This converts a local, differential equation into a global, integral relationship. In this work, the finite element equations are derived using the MWR, as discussed in Zienkiewicz (Ref 18, Sec. 3.4).

GLOBAL FINITE ELEMENT EQUATIONS. Let the distribution function, $f(z,v,t)$, be approximated by a set of N trial functions, $N_i(z,v)$, $i=1,\ldots,N$. That is,

$$f(z,v,t) \approx \sum_{j=1}^{N} N_j(z,v) f_j(t) \qquad (22)$$

where $f_j(t)$ is a nodal value of f; $f_j(t)=f(z_j,v_j,t)$. Likewise, let

$$E(z,t) \approx \sum_{k=1}^{N_z} M_k(z) E_k(t) \qquad (23)$$

where $M_k(z)$ are a set of N_z trial functions for the electric field, and $E_k(z)=E(z_k,t)$ are the E-field nodal values. These approximations for $E(z,t)$ and $f(z,v,t)$ are used in Eqn (5). When the result is multiplied by $W_i(z,v)$, $i=1,\ldots,N$, the MWR weights, and summed and integrated over the entire region, the following equation is obtained:

$$\sum_{i=1}^{N} \sum_{j=1}^{N} \int_z \int_v [W_i(z,v) N_j(z,v) \frac{\partial f_j}{\partial t}(t) + v W_i(z,v) \frac{\partial N_j}{\partial z}(z,v) f_j(t)$$

$$- \quad M_k(z) E_k(t) W_i(z,v) \frac{\partial N_j}{\partial v}(z,v) \; f_j(t)] \, dvdz = 0 \qquad (24)$$

Recall that the source function, $S(z,v,t)$, has been set to zero because the electrons are emitted via the imposition of an appropriate boundary condition. This equation can be written in a more condensed matrix form:

$$[A]^{NxN}\left\{\frac{df}{dt}(t)\right\}^{Nx1} + [A_z]^{NxN}\left\{f(t)\right\}^{Nx1} - [A_v]_J^{NxN}E_J(t)\left\{f(t)\right\}^{Nx1} = 0 \qquad (25)$$

with the help of the following definitions:

$$(A)_{ij} = \int_z\int_v W_i(z,v)N_j(z,v)\; dvdz \qquad (26a)$$

$$(A_z)_{ij} = \int_z\int_v vW_i(z,v)\frac{\partial N_j}{\partial z}(z,v)\; dvdz \qquad (26b)$$

$$[(A_v)_J]_{ij} = \frac{e}{m}\int_z M_J(z)\left[\int_v W_i(z,v)\frac{\partial N_j}{\partial v}(z,v)\; dv\right] dz \qquad (26c)$$

Thus, $[A]$, $[A_z]$, and the $[A_v]$ are NxN matrices, and $\{f(t)\}$ is an Nx1 matrix (a column vector).

Once the weight and trial functions are chosen, and the integrals in Eqns (26) are performed, Eqn (25) can be solved as a set of N first order, ordinary differential equations in time. Applying the same approach to Ampere's Law in one dimension, Eqn (6), one finds:

$$[D]^{N_z x N_z}\left\{\dot{E}(t)\right\}^{N_z x1} - [D_v]^{N_z x N_z}\left\{f(t)\right\}^{N_z x1} = 0 \qquad (27)$$

where,

$$(D)_{ij} = \int_z P_i(z) M_j(z)\ dz \qquad (28a)$$

$$(D_v)_{ij} = \frac{e}{\varepsilon_o} \int_z P_i(z) \left[\int_v v Q_j(z,v)\ dv \right] dz \qquad (28b)$$

and where the dot above the E means differentiation with respect to time. The $P_i(z)$, $i=1,\ldots N_z$, are the weight functions; $Q_j(z,v)$, $j=1,\ldots N_z$, are the trial functions for $f(z,v,t)$; and the $M_j(z)$ are the trial functions for $E(z,t)$.

Note that in this general formulation of the finite element equations, the nodal points are not necessarily the same in both equations. That is, they could be solved in two separate meshes.

ELEMENT SHAPE AND MESH DESCRIPTION. Before proceeding further, it is necessary to discuss the choice of element and mesh configuration, and the weight and trial functions which are compatible with these choices. The simplest element shape that can be used for the Vlasov Equation is a rectangular element in (z,v) space. There are many advantages in using rectangles in this problem, and some disadvantages. In order to demonstrate the methods useful in the application of the FEM to one-dimensional SGEMP, I chose rectangles. For a detailed discussion of the advantages/disadvantages of different element shapes and less retricted meshes, see Appendix C.

A rectangular mesh is regular. That is, for linear Lagrangian elements, the node pattern consists of the set of (z_I, v_J) with

$I=1,\ldots,N_v$; $J=1,\ldots,N_z$. For every z_I there are N_v v_J's and for every v_J , there are N_z z_I's. A typical rectangular mesh is depicted in Fig. 2. Of course, the mesh can, in general, be non-uniform in either the z or v direction independently.

THE TRIAL FUNCTIONS. The description of the trial functions (sometimes called approximating functions or shape functions) can most easily be described in the local coordinate system of the element. For rectangles, the simplest trial functions which can be used are linear polynomials with nodes at each of the four corners, as shown in Fig. 3. These trial functions are members of the Lagrange family of polynomials. They are also belong to a family of polynomials which are especially suited for the FEM because of their simplicity. Zienkiewicz refers to the entire set as the Serendipity family (Ref 18, Sec. 7.5). They satisfy the essential requirement of the finite element approximation: continuity of the unknown function across element interfaces. These linear functions are defined in the local coordinate system by:

$$N_i(\xi,\eta) = \frac{1}{4}(1 + \xi_i\xi)(1 + \eta_i\eta) \qquad (29)$$
$$i = 1,\ldots,4$$

where the transformation from the global to the local system is made by:

$$\xi = \frac{1}{a}(z - z_c) \quad (30a); \qquad \eta = \frac{1}{b}(v - v_c) \quad (30b)$$

The constants, a, b, z_c and v_c are defined in Fig. 3. Note that each

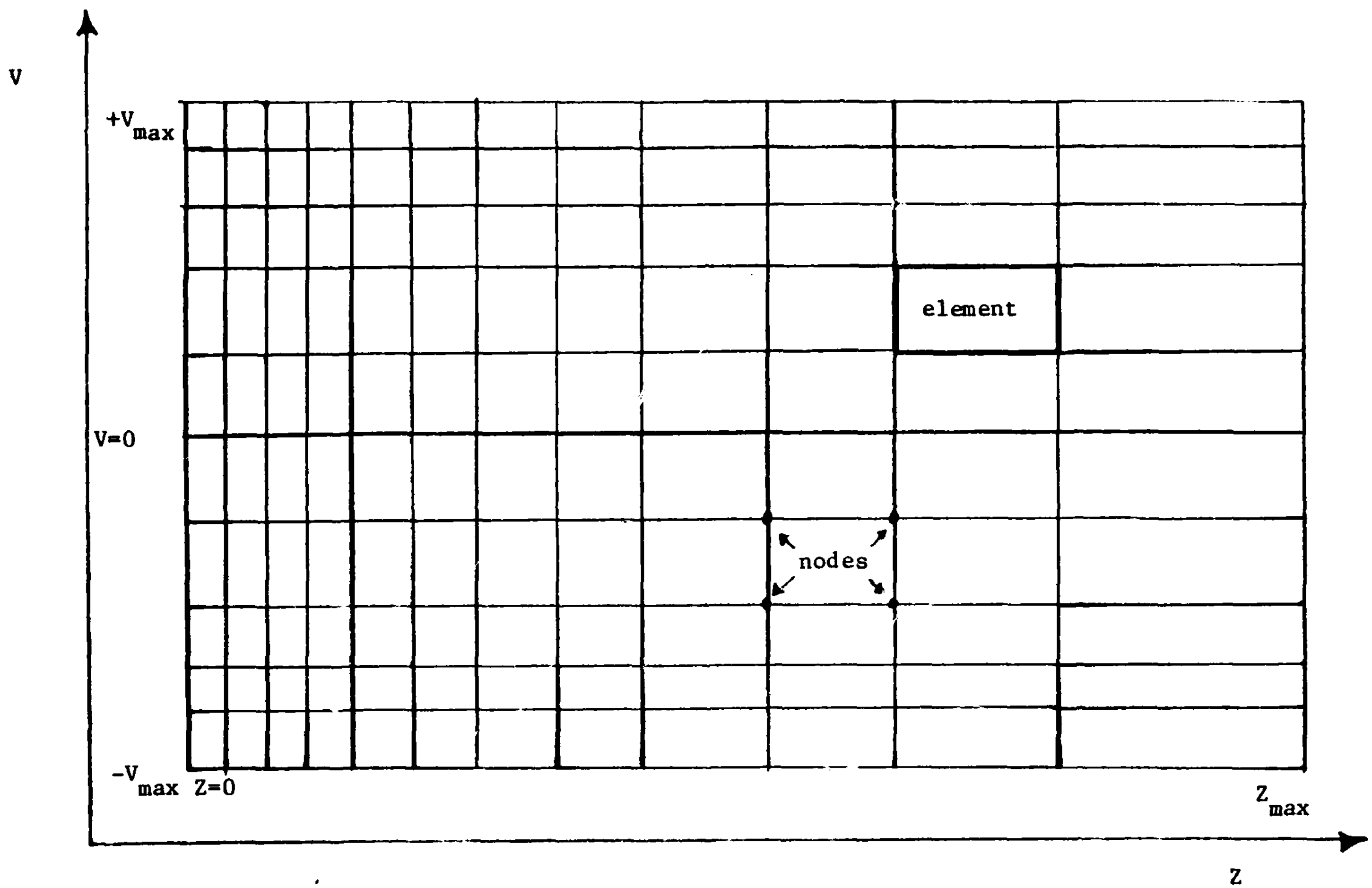

Fig. 2 Typical Finite Element Rectangular Mesh

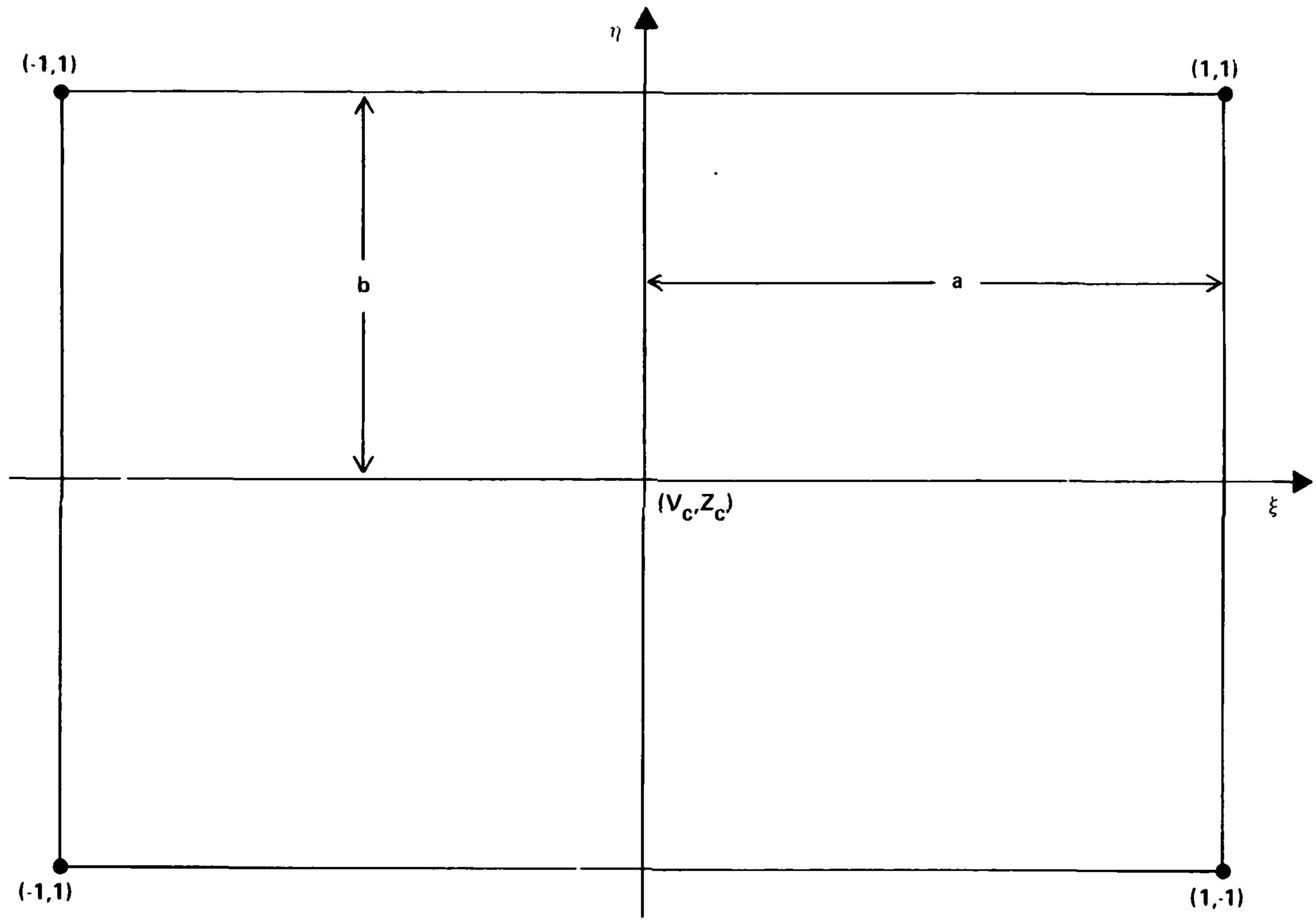

Fig. 3 Local Coordinate System for Rectangular Element

of these functions has the property of being unity at one node, and zero at the other three nodes, with a linear variation in between.

Of course, the variation in the ξ and η directions are independent of one another, and as such, can be treated separately. Thus, let

$$L_1(\xi) = \frac{1}{2}(1 - \xi) \qquad (31a)$$

$$L_2(\xi) = \frac{1}{2}(1 + \xi) \qquad (31b)$$

with like definitions in the η -direction. These are the basic linear trial functions in one dimension, sometimes called tent functions because they construct a tent-like shape when they are built on a series of nodes (see Fig. 4a). The rectangular functions of Eqn (29) are built from these. Using the nodal numbering system of Fig. 3:

$$N_1(\xi,\eta) = L_1(\xi)L_1(\eta) \qquad (32a)$$

$$N_2(\xi,\eta) = L_2(\xi)L_1(\eta) \qquad (32b)$$

$$N_3(\xi,\eta) = L_2(\xi)L_2(\eta) \qquad (32c)$$

$$N_4(\xi,\eta) = L_1(\xi)L_2(\eta) \qquad (32d)$$

Just as the combination of tent functions over one-dimensional elements produce the global, piecewise trial functions shown in Fig. 4a, the global functions required for the two-dimensional problem, $N_i(z,v)$, $i=1,\ldots N$ are built from the local trial functions, $N_i(\xi,\eta)$, $i=1,\ldots,4$. Figure 4b shows the tent functions for one element in two dimensions, and Fig. 4c depicts the tent functions at one node over a series of

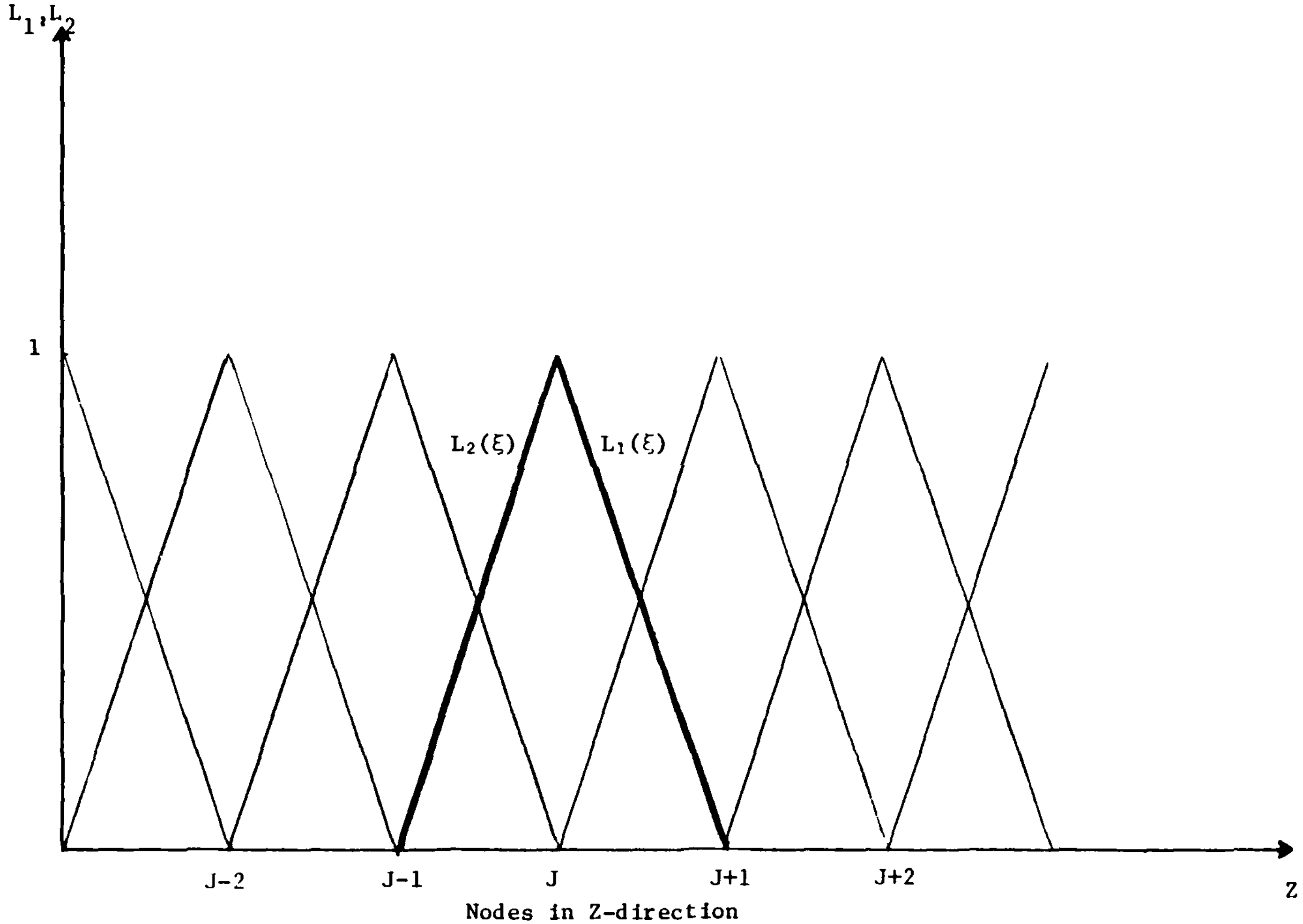

Fig. 4a Construction of Tent-Functions From Linear Trial Functions for Each Element

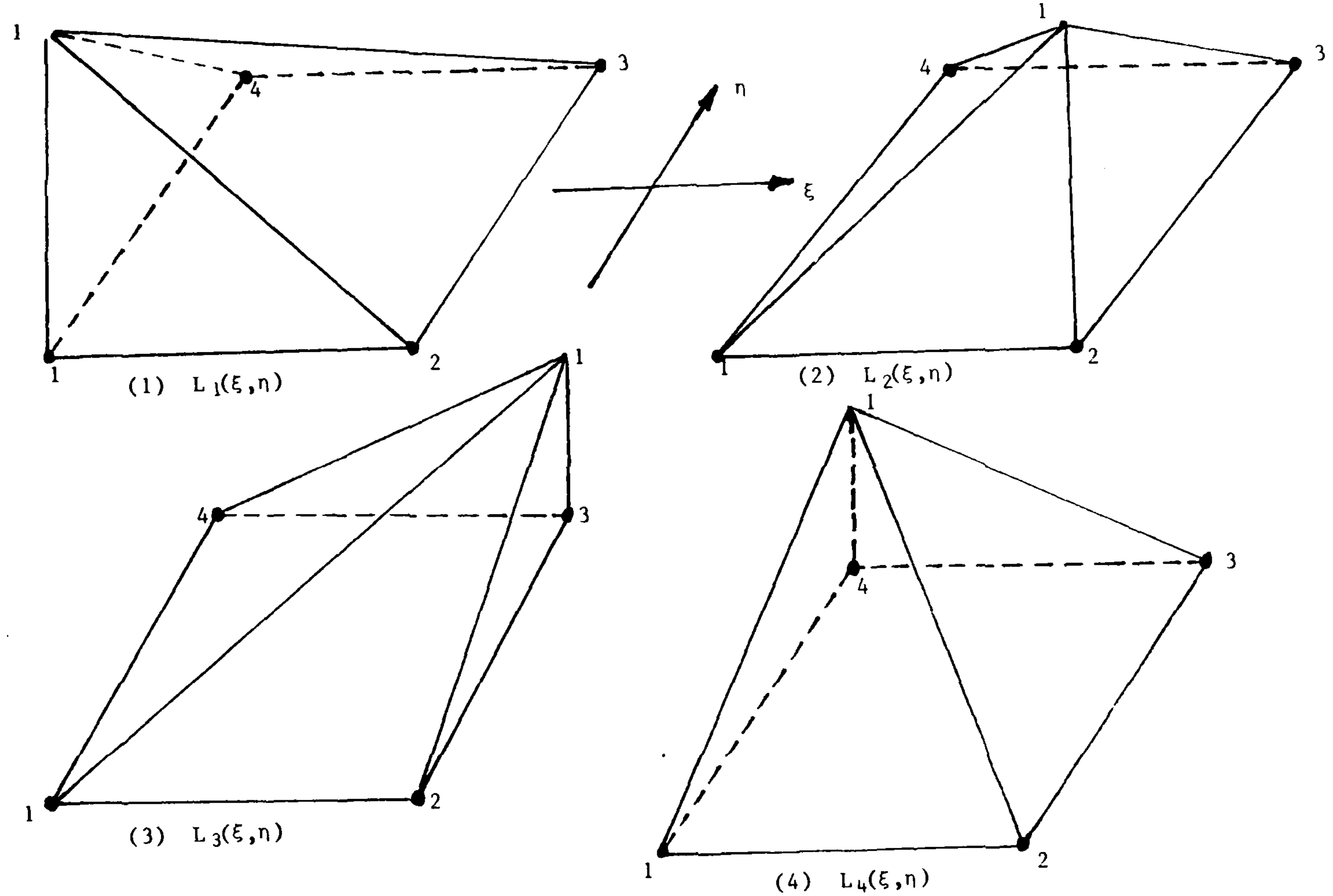

Fig. 4b Tent-Functions for a Rectangular Element in 2D

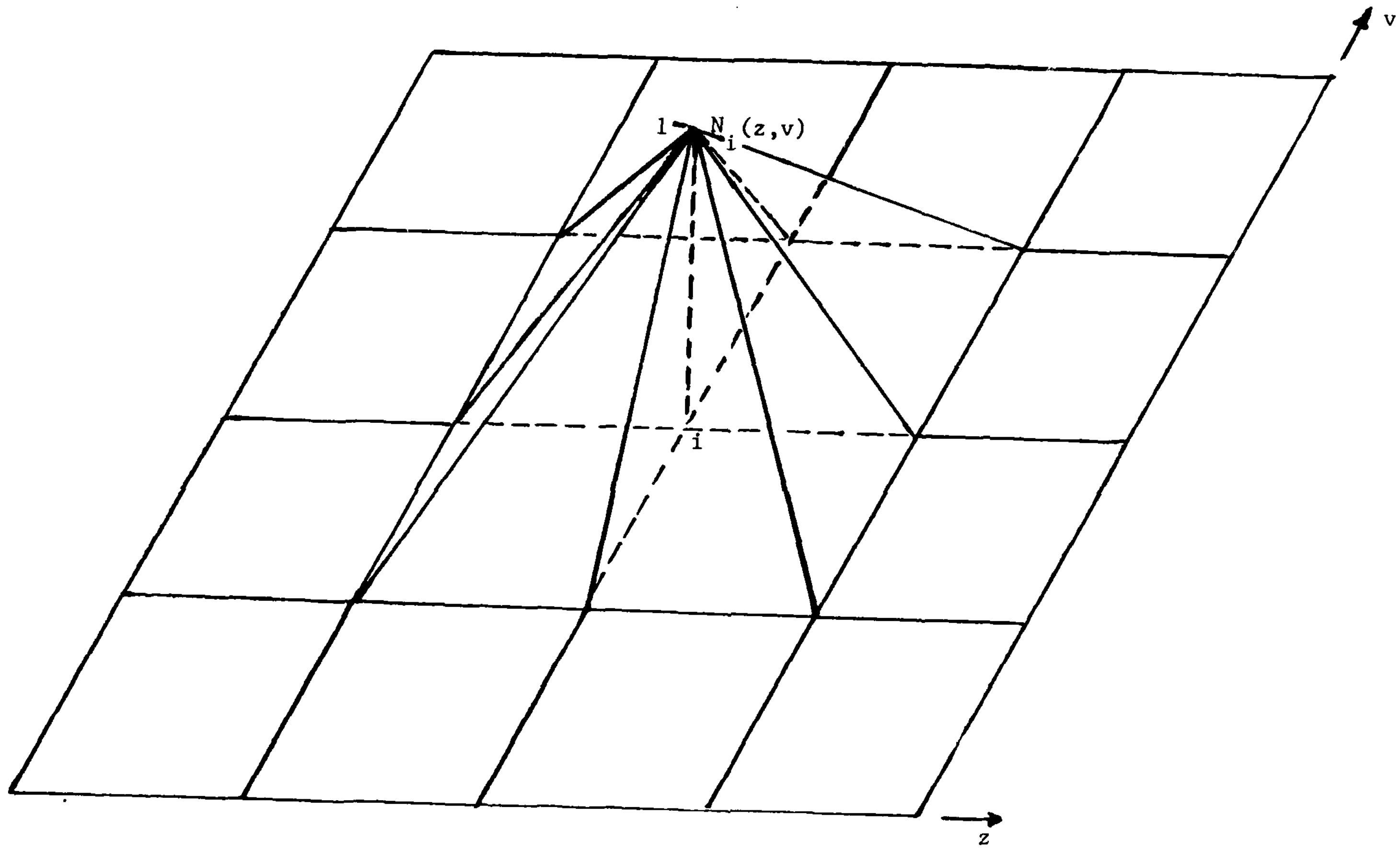

Fig. 4c Tent-Functions in 2D for a Rectangular Mesh

rectangles.

WEIGHT FUNCTIONS AND UPWINDING. The residual weights, $W_i(z,v)$, $i=1,\ldots N$, are also piecewise polynomials and so can be constructed most easily in the local coordinate representation. One of the more common choices for the weight functions is, $W_i(z,v) = N_i(z,v)$, for all i. This is sometimes referred to as the Galerkin Method. However, an upwinding procedure will be used (Ref 33, and Ref 19, Chapter 1) in anticipation of special requirements for the advection term of the Vlasov Equation. In this approach, Galerkin weighting appears as a special case. Referring to the local system, let:

$$W_1(\xi,\eta) = [L_1(\xi) + \alpha_1 F(\xi)][L_1(\eta) + \alpha_4 F(\eta)] \tag{33a}$$

$$W_2(\xi,\eta) = [L_2(\xi) - \alpha_1 F(\xi)][L_1(\eta) + \alpha_2 F(\eta)] \tag{33b}$$

$$W_3(\xi,\eta) = [L_2(\xi) - \alpha_3 F(\xi)][L_2(\eta) - \alpha_2 F(\eta)] \tag{33c}$$

$$W_4(\xi,\eta) = [L_1(\xi) + \alpha_3 F(\xi)][L_2(\eta) - \alpha_4 F(\eta)] \tag{33d}$$

The α_i are the upwinding parameters. Note that Galerkin weighting occurs when $\alpha_i=0$, for all $i=1,\ldots,4$. The side for each α_i is shown in Fig. 5. The function $F(\cdot)$ is chosen so that $F(\cdot)=0$ at the nodes. This preserves continuity of the weight functions at element interfaces. If $F(\cdot)$ is a positive function, the sign of α_i is picked to match it with the direction of flow of electrons. Thus, for α_1 and α_3, the sign will be positive when $v>0$, and negative when $v<0$. For α_2 and α_4, the sign is always negative because the electric field decelerates the electrons during the times of interest. Finally, the integral of $F(\cdot)$ over the element should be unity. A function which fits all these requirements

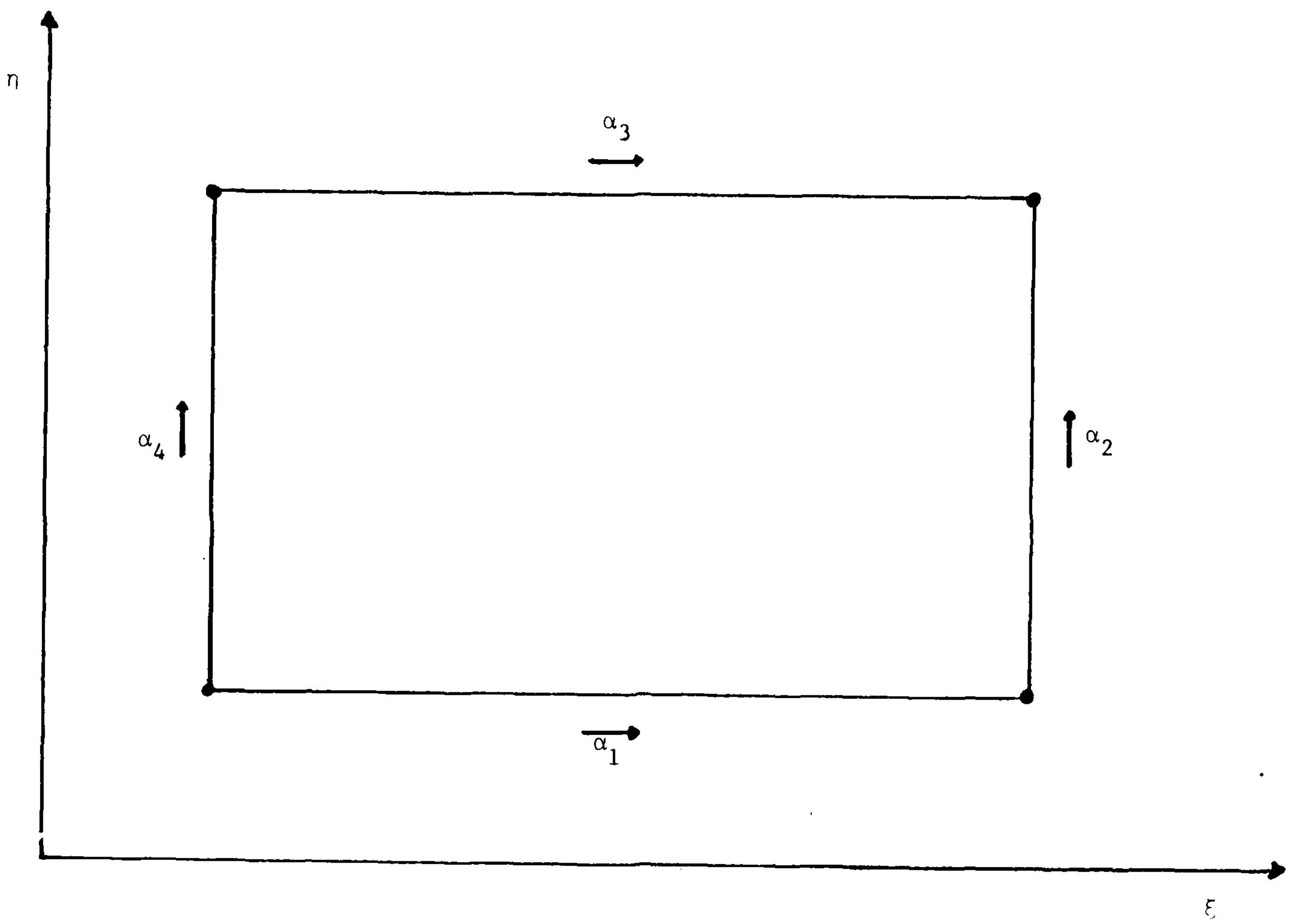

Fig. 5 Upwinding Parameter Sides And Direction for a Rectangle

is:

$$F(x) = -\frac{3}{4}(1 - x)(1 + x) = -3L_1(x)L_2(x) \qquad (34)$$

Equations (33) have been constructed from the following one dimensional expressions for each side of the rectangle:

$$W_i(x) = L_i(x) + (-1)^{i+1}\alpha F(x) \qquad (35)$$
$$i = 1,2$$

The shape of one of these weight functions, $W_1(x)$, is depicted in Fig. 6 for several α's. It is the biasing of the weights towards one node with repect to the other node that gives upwinding an advantage for propagation problems.

ELEMENT MATRICES. The actual evaluation of Eqns (26) and (28) is normally done in the local coordinate system of the element. Then, the transformation is made to the global system. This transformation is known as the "assembly" process of the FEM and involves a Boolean mapping of the local numbering system for the nodes to the global numbering system (Ref 34, Chapter 6). In symbolic form, for example,

$$[A]^{NxN} = \mathop{\mathcal{A}}_{e=1}^{N_e} [a^{(e)}]^{4x4} \qquad (36)$$

which says that the global NxN [A] matrix is constructed from a 4x4

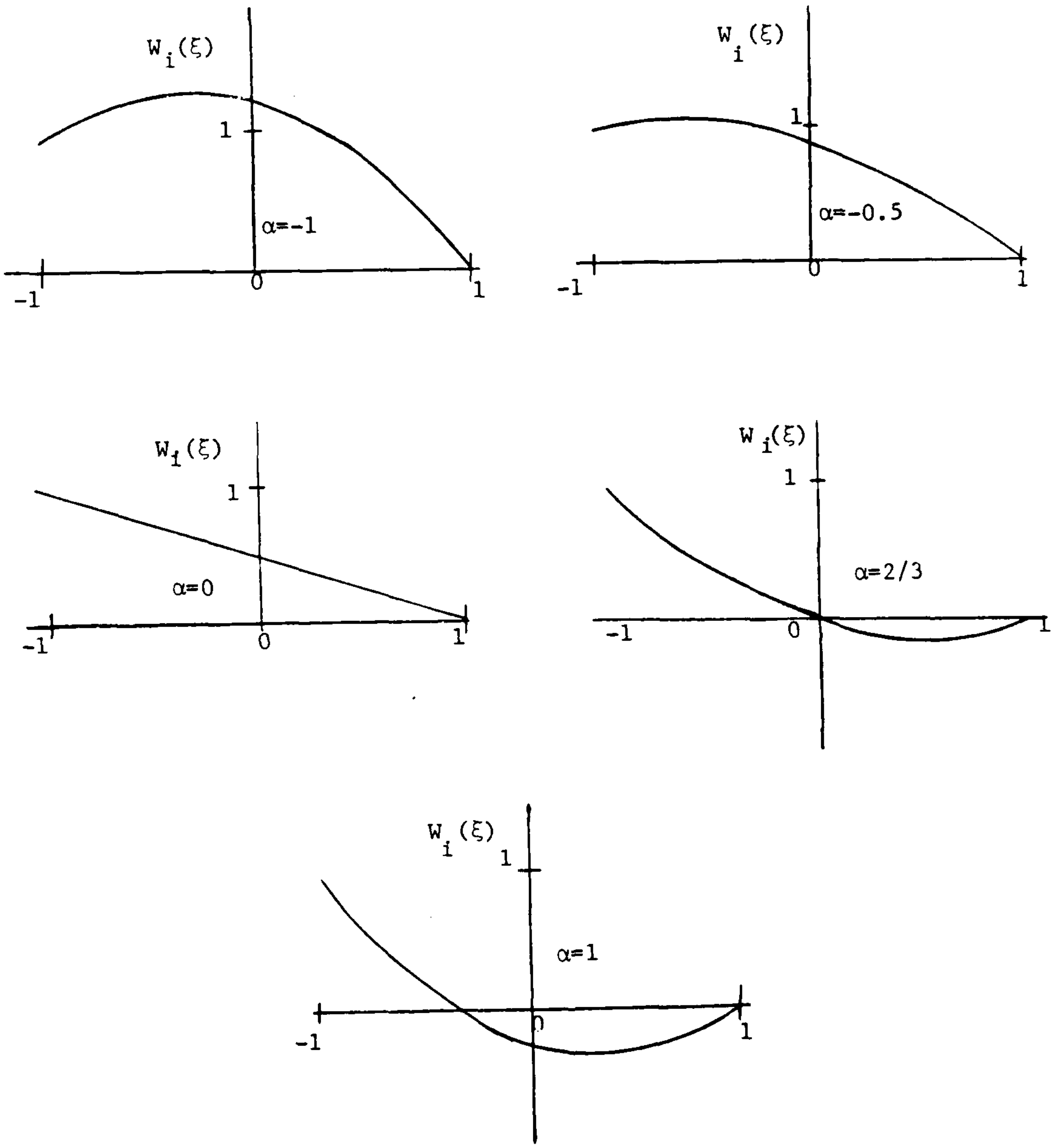

Fig. 6 Weight Functions in 1D
For Various Values of Alpha

element matrix (for linear rectangular elements) by "summing" over the number of elements, N_e, in the system. The script "$\mathcal{A}$" is used to denote that this sum is a special assembly procedure defined by a Boolean transformation. Appendix D has the details on the exact meaning of Eqn (36).

The expressions for $[a^{(e)}]$ and $[a_z^{(e)}]$ are straightfoward:

$$(a^{(e)})_{ij} = ab\int_{-1}^{+1}\int_{-1}^{+1} W_i(\xi,\eta)N_j(\xi,\eta)\, d\xi d\eta \qquad (37a)$$

$$(a_z^{(e)})_{ij} = b\int_{-1}^{+1}\int_{-1}^{+1} W_i(\xi,\eta)(b\eta + v_c)\frac{\partial N_j}{\partial \xi}(\xi,\eta)\, d\xi d\eta \qquad (37b)$$

In these equations, the Jacobian of the transformation from global to local coordinates, a•b, has been included.

The expression for matrix $[A_v]_J$, Eqn (26c), is a little bit more difficult to write in local coordinates because of the explicit dependence on each $M_J(z)$. However, $M_J(z)$ is a tent function over the Jth node for the linear approximation of regularly-spaced rectangles. Therefore, $M_J(z)$ in Eqn (29c) is either $L_1(\xi)$ or $L_2(\xi)$ in the local system. The assembly of $[A_v]_J$ does not occur through Eqn (36), but rather via:

$$[A_v]_J^{NxN} = \mathop{\mathcal{A}}_{e=1}^{N_e} \{a_{v1}^{(e)^{4\times4}} \;,\; a_{v2}^{(e)^{4\times4}}\} \qquad (38)$$

That is, $[A_v]_J$ is built from two element matrices, rather than one, and the way that the matrices are combined depends not only on the Boolean transformation, but also on the Jth position of the global column of nodes. See Appendix D for details.

Explicitly, then,

$$(a_{v\ell})_{ij} = a\int_{-1}^{+1}\int_{-1}^{+1} L_\ell(\xi)W_i(\xi,\eta)\frac{\partial N_j}{\partial\eta}(\xi,\eta)\,d\xi d\eta \qquad \ell = 1,2 \tag{39}$$

Now, using Eqns (32) and (33), the elemental matrices can be evaluated in closed form to obtain:

$$(a^{(e)})_{ij} = \frac{ab}{4}\,(1 + \frac{1}{3}\xi_i\xi_j + \eta_i\alpha_i)(1 + \frac{1}{3}\eta_i\eta_j + \xi_i\alpha_{i-1}) \tag{40a}$$

$$(a_z^{(e)})_{ij} = \frac{b}{12}\xi_j(1 + \xi_i\alpha_k)[(3 + \eta_i\eta_j + 3\eta_i\alpha_p)v_c + (\eta_i + \eta_j + \frac{3}{5}\eta_i\eta_j\alpha_p)b] \tag{40c}$$

$$(a_{v1}^{(e)})_{ij} = \frac{a}{20}\eta_j\frac{(1 + \eta_i\alpha_p)}{(2 + \xi_j)}[5 + \frac{1}{2}\xi_i(9 + 3\xi_j)\alpha_k] \tag{40c}$$

$$(a_{v2}^{(e)})_{ij} = \frac{a}{20}\eta_j\frac{(1 + \eta_i\alpha_p)}{(2 + \xi_{j+2})}[5 + \frac{1}{2}\xi_i(9 + 3\xi_{j+2})\alpha_k] \tag{40d}$$

where $i,j=1,\ldots,4$; and all subscripts are cyclic (that is, $j-1=4$ when $j=1$, and $j+2=1$ when $j=3$, etc.). The following replacement rules are in effect for k and p:

$k = 1$ when $i = 1, 2$
$k = 3$ when $i = 3, 4$
$p = 4$ when $i = 1, 4$
$p = 2$ when $i = 2, 3$

Example derivations for these equations are shown in Appendix E.

CURRENT DENSITY CALCULATION. The only remaining element matrices to evaluate are $[d^{(e)}]$ and $[d_v^{(e)}]$ which are associated with Ampere's Law. There is a process that can be used for a rectangular mesh which eliminates the need to carry out the integrals of Eqns (28). Everywhere that a nodal value of $E(z_J,t)$ is needed, nodal values of $f(z_J,v_J,t)$ exist. Therefore, a simple numerical integration in the v-direction can be used to evaluate Eqn (6) which will determine $E(z_J,t)$ for all J. In other types of meshes, this would not be possible (see Appendix C).

Since $f(z,v,t)$ is assumed linear in v, the integration required in Eqn (6) is quadratic in v. Therefore, Simpson's rule (Ref 35, Chapter 14) will evaluate the integral exactly over each element in this approximation. Thus:

$$E_J(t) = \frac{e}{6\epsilon_o}\sum_{k=1}^{N_v-1}(v_{k+1} - v_k)[2v_k f(z_J,v_k,t) + v_k f(z_J,v_{k+1},t)$$

$$+ v_{k+1} f(z_J,v_k,t) + 2\, v_{k+1} f(z_J,v_{k+1},t)] \qquad (41)$$

N_v = number of nodes in v-direction.

TIME INTEGRATION. Equations (25) and (41) are first order, coupled, ordinary differential equations in time. The time integration is performed by using a two-step procedure based on the Lax-Wendroff method (Ref 19, Chapter 2). The algorithm is defined by the following equations:

$$f(t + \frac{\Delta t}{2}) = f(t) + \frac{\Delta t}{2}\dot{f}(t) \qquad (42a)$$

$$f(t + \Delta t) = f(t) + \Delta t\dot{f}(t + \frac{\Delta t}{2}) \qquad (42b)$$

This scheme is accurate to second order. Applying this method to Eqns (25):

1st Step:

$$[A]\{f\}_{i+\frac{1}{2}} = [A]\{f\}_i - \frac{\Delta t}{2}[A_z]\{f\}_i + \frac{\Delta t}{2}\sum_{J=1}^{N_z}[A_v]_J E_J^i\{f\}_i \qquad (43a)$$

2nd Step:

$$[A]\{f\}_{i+1} = [A]\{f\}_i - \Delta t[A_z]\{f\}_{i+\frac{1}{2}} + \Delta t\sum_{J=1}^{N_z}[A_v]_J E_J^{i+\frac{1}{2}}\{f\}_{i+\frac{1}{2}} \qquad (43b)$$

The electric field is determined from Eqn (41) using the same procedure:

1st Step:

$$E_J^{i+\frac{1}{2}} = E_J^i + \frac{e\Delta t}{12\varepsilon_o}\sum_{k=1}^{N_v-1}(v_{k+1} - v_k)[2v_k f_i(z_J,v_k) + v_k f_i(z_J,v_{k+1})$$
$$+ v_{k+1} f_i(z_J,v_k) + 2v_{k+1} f_i(z_J,v_{k+1})] \qquad (44a)$$

2nd Step:

$$E_J^{i+1} = E_J^i + \frac{e\Delta t}{6\varepsilon_o}\sum_{k=1}^{N_v-1}(v_{k+1} - v_k)[2v_k f_{i+\frac{1}{2}}(z_J,v_k) + v_k f_{i+\frac{1}{2}}(z_J,v_{k+1})$$
$$+ v_{k+1} f_{i+\frac{1}{2}}(z_J,v_k) + 2v_{k+1} f_{i+\frac{1}{2}}(z_J,v_{k+1})] \qquad (44b)$$

The procedure for marching in time is to start with Eqn (43a) to determine $\{f\}_{i+\frac{1}{2}}$. Also, Eqn (44a) will fix $\{E\}_{i+\frac{1}{2}}$. Then, Eqns (44b) and (43b) calculate $\{E\}_{i+1}$ and $\{f\}_{i+1}$ respectively. The whole process can now be repeated. Note that since E and f are determined at the same time intervals, it is unimportant which order they are computed.

COMPUTATIONAL IMPLEMENTATION. The one-dimensional SGEMP boundary layer problem has now been reduced to a set of algebraic equations, Eqns (43) and (44). Now, a numerical technique must be picked to solve these equations, and the boundary conditions properly applied.

The matrices $[A]$, $[A_z]$, and $[A_v]_J$ are NxN, where N = total number of nodal points. Since there are N_z of the $[A_v]_J$, the problem size in terms of computer memory for just the matrices is $NxNx(N_z+2)$. Thus, if $N_z=20$ and $N_v=10$, the rectangular mesh will have 200 nodes, with the matrices having 880,000 members! Fortunately, most of these are zero; that is, the matrices are extremely sparse. In fact, it can be shown that for the rectangular mesh,

$$N_\phi(A,A_z) = (3N_z - 2)(3N_v - 2) \qquad (45a)$$

$$N_\phi(A_v) = 21N_zN_v - 14N_z - 18N_v + 12 \qquad (45b)$$

where N_ϕ means the maximum number of non-zero members for the specified matrices. Also, Eqn (45b) includes all N_z of the NxN matrices. Thus, for the 20 x 10 problem, at most there are only 5376 non-zero members.

Because of this, sparse matrix techniques may be used to solve the equations. I chose a fully packed scheme which stores only the non-zero members of the arrays. Pointer arrays are used to specify which row and column each member is in. The algebraic solution is done using a

Gauss-Seidel iteration technique (Ref 35, Sec. 20.8) in fully packed form (Ref 36). Matrix [A] is the only one which needs to be inverted, and is diagonally dominant for most values of α_1. Thus, the Gauss-Seidel method is guaranteed to converge.

The boundary conditions are implemented by modifying the load vector, {b} , for the form [A] {x} = {b} , as well as the appropriate row and column of [A] (Ref 18, Chapter 20). This reduces the number of unknowns in {x} by the number of boundary values needed to be specified. Using Eqn (16) and (17), the following boundary condition on f specifies the source of electrons:

$$f(0,v,t) = \frac{mY\phi_o}{w_1} E_1\left(\frac{mv^2}{2w_1}\right) \quad T(t) \quad [\mathrm{sec/m^4}] \qquad (46)$$

$$v>0$$

This is valid for an exponential energy source.

The next chapter presents the results obtained from the solution of the equations described in this chapter for several conditions.

IV. Results

In this chapter, the numerical results obtained by the application of the techniques presented in Chapters II and III are given. These results are organized in order of increased computational difficulty. First, sample data are given for pure advection, or wave propagation. Then, both SGEMP equations are solved for the linear case. The physical implications are analyzed and compared with the computer generated results. Next, the nonlinear set of equations are solved, first with a linear time history, and then with an exponential time dependence. This is compared with "particle pushing" techniques and quasi-static theoretical analysis. Finally, general considerations about mesh sensitivity, particle conservation and convergence criteria shall be analyzed.

PROPAGATION STUDIES. The simplest form that Eqn (5) can have and still carry some physical meaning is obtained by dropping the nonlinear term to give:

$$\frac{\partial f}{\partial t}(z,v,t) + v\frac{\partial f}{\partial z}(z,v,t) = 0 \qquad (47)$$

This equation describes pure advection, or propagation, of the unknown function, f(z,v,t), at velocity, v. It is still a first order, hyperbolic, partial differential equation, but is now linear. Given initial conditions that prescribe the shape of the distribution, say $f_o(z,v) = f(z,v,0)$, then the exact solution to Eqn (47) is that function which translates the shape of f at the velocity, v, along the z axis. Therefore, the solution to Eqn (47) can be represented by:

$$f(z,v,t) = f_o(z - vt,v) \qquad (48)$$

This problem, and numerical methods to solve it, has been the subject of several studies (Ref 19, Chapter 19 and Ref 27). In particular, a very stringent propagation test can be done when Eqn (47) is solved using discontinuous initial conditions in z. A square wave pulse meets these conditions.

The primary purpose in doing such a test is to determine how accurately the finite element technique treats a propagating signal. Since oscillations are a well-known result of numerical solutions to wave equations, this test also helps to study the effect of various upwinding parameters on these oscillations. Several computer runs were made to evaluate different α_i. The test was done in a manner similar to Book and Boris (Ref 27). The pulse existed only at one velocity, with $v\Delta t/\Delta z = 0.2$. The background density was 0.5 and the pulse height was 2.0 (both quantities measured in arbitrary units). All the $|\alpha_i|$, $i=1,\ldots,4$ were set to the same magnitude, with α_1 and α_3 positive for positive v_c and negative for negative v_c. Both α_2 and α_4 were always negative. The results of this study are shown in Fig. 7, after 100 time steps. They are superimposed upon the initial square wave. Note

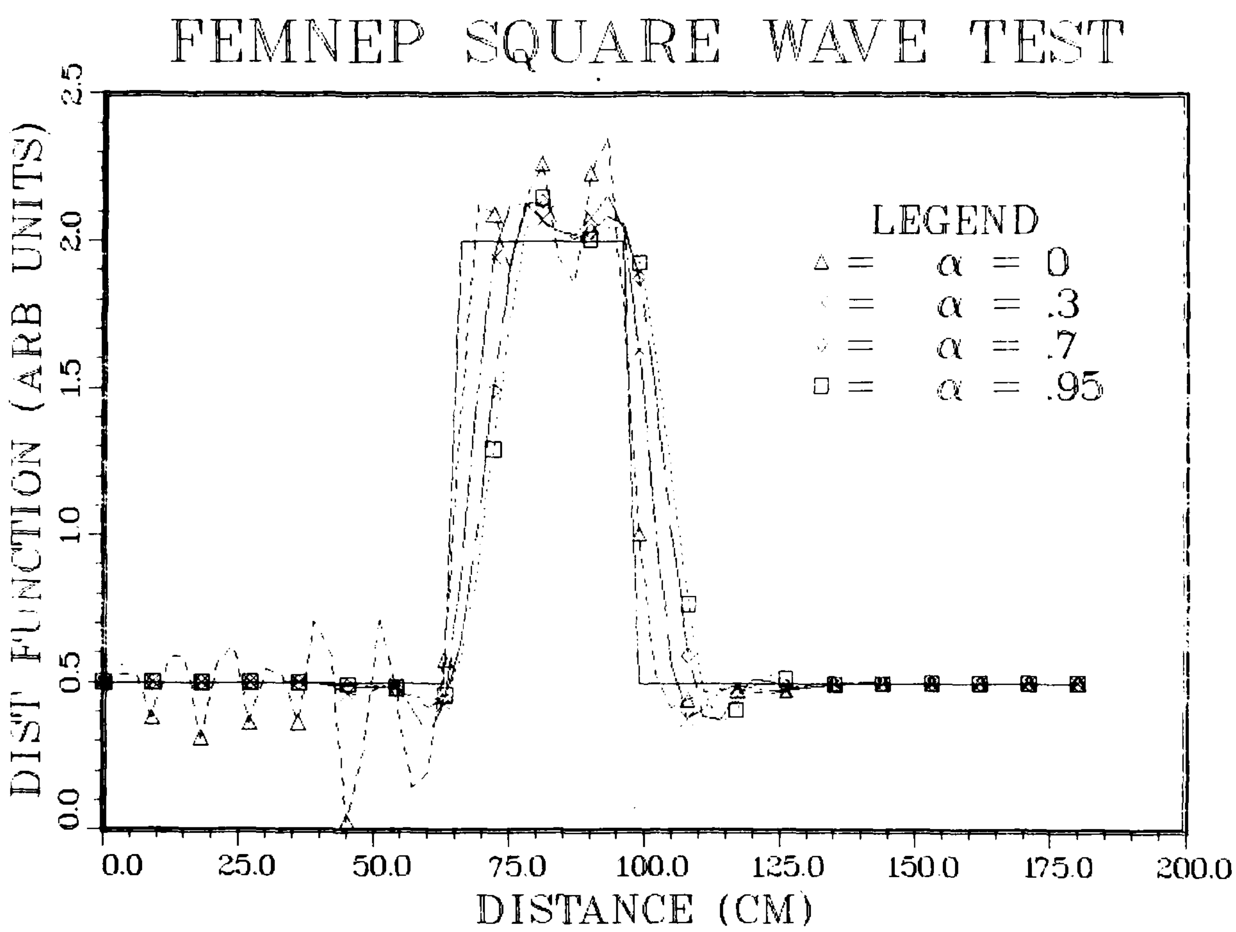

Fig. 7 Effect of Upwinding on Square Wave Propagation

the characteristic oscillations in front of, and trailing, the pulse. It is clear that the effect of increasing the magnitude of α from 0 to 1 is to reduce the oscillations, while introducing dispersion in the pulse.

There is, therefore, a trade-off between oscillatory behavior and dispersion. A value of about 0.5 appears to be a logical choice for a compromise. However, for practical considerations, another value makes more sense for most problems. Consider Eqn (40a). When $|\alpha_i| = 2/3$, and the conditions on the sign of the α_i are met as described above, $a_{12} = a_{13} = a_{31} = a_{32} = a_{41} = a_{42} = 0$. Because six out of 16 members of this element matrix are zero, there is a considerable reduction in the number of non-zero members of [A]. The savings is slightly more than a factor of two for a regular, rectangular mesh. Since this is the coefficient matrix for the system of of algebraic equations which determines f(z,v,t), execution time is halved by using $|\alpha_i| = 2/3$, $i=1,\dots,4$. This is due to the decrease in the number of arithmetic operations required by the Gauss-Seidel iteration scheme. Only the non-zero members of [A] are used for the tightly-packed scheme used in FEMNEP. For the square-wave test, there are 847 non-zero members of [A] when $|\alpha_i| = 2/3$. But, when $|\alpha_i| \neq 2/3$, there are 1810. This is the maximum possible for the rectangular mesh, $N_\phi(A)$, as calculated by Eqn (45a), with $N_z = 61$ and $N_v = 4$, used for this problem.

However, an interesting feature of using the value of $|\alpha_i| = 2/3$ is that the Gauss-Seidel iteration technique does not converge for the square-wave discontinuous pulse. For all other values of α tried, the method converged for this problem, including $\alpha = 0.650$ and $\alpha = 0.670$. Also, the iteration scheme worked well for all values of α_i, including

$=2/3$, for smoothly varying input pulses. The only exception to this observation occurs when $|\alpha| \to 1$, at which point the Gauss-Seidel technique no longer converges. The last section in this chapter on "Convergence Criteria" gives a comparison of the computer execution time for $|\alpha_i| =2/3$, and $|\alpha_i|=0.60$.

ELECTRIC FIELD FROM THE LINEAR VLASOV EQUATION. The next test that can be made on the finite element technique is to add the electric field to the solution. The nonlinear term, $E(z,t)\frac{\partial f}{\partial v}(z,v,t)$ is still ignored. In the finite element approximation this implies that $\sum_{J=1}^{N_z}[A_v]_J E_J(t)\{f(t)\}$ is zero in Eqn (25). Of course, the physical implication of making the equations linear is to prevent the electrons from interacting with each other. That is, an electric field is built up by the removal of negative charge from the surface, but the electrons, themselves, are not affected by it. The linear equations allow for the separation of charge with no boundary layer build up. In effect, a parallel plate capacitor of infinite cross sectional area is the physical model described by the linear equations. If Q represents the charge per unit area which has been emitted from the surface, then, after all charge has proceeded past distance z_o, the electric field in rationalized MKS units is:

$$E(z) = \frac{Q}{\varepsilon_o} = \frac{N_p}{\varepsilon_o}\text{, for all } z<z_o \qquad (49)$$

and N_p = number of electrons per square meter.

The purpose of running this test is to check the effect of boundary conditions, normalization procedures and the integrations of Eqn (41).

The test was performed by injecting 5.0×10^6 electrons/cm^2 into a 4x20 point v–z mesh. The electrons were given only one velocity, with the condition that $v\Delta t/\Delta z = 0.2$. The α's were all set with the same magnitude for each element. The α_1 and α_3 were positive, while the α_2 and α_4 were negative. Figures 8 and 9 show the results of this test for two cases, $|\alpha_i| = 2/3$ and $\alpha_i = 0$. Both the electric field vs z, and the distribution function vs z are shown at various times. The incident pulse time history was of the form:

$$T(t) = \frac{\alpha\beta}{\alpha-\beta}\left(-e^{-\alpha t} + e^{-\beta t}\right) \qquad (50)$$

with α = 2/shake

β = 6/shake

where, 1 shake = 10 nanosec.

Using Eqn (49), the theoretical value for the electric field, if all 5×10^6 particles have passed z_o, is E_{th} = 905.0 volts/m. Table I shows E vs z produced by the finite element equations at t=20.2 shakes (202 time steps). From the table and the graphs, it is easy to see the effect of using some upwinding, versus not using any, on the electric fi . The effect on the distribution function is even more dramatic. From Fig. 9, not only are trailing oscillations severe without upwinding, but reflections off the end of the mesh at z = 95 cm are are very apparent. This is quite visible in Fig. 9(f) and 9(g), where

TABLE I

Electric Field for Two Values of Alpha in a Linear Problem

z(cm)	E(z) (volts/m) $\alpha = 0$	E(z) (volts/m) $\alpha = 2/3$
0	904.4	904.4
5	913.5	904.4
10	898.3	904.4
15	889.9	904.4
20	922.8	904.4
25	906.5	905.8
30	899.7	905.6
35	897.5	906.4
40	899.2	906.7
45	931.5	906.6

E_{th} = 905.0 volts/m

the reflected distribution function is growing in magnitude, while with upwinding, Fig. 8(f)and 8(g), reflections do not exist. This wiil be particularly important when electrons are allowed to return to the surface with negative velocity. Reflections in the distribution function from returning electrons would be disastrous from three standpoints: first, positive reflections in the distribution function would represent particles external to the object which are not really there; second, growing reflections represent an instability in the calculation; and third, negative reflections giving rise to a negative distribution function have no physical meaning and can cause instabilities in nonlinear calculations.

LINEARLY RISING PULSE. The next type of solution presented is for the case of a linearly rising pulse, with an exponential (blackbody-like) energy spectrum. This is a truly nonlinear problem, so that the full set of equations must be used. As a check on the results, the

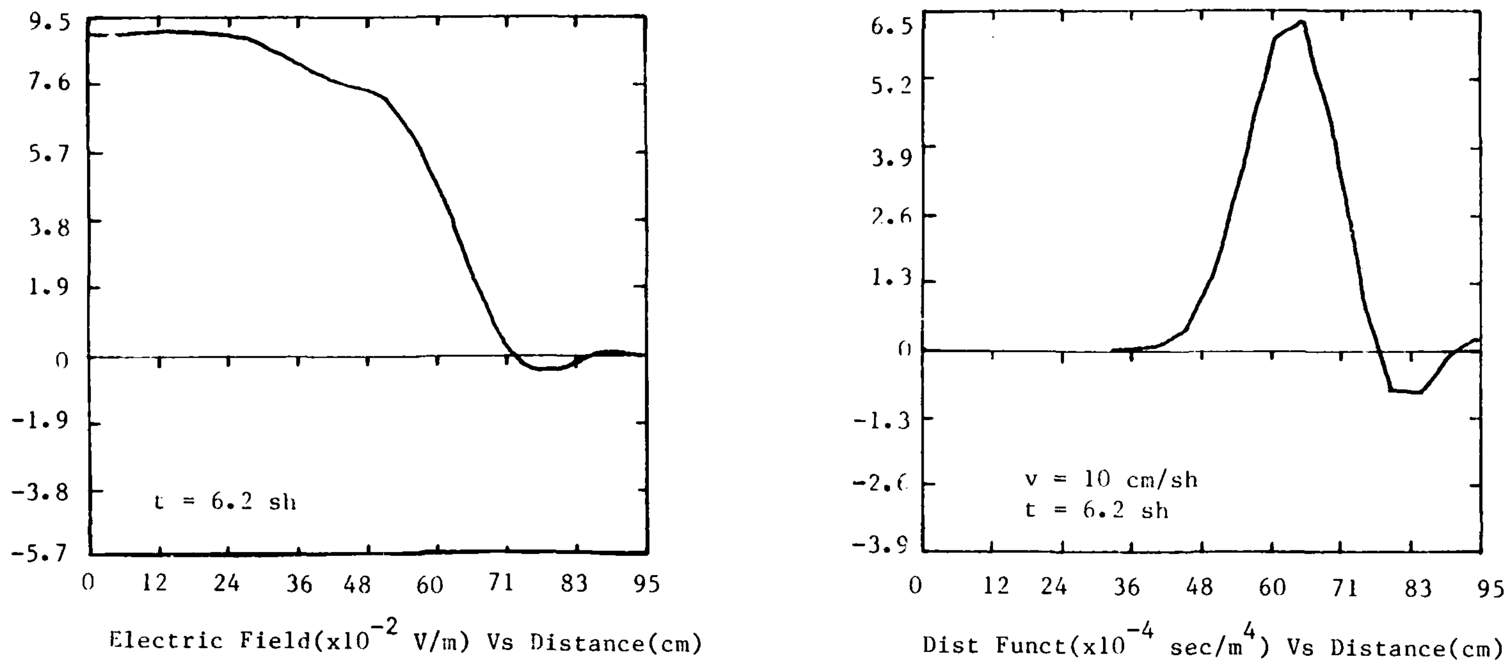

(a)

(b)

Fig. 8 Electric Field and Distribution Function
Vs Distance for Linearized Equations, α=2/3

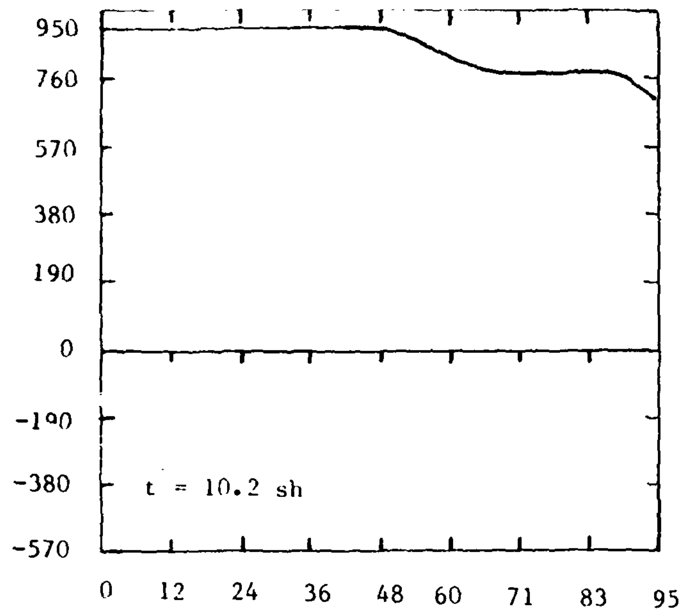

Electric Field(V/m) Vs Distance(cm)

(c)

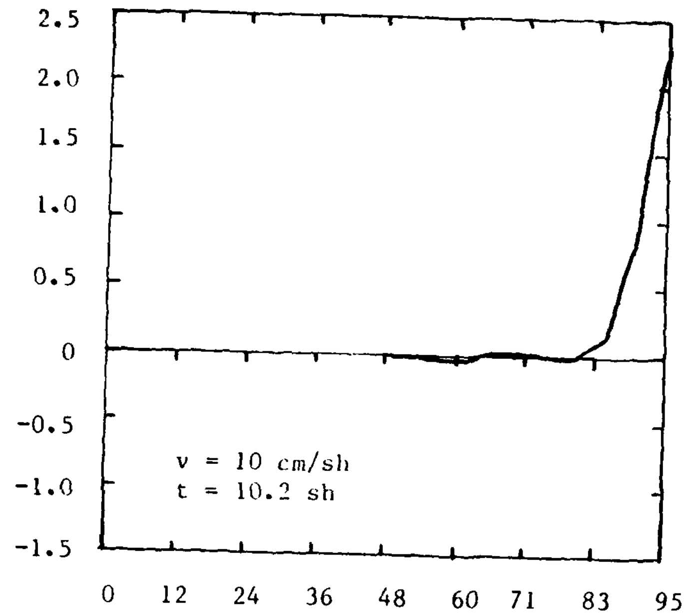

Dist Funct($x10^{-4}$ sec/m^4) Vs Distance(cm)

(d)

Fig. 8 (continued)

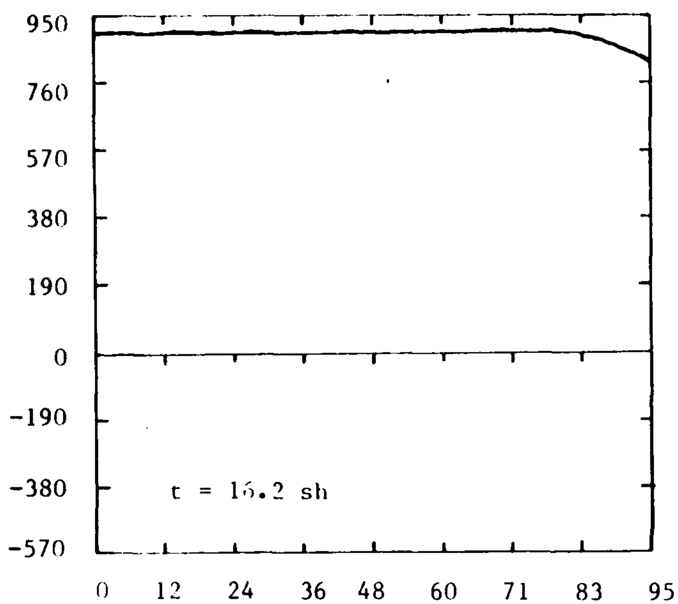

Electric Field(V/m) Vs Distance(cm)

(e)

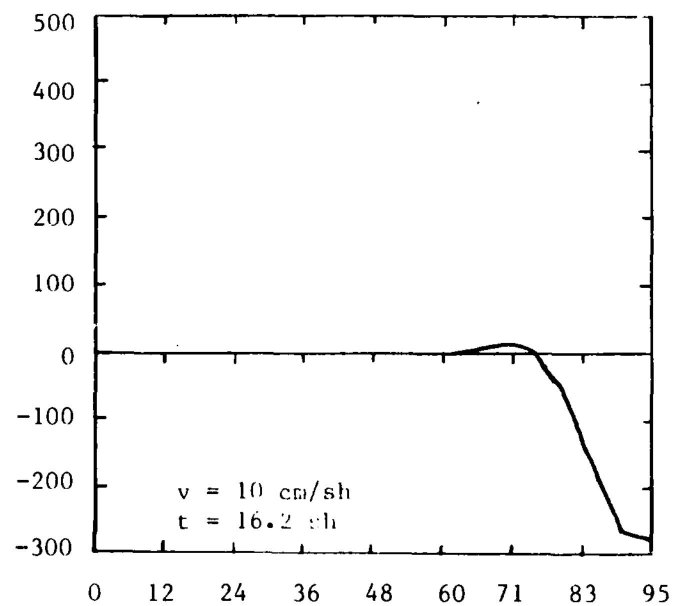

Dist Funct(sec/m^4) Vs Distance(cm)

(f)

Fig. 8 (continued)

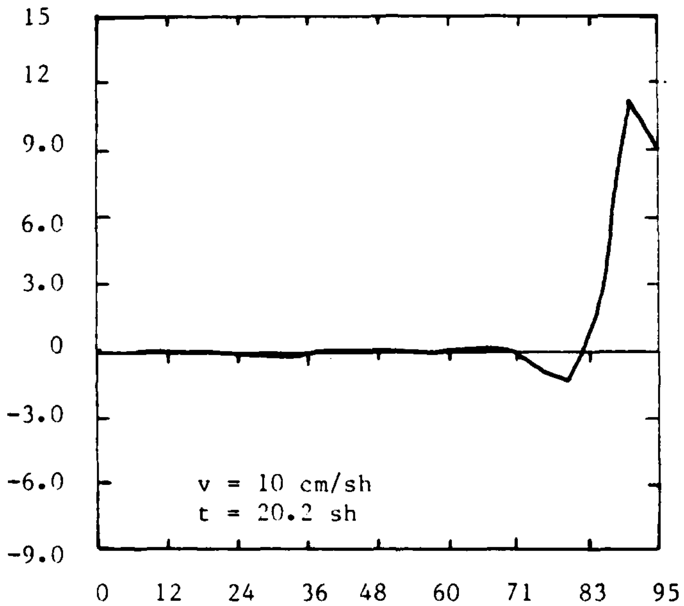

Dist Funct (sec/m^4) Vs Distance(cm)

(g)

Fig. 8 (continued)

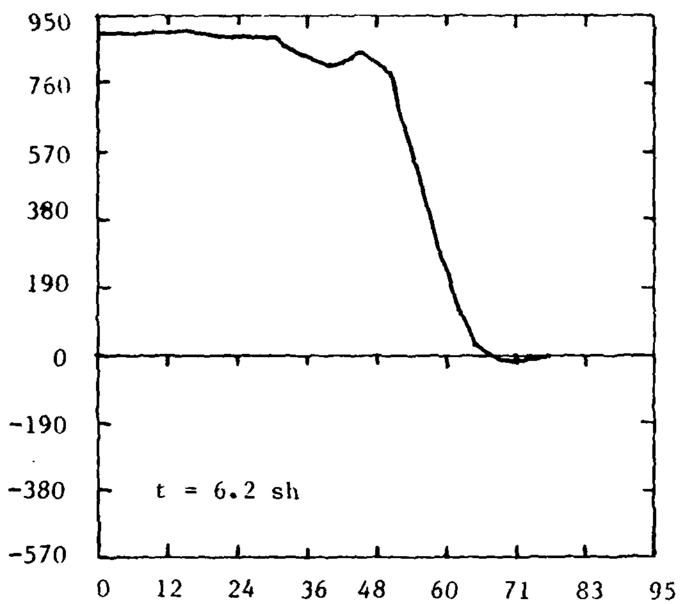

Electric Field(V/m) Vs Distance(cm)

(a)

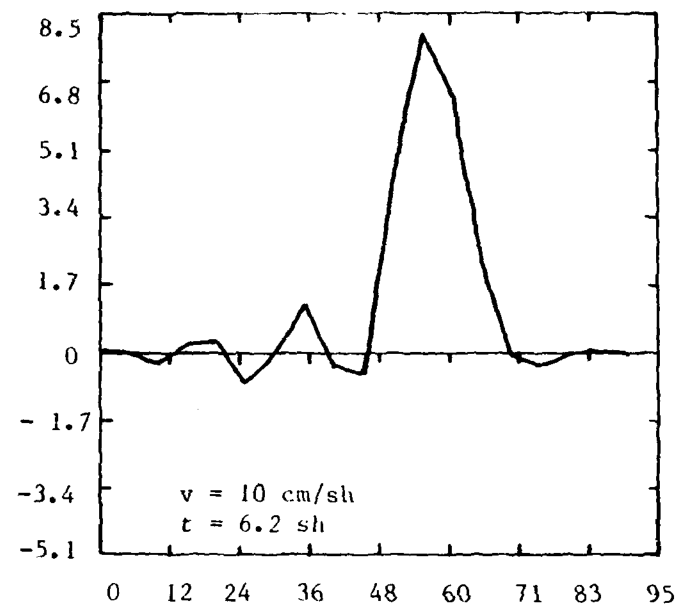

Dist Funct(x10^{-4} sec/m^4) Vs Distance(cm)

(b)

Fig. 9 Electric Field and Distribution Function Vs Distance for Linearized Equations, α=0

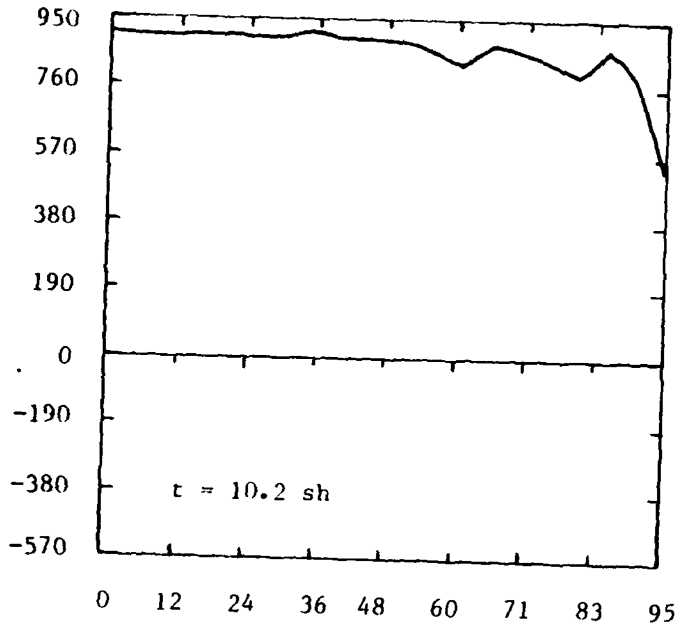

Electric Field(V/m) Vs Distance(cm)

(c)

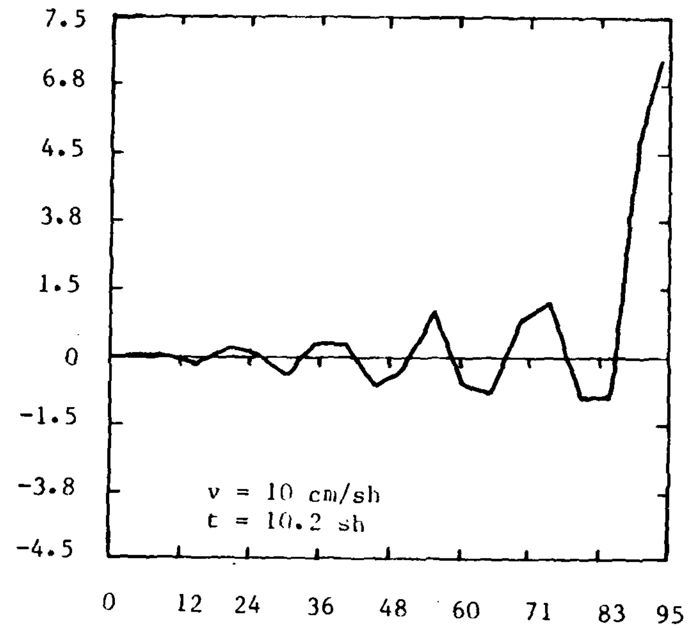

Dist Funct($x10^{-4}$ sec/m^4) Vs Distance(cm)

(d)

Fig. 9 (continued)

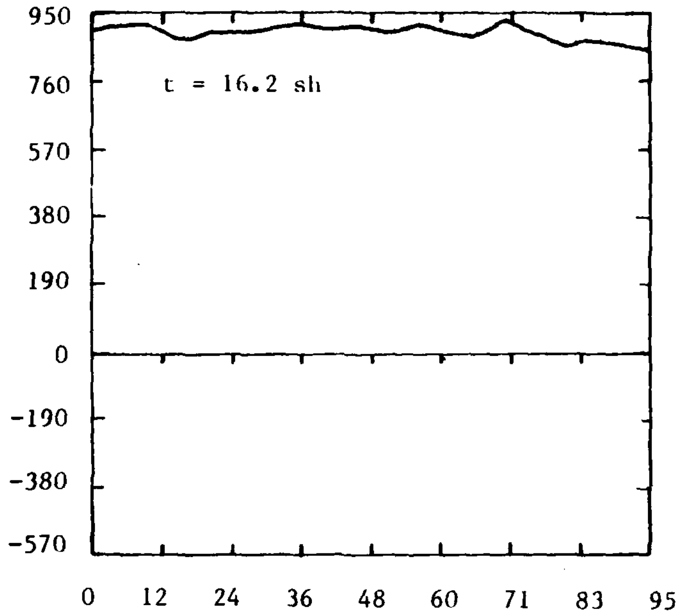

Electric Field(V/m) Vs Distance(cm)

(e)

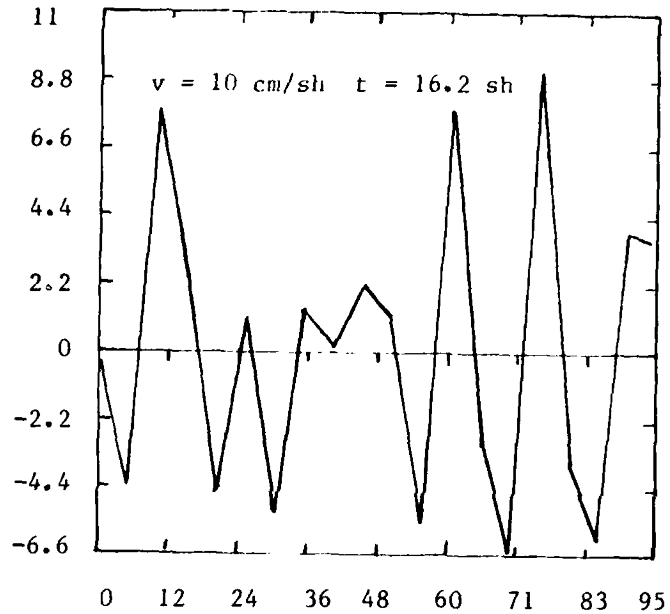

Dist Funct($x10^{-3}$ sec/m^4) Vs Distance(cm)

(f)

Fig. 9 (continued)

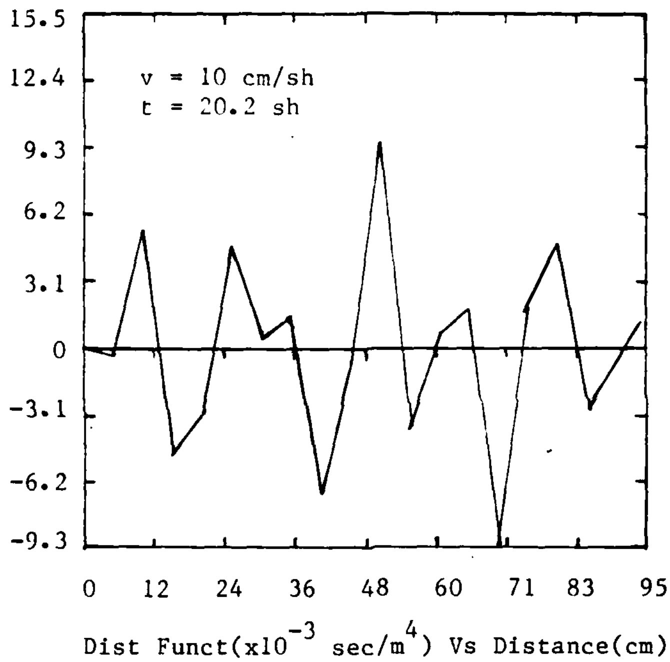

(g)

Fig. 9 (continued)

finite element solution is compared first with steady-state theory (Ref 5). This is permissible because whenever the photon flux rises linearly with time, the electron behavior can become quasi-static under certain conditions. Then, the time dependent term in the Vlasov Equation can be ignored. If the energy spectrum is assumed to be exponential, the remaining equations can be reduced to quadratures and a semi-analytic form for the solution produced.

The time dependence for this case is given by the ramp function:

$$T(t) = \begin{cases} bt & 0 \leq t \leq t_m \\ 0 < t < t & \end{cases} \qquad (51)$$

$$b = \text{rise rate } (\text{sec}^{-2})$$

Unit normalization of this function yields, $b=2/t_m^2$. In order to run the same sample problem that is carried out in Section 11 of Ref 5, the flux, ϕ_o, must be set to 1/3 cal/cm , with t_m =1 shake. The material of the object is assumed to be Aluminum, so the material yield, Y, is given as 2.57×10^{12} electrons/cal, again taken from Ref 5. Also, the exponentiation energy for this material is, w_1 =4.77 keV.

Using these parameters, the analysis given by Carron in his report will be valid for Eqn (51) for $0.1 \leq t \leq 1$ shake. During this time, most of the electrons will be in steady-state conditions. However, all the electrons do not reach steady-state at the same time, since they have a distribution of energies. Thus, caution must be used in any detailed comparison. One-dimensional SGEMP can be solved exactly when all the electrons are in steady-state, but the application to any type of time dependent problem must be considered only an estimate. Nonetheless, it is instructive to compare this theory with a dynamic calculation like FEMNEP, for it is the closest one can come to an analytic solution for a nonlinear problem.

Figure 10 displays an example of what a typical (z,v) mesh looks like for the linearly rising pulse problems. It is now necessary to allow particles to return to the surface, which means that negative velocities must be included in the mesh. The sign of α_i must always be chosen in the direction of motion of particles through the mesh in both the v and z variables. These directions are shown in Fig. 10. Equation (51) and Eqn (46) were used to input the source of electrons.

Several different mesh sizes were tried, and compared with steady-state theory. The results are given in Fig. 11, superimposed on the theoretical predictions. For all these calculations, $|\alpha_i| = 2/3$. In order to make the comparisons easier, the meshes were set up using uniform spacing in both z and v for this case (except near zero velocity where 20 cm/sh = 1 keV is the smallest velocity allowed).

Figure 11 clearly shows that as the mesh size is decreased, convergence is obtained. The convergence is not to the steady state values, however. But, this is to be expected. Note that close-in, out to about three Debye lengths (where a Debye length is approximately 0.27 cm, according to Carron) FEMNEP's results agree to within [illegible]% (recall that the boundary layer is defined as a few Debye lengths thick). Figure 11 also shows that at 10 Debye lengths, steady-state theory and the calculated results differ by more than a factor of two. Physically, this is expected. The higher energy electrons which penetrate the boundary layer have not reached steady-state conditions. But, most of the lower energy electrons which are trapped in the layer have come to

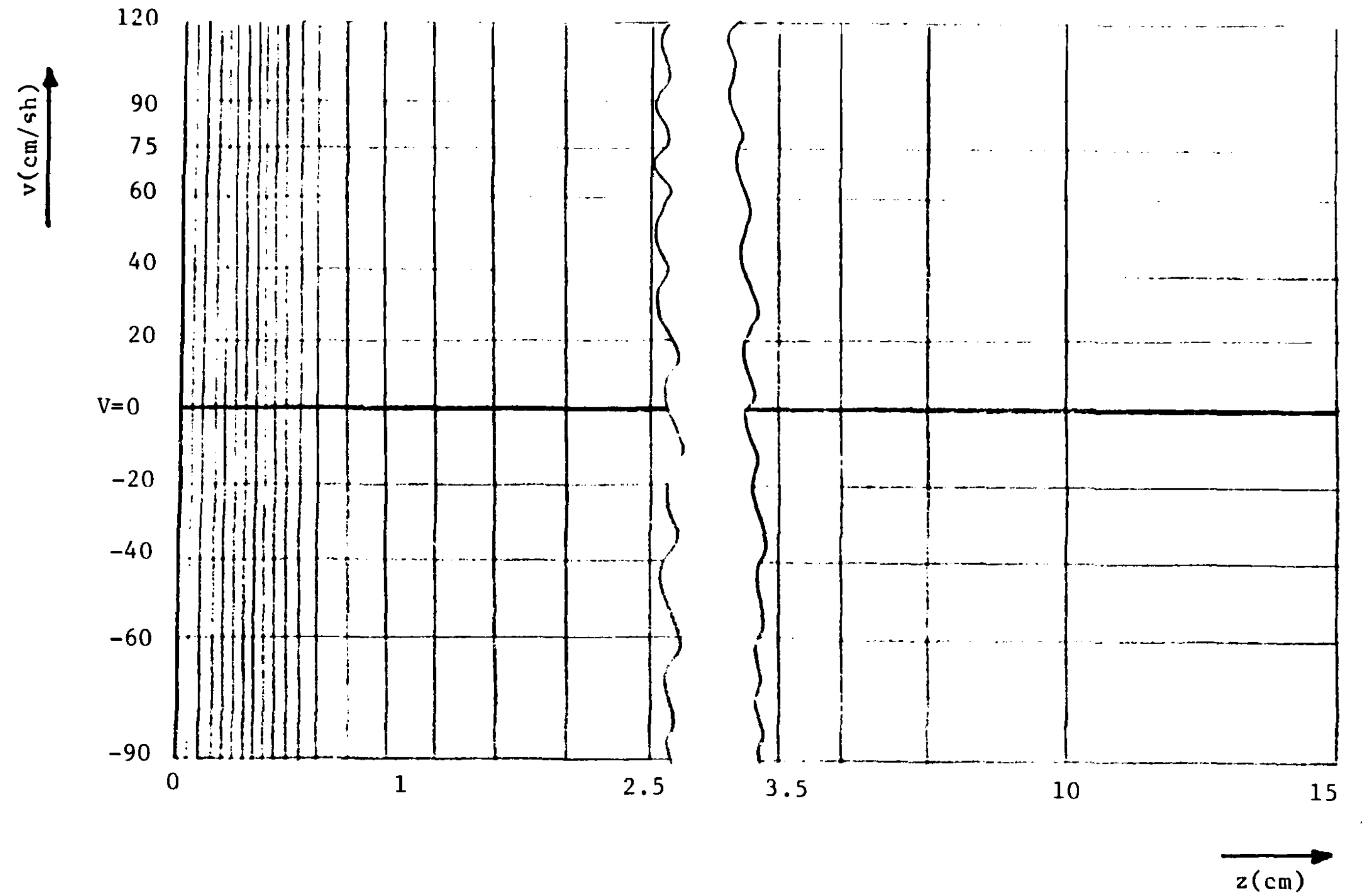

Fig. 10 Sample Calculational Mesh For Lineary-Rising Pulse Problem

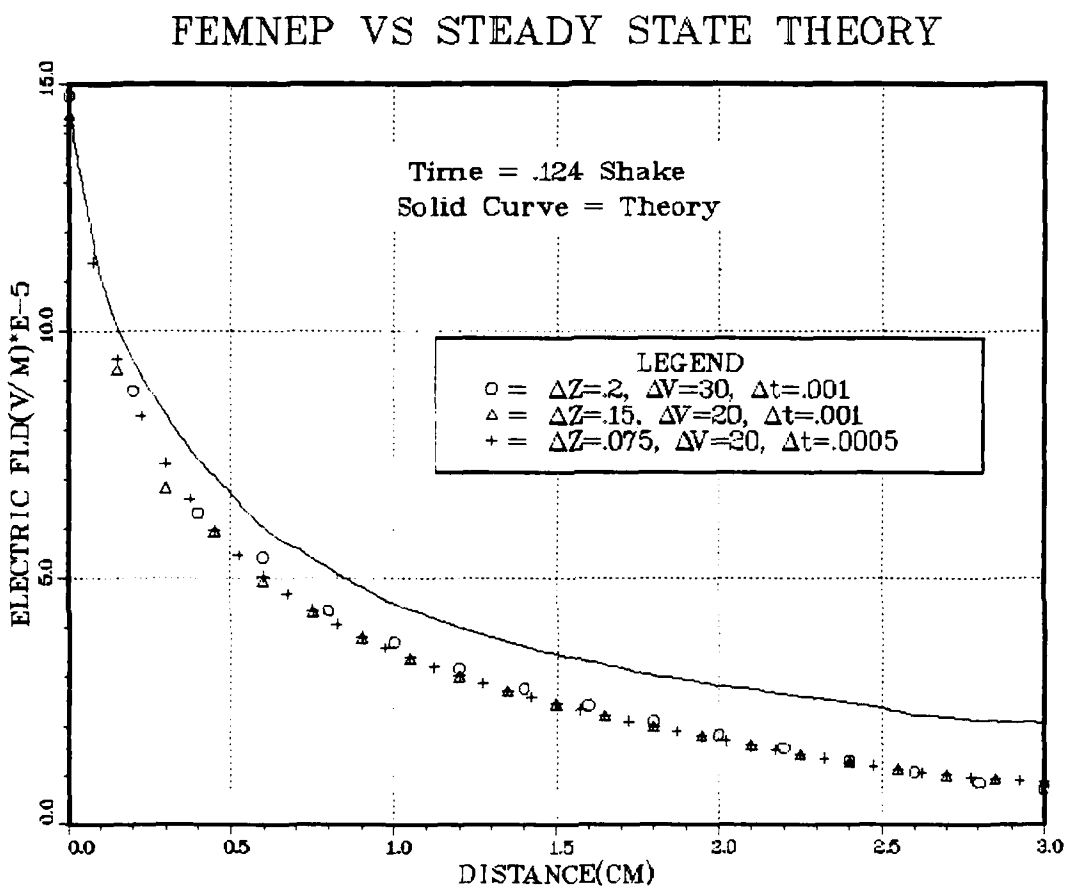

Fig. 11 Finite Element Comparison with Steady State Theory for Linearly Rising Pulse

equilibrium.

The next comparision of a linearly rising pulse is made with a scaled "particle-pushing" program (Ref 7), called SCAL1D. Figures 12 and 13 demonstrate the electric field comparison obtained as a function of distance and time. Both figures show results at early time, that is, before 1 nsec. The problem being solved is exactly the same one used in the last paragraph. The mesh scheme is similar to Fig. 10. However, at these early times, the electrons are not in equilibrium, and the full time dependent solution is being tested. These data show that FEMNEP compares very favorably with SCAL1D. For all times and distances shown, the agreement is no worse than 25%. In many cases, it is much better than that. This result further supports the conclusion reached in the last section which suggested that at t = 0.124 shake many high energy electrons have not reached steady-state. This causes the agreement between FEMNEP and steady-state theory to deteriorate beyond several Debye lengths.

EXPONENTIAL TIME HISTORY. One final comparison has been made using the finite element computer program in a calculation with an exponential time history, Eqn (18). This time, the results are compared to another "particle-pushing" program called MAD1 (Ref 8). The major difference between this code and SCAL1D is that the MAD1 code inputs the energy spectrum of the electrons from a one-dimensional emission code, rather than treating it as an analytic form. Of course, none of the unknown variables are scaled in MAD1 as they are in SCAL1D.

The problem parameters used for this comparison are as follows: a 5 keV blackbody photon spectrum, normally incident on Aluminum with a time

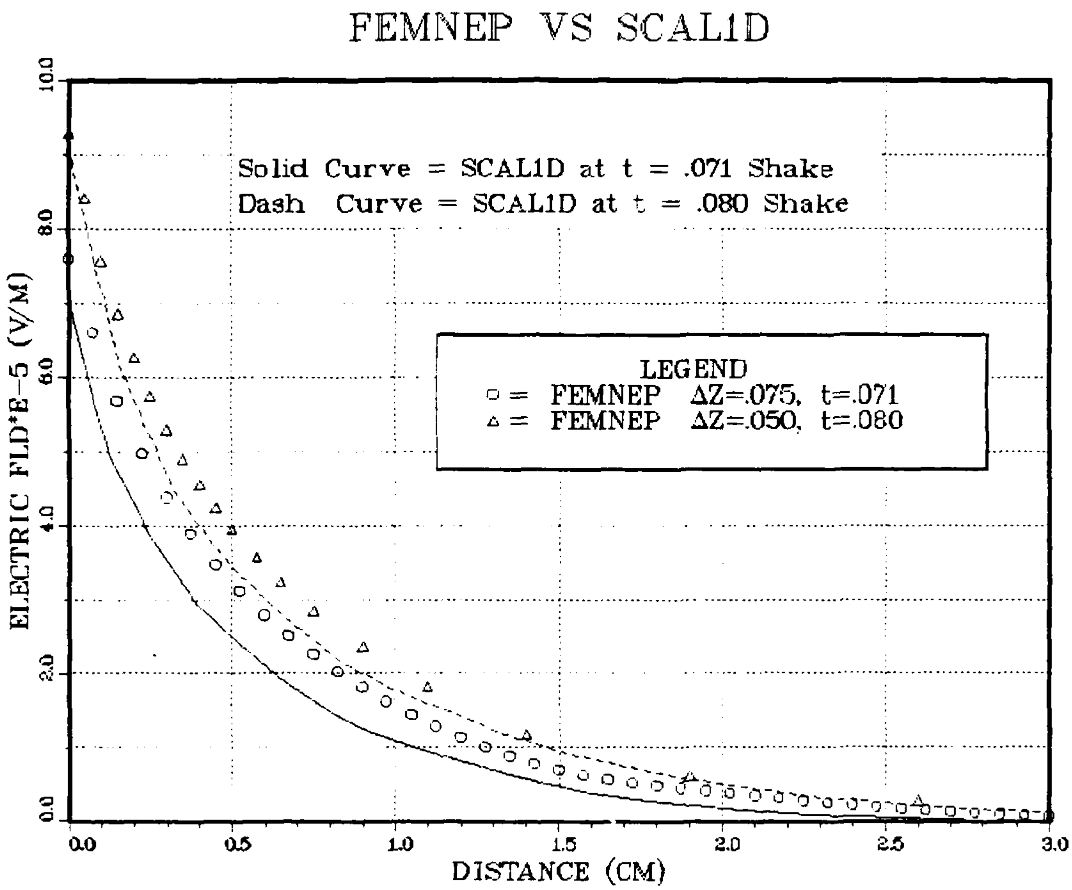

Fig. 12 Finite Element Comparison with Scaled Results, Electric Fields Vs Distance

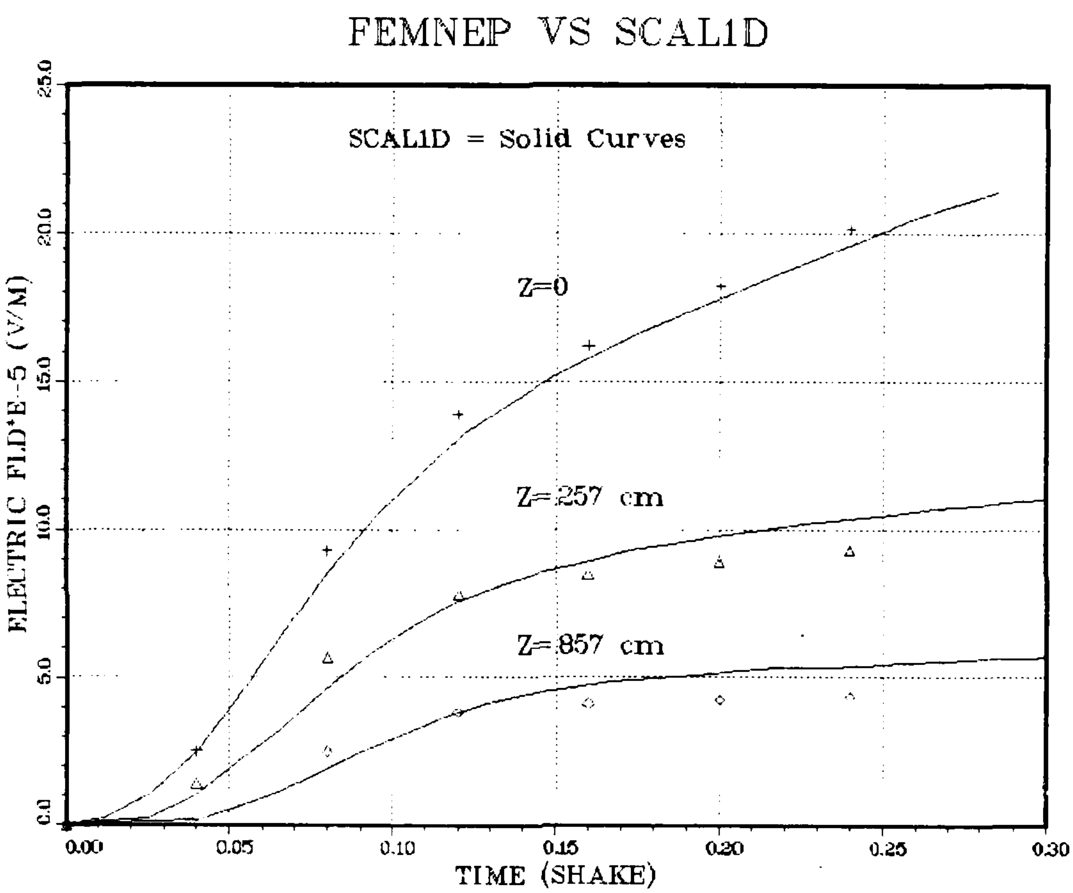

. 13 Finite Element Comparison with Scaled Results, Electric Field Vs Time history defined by:

$$c_1 = 2.0/\text{shake}$$
$$c_2 = 2.5/\text{shake}$$
$$c_3 = 1.569/\text{shake}$$
$$c_4 = 4.0 \text{ shakes}$$

and, the total X-ray fluence, $\phi_o = 0.1$ cal/cm^2.

For the finite element calculation, the same source parameters were used as in the previous case; that is, $Y = 2.57 \times 10^{12}$ electrons/cal and $w_1 = 4.77$ keV, assuming that the blackbody radiation is represented by an exponential energy distribution of electrons.

Using the identical upwinding parameters as before, $|\alpha_i| = 2/3$, for all i, the finite element calculation was performed in a nonuniform grid. This was necessary so that distances out to five meters could be used, while still resolving the Debye length close to the surface. Table II summarizes all the input parameters for both the MAD1 and FEMNEP runs. It is interesting to note that the MAD1 calculation was done with a uniform z-spacing of 1.5 cm. The FEM required smaller spacing in close (see next section on mesh sensitivity for discussion of z-spacing requirements for FEMNEP).

Figures 14 and 15 show the comparison of the electric field versus time on the surface, and electric field versus distance at t=4.0 shakes. The discrepancy at very early time in Fig. 14 is due to the fact that MAD1 must start its calculation at t=-2 shakes to avoid injecting too many particles in the beginning. The agreement over most of the z and v range is excellent.

MESH SENSITIVITY STUDIES. The purposes of this section are twofold: (1) to describe the important restrictions and requirements on mesh spacing and time step sizes, and (2) to demonstrate the convergence of the FEM as mesh size decreases. Examples are given which show that

TABLE II

Input Parameters for MAD1 VS FEMNEP Comparisons

	MAD1	FEMNEP
CLASSIFICATION	Particle Pusher	Vlasov Eqn Solver
NUMERICAL METHOD	Finite Differences	Finite Elements
SOURCE ENERGY SPECTRUM	From QUICKIE2 Code (Ref 31)	Assumed Exponential
SOURCE ANGULAR DISTRIBUTION	Assumed cos θ	Assumed cos θ
NO. OF EMISSION ENERGY BINS	20	5
NO. OF EMISSION ANGULAR BINS	9	Analytic
EQN USED FOR E-FIELD CALCULATION	Gauss' Law	Ampere's Law
Z-SPACING	Uniform	Non-uniform
ΔZ	1.5 cm	0.18 cm minimum 50 cm maximum
TOTAL Z CELLS	400	44
TIME ALGORITM	2nd Order centered finite difference	2nd Order Lax-Wendroff
Δt	0.01 shake	0.001 shake
NO. OF TIME STEPS TO 6.0 SHAKES	800 (calculation starts at t = -2.0 shakes)	6000

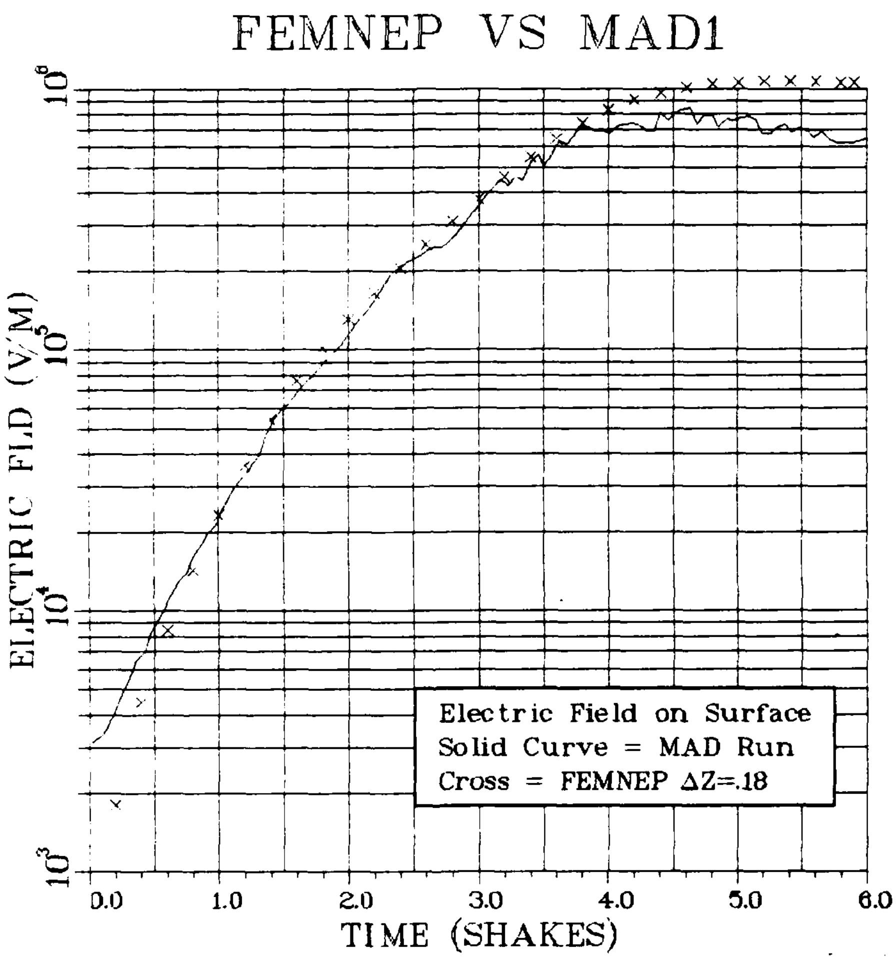

Fig. 14 Finite Element Comparison with MAD1 Program, Electric Field Vs Time

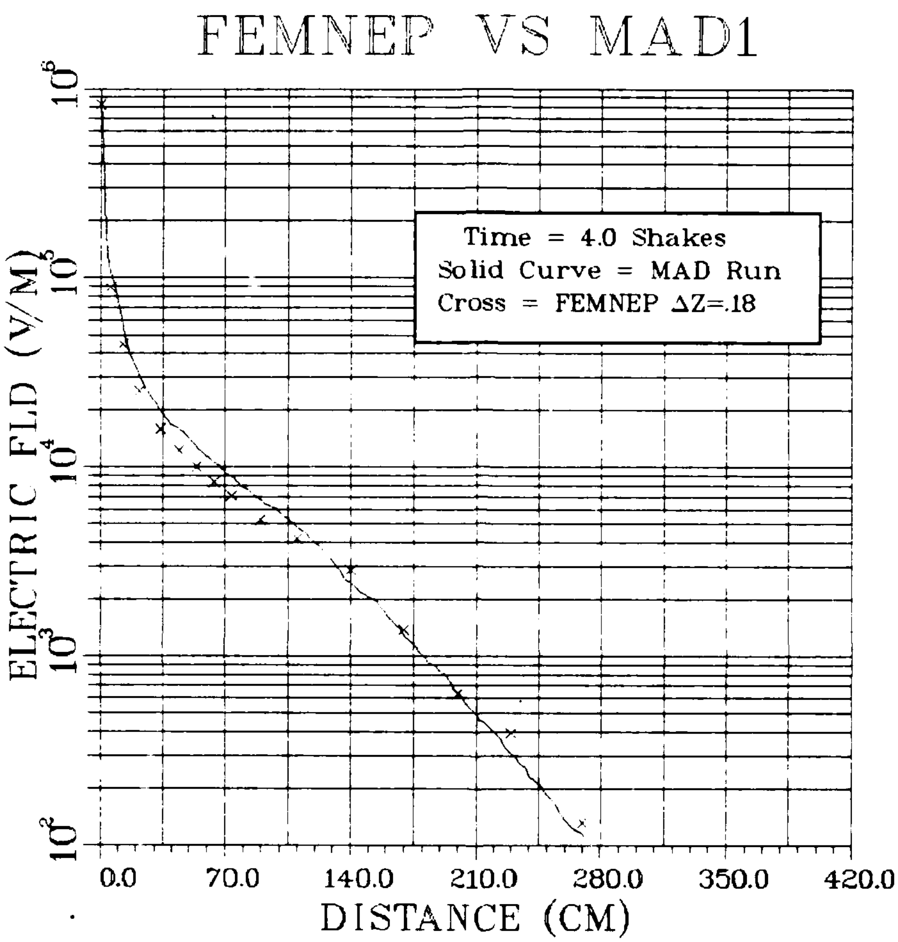

Fig. 15 Finite Element Comparison with MAD1 Program, Electric Field Vs Distance

certain recommendations must be followed to preserve the integrity of the finite element solutions. And, results will be presented indicating the finite element solutions converge, for decreasing mesh sizes, to the same data that a particle code produces.

The first area of concern are the Courant-Friedrichs-Lewy conditions of Eqns (10) and (11). They impose restrictions on the relative sizes of the Δz and Δt spacing. Figures 16 and 17 show what occurs to the electric field and distribution function when Δt is increased from 0.0001 shake to 0.002 shake for a fixed Δv and Δz mesh of 30 cm/sh and 0.1 cm, respectively. This is a variation of 0.09 to 1.8 for the Courant factor, $v\Delta t/\Delta z$ when v=90 cm/sh (the largest velocity in the mesh which particles were allowed to travel). The results show vividly that the Courant condition of Eqn (14) must be adhered to strictly to preserve stability. The cross-over from stability to instability occurs at Δt=0.001111 shake, or $v\Delta t/\Delta z=1$. The results also show that once $v\Delta t/\Delta z$ becomes less than one, stability is quickly achieved, and no matter how small Δt is taken to be, there is no noticeable change in the electric field profiles. There is, however, an improvement in particle conservation, which will be taken up in the next section. An indication that there is a net effect by making Δt small enough can be seen in Fig. 17. Oscillations of the distribution function are seen at the highest velocity profile (v=90 cm/sh) for large Δt.

A comment should be made at this point about the other Courant condition, Eqn (11). This condition can be re-written in terms of the electric field, with the help of Eqn (9):

$$\frac{\Delta v[\text{cm/sh}]}{\Delta t[\text{sh}]} > 1.76 \quad 10^{-7} E[\text{volts/m}] \qquad (52)$$

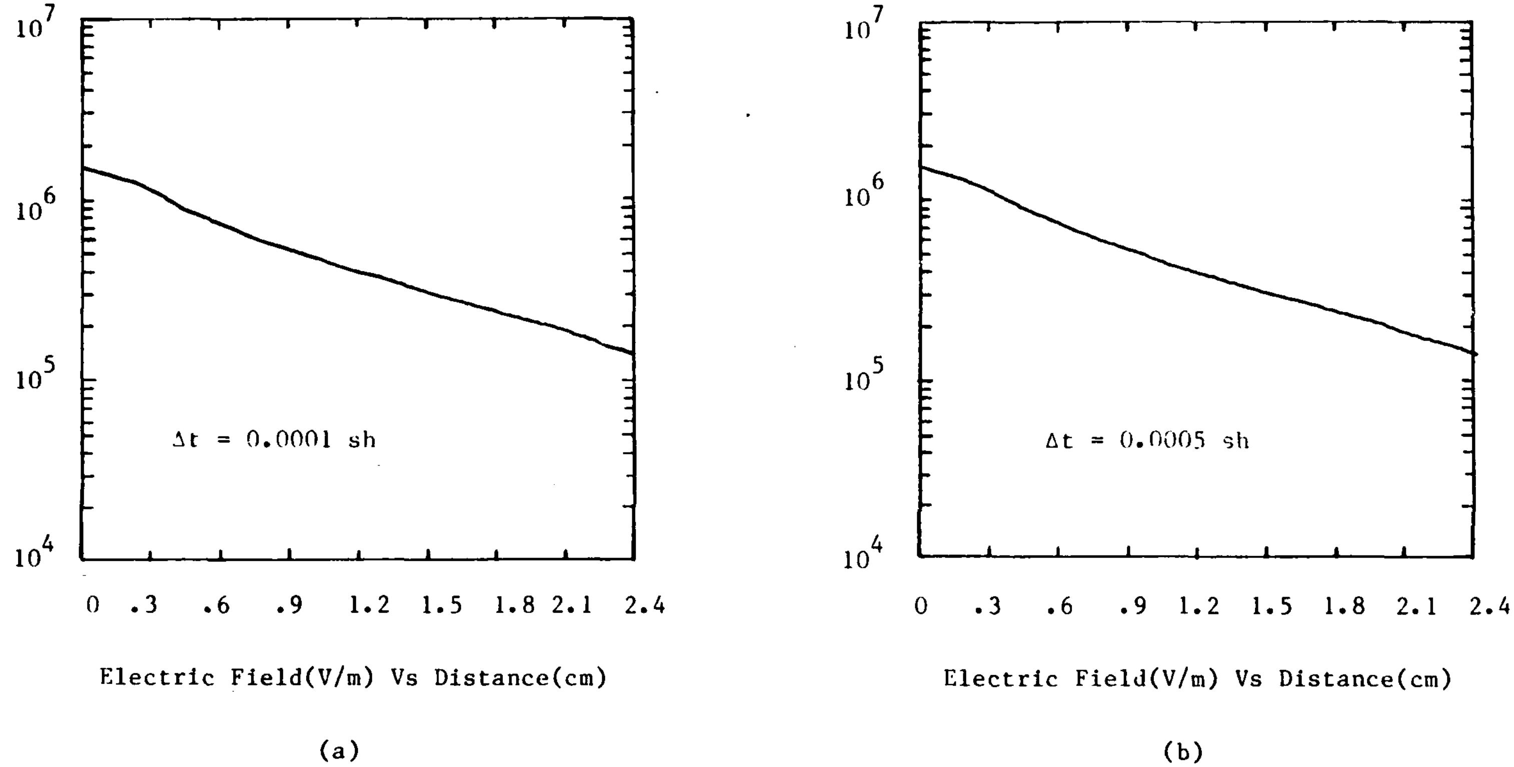

Fig. 16 Sensitivity Study Showing Electric Field Vs Distance for Various Time Steps

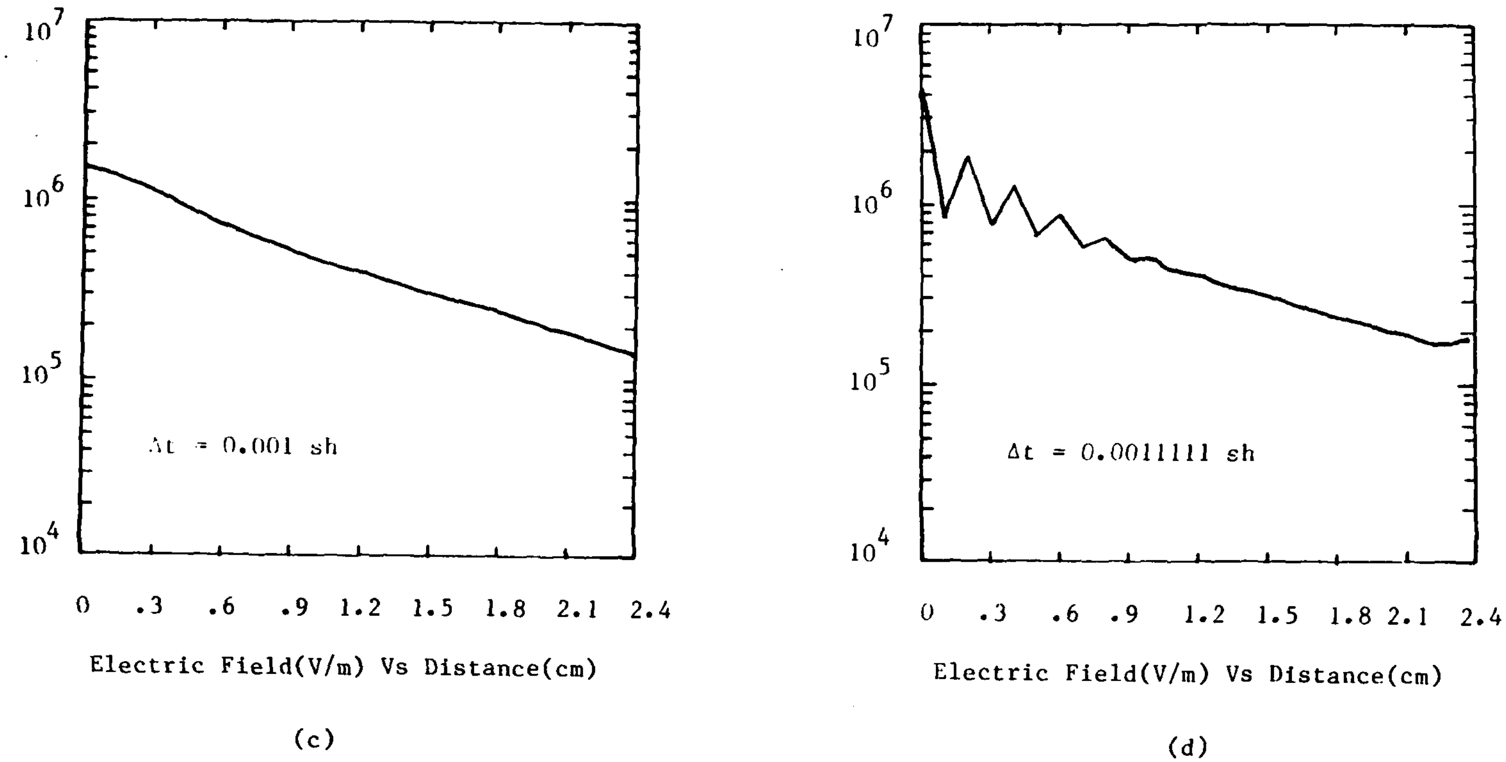

Fig. 16 (continued)

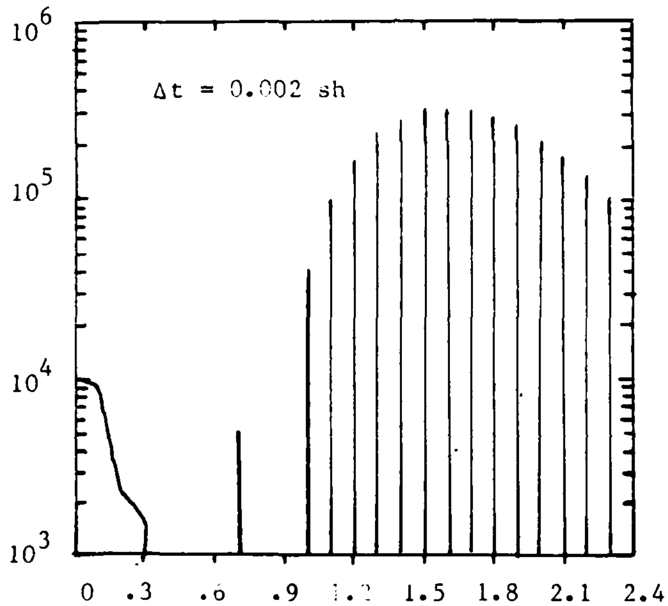

Electric Field(V/m) Vs Distance(cm)

(e)

Fig. 16 (continued)

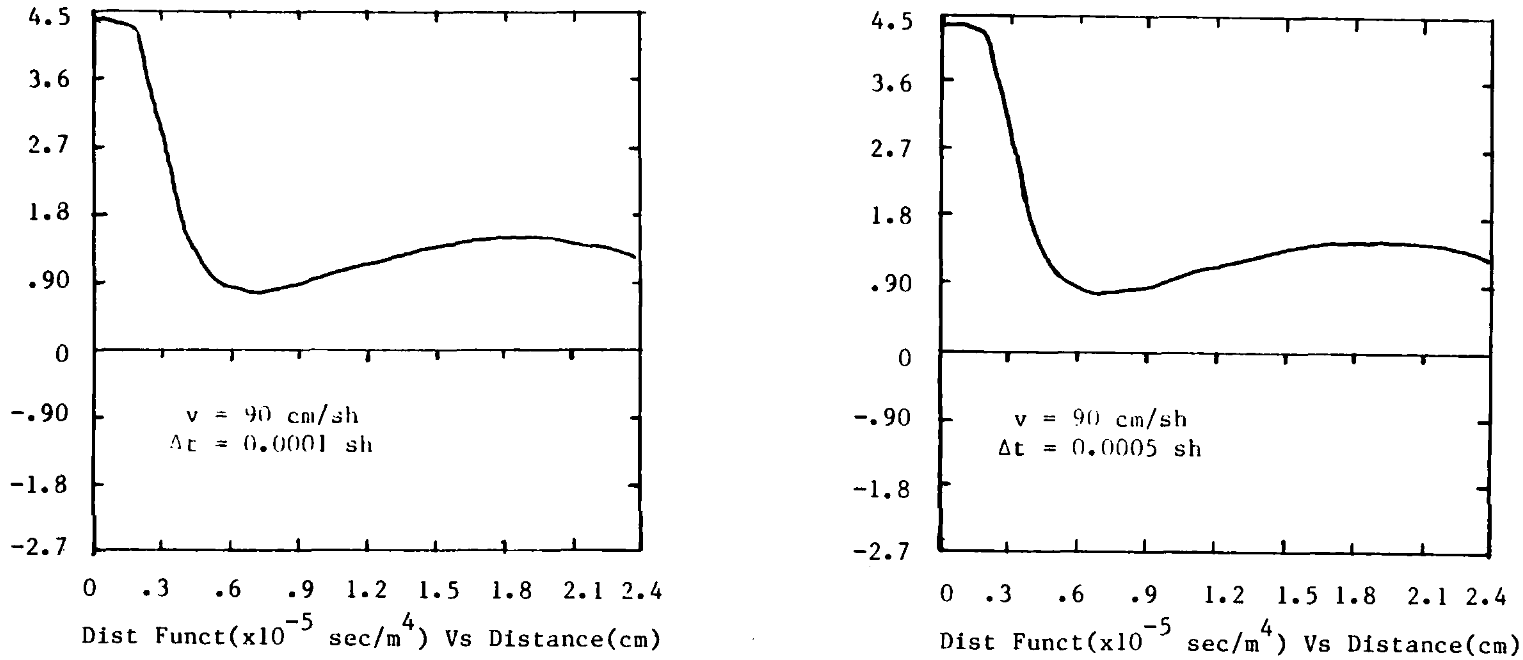

(a) (b)

Fig. 17 Sensitivity Study Showing Distribution Function Vs Distance for Various Time Steps

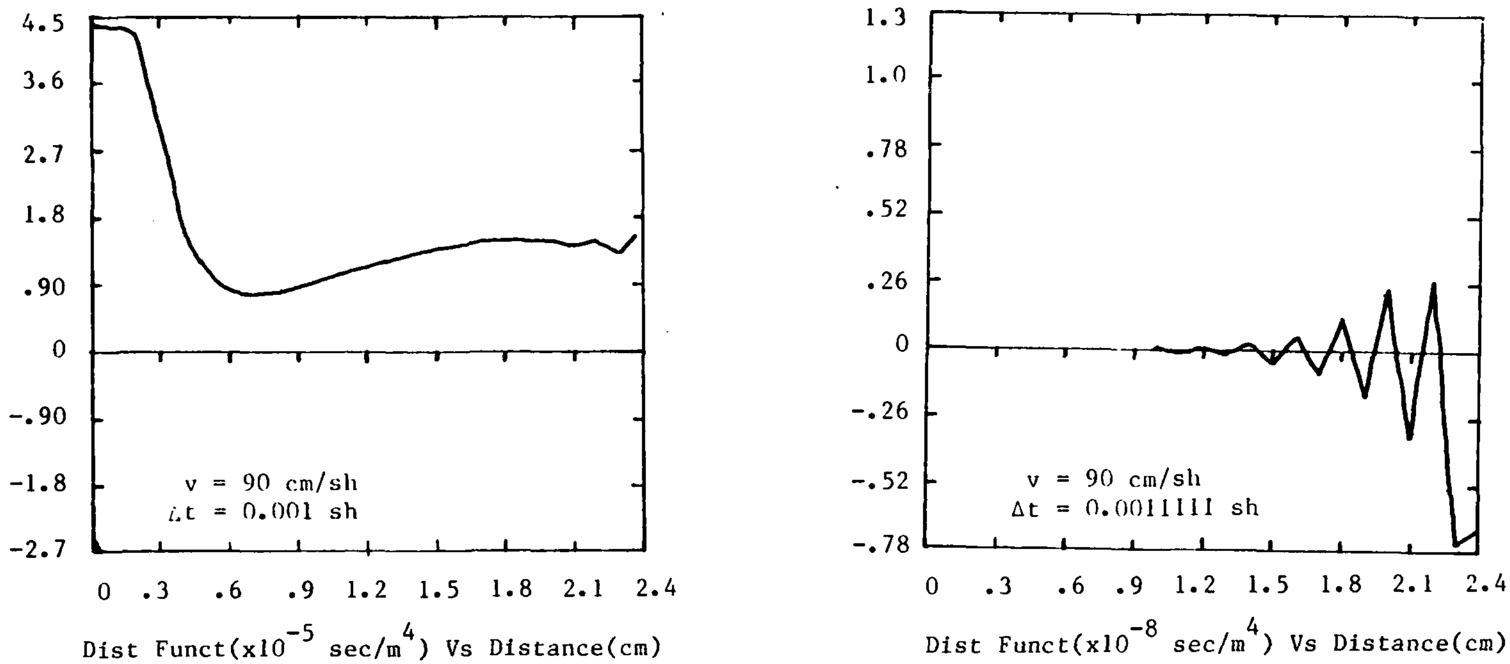

(c) (d)

Fig. 17 (continued)

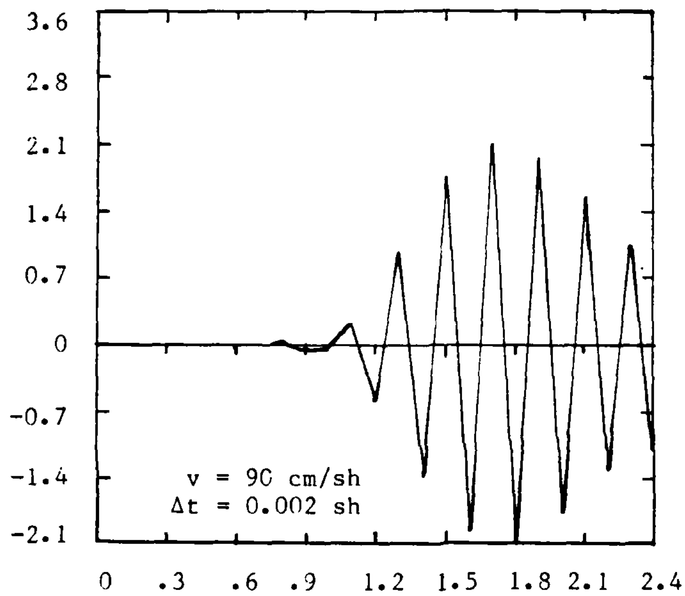

Dist Funct(x10^{-9} sec/m^{4}) Vs Distance(cm)

(e)

Fig. 17 (continued)

The above equation will be satisfied for all practical situations. The Δv spacing will not be much smaller than 10 cm/sh=0.29 keV, and Δt is typically about 0.01 shake or less. Therefore, the smallest that the left-hand-side of Eqn (52) would ever get is about 1000 cm/sh . In order for Eqn (52) not to hold true, E must be larger than 1.0×10^{10} volts/m---very large indeed. Also, very conservative figures have been used to determine $\Delta v/\Delta t$. For example, the calculations presented in this dissertation used a $\Delta v/\Delta t$ closer to 20,000 cm/sh ,which pushes the critical value of E even higher. Consequently, this Courant condition is easily satisfied for all practical one dimensional SGEMP problems.

The importance of choosing a sufficiently small Δz spacing was discussed in Chapter II. The physical nature of the Debye length requires Δz to be able to resolve it. One way of experimentally measuring the Debye length in a calculation is to take it as the distance the electric field falls by a factor of 2/e. This comes from the screening factor of $\exp(-z/\lambda_D)$ in the static equations for the electric potential (Ref 28). From Fig. 11, E falls from 14.5×10^5 volts/m to 10.5×10^5 volts/m (factor of 2/e) in about 0.15 cm. If the z-spacing exceeds 0.2 cm, the results should be suspect. The same problem as shown in Fig. 11 was run with a z-spacing of 0.4 cm. These data are presented in Fig. 18, along with the steady-state predictions, and the Δz=0.20 run for comparison. Not only is the curve for Δz=0.40 cm less accurate, as might be expected, but the shape of the curve shows oscillations. In fact, at distances beyond 3 cm , E becomes negative and oscillating.

The restrictions on the Δv and Δz mesh sizes mentioned above are the minimum requirements in relation to Δt step size. However, there

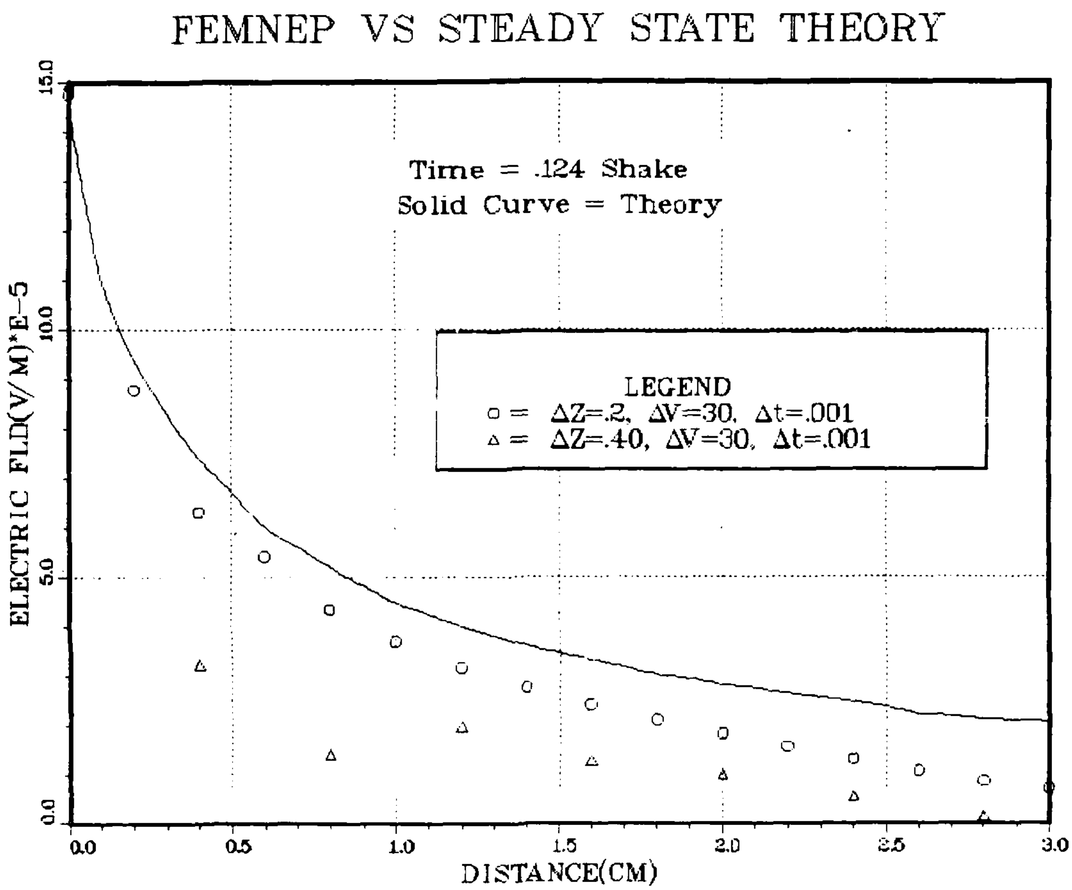

Fig. 18 Finite Element Calculation Showing the Effect of Δz Spacing Large Compared to Debye Length

AD-A101 144 AIR FORCE INST OF TECH WRIGHT-PATTERSON AFB OH SCHOO--ETC F/G 12/1
THE FINITE ELEMENT METHOD APPLIED TO THE SYSTEM-GENERATED ELECT--ETC(U)
FEB 81 J A GAUDET

UNCLASSIFIED AFIT/DS/PH/81-1 NL

2 OF 2
AD
A101144

END
DATE
FILMED
7-81
DTIC

TABLE III

Electric Field at Various Distances

Under Mesh Refinement at t = 0.08 shake

RUN#	Δz (cm)	Δv (cm/sh)	E(0) (MV/m)	E(.257cm) (MV/m)	E(.857cm) (MV/m)
1	.05*	30	.9670	.6794	.3438
2	.05*	20	.9304	.5694	.2516
3	.05*	15	.8998	.5105	.2136
4	.05*	10	.8573	.4605	.1932
5	.025	10	.8526	.4600	-
6	.05	5	.8093	.4355	-
7	.05	1*	.7950	.4477	-
SCAL1D	-	-	.8455	.4585	.1876

(MV/m = Megavolt/meter)

* non-uniform mesh, number represents the smallest mesh interval

are other considerations equally as important with regard to the convergence and accuracy of the method. In order to demonstrate that the FEM does produce results which converge to other known data, a series of runs were made in which the mesh spacing was systematically reduced. The data were then compared with the most accurate and detailed particle code results available for one-dimensional SGEMP, the SCAL1D program. Table III summarizes the results of this study.

The data in Table III are analyzed the following way: as the v mesh size decreases, the electric fields approach converging values. At the last refinement, the difference in the calculated fields does not exceed 6%, and over much of its range, it is better than 4%. Also, for the two values for which the FEMNEP data can be compared with SCAL1D results directly, without interpolation, they lie within 6.5%. The crossover of the bottom two curves is due to the non-uniform spacing in the z-direction for this run. A graphical representation of these results appear in Fig. 19. When this data is coupled with the z-mesh refinement studies of Fig. 11, convergence of this finite element approach to the one-dimensional SGEMP boundary layer is shown. Also, the comparison of FEMNEP data with the particle code SCAL1D demonstrates the validity of the technique.

As discussed above, the Courant condition for the v-mesh does not apppear to play a significant role in the choosing of a Δv since it is normally satisfied for practical SGEMP problems. However, Fig. 20 shows that the v-step can not be picked arbitrarily small, without regard to the z-step. The build-up of the knee in the curve for Δz = .05 cm is not normal. It is a result of choosing too small a Δv for this Δz. Note that the knee is not present for the Δz = .05 cm, Δv = 20 cm/sh curve. (This curve diverges from the other two curves beyond z = .15 cm because a different boundary condition was used at z = .5 cm.) The problem is corrected by making Δz smaller. This coupling effect between Δz and Δv appears to get more severe as the number of time iterations increases, and impacts the flexibility of grid make-up for problems with long run times.

PARTICLE CONSERVATION. The computer program, FEMNEP, keeps track of the number of electrons emitted at each time step, and the number

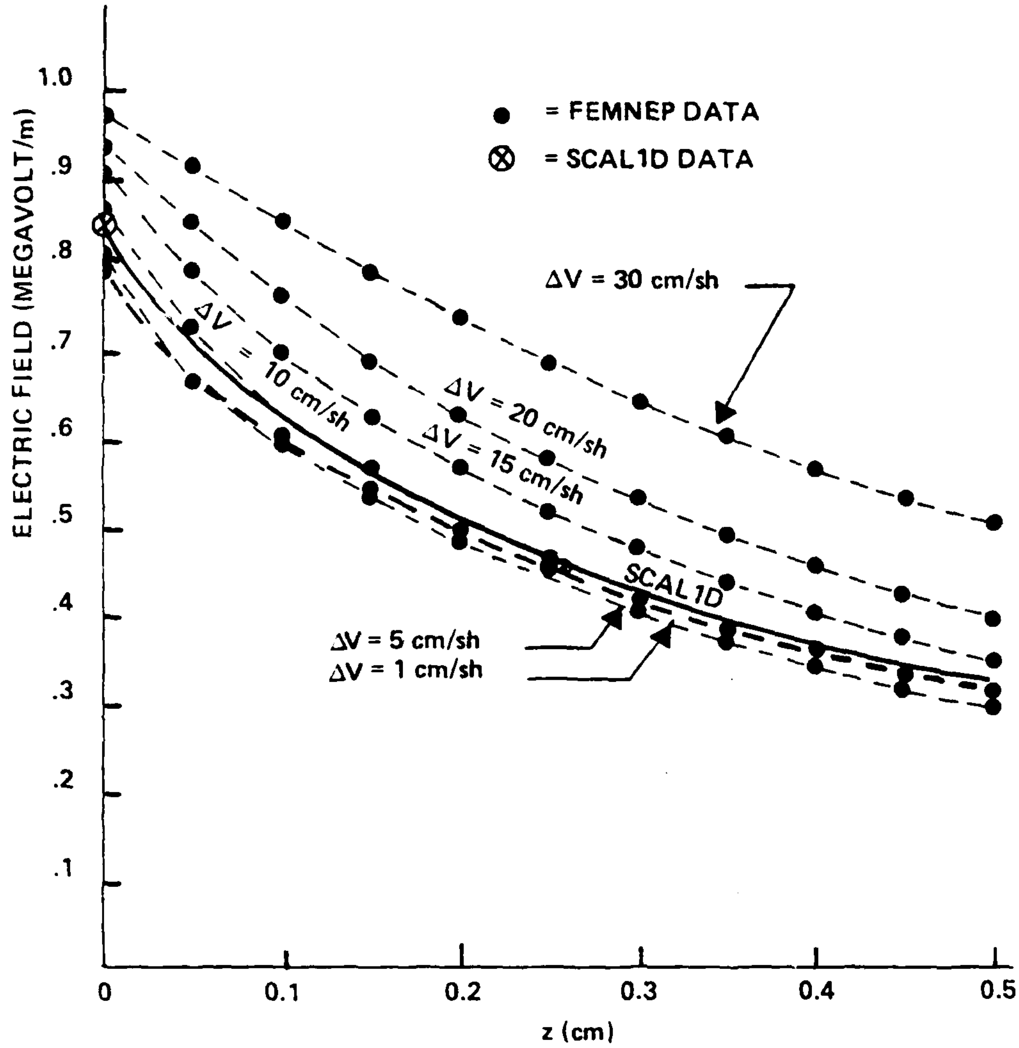

Fig. 19 Electric Field Vs Distance at t = 0.08 sh, Showing Convergence to SCAL1D Results

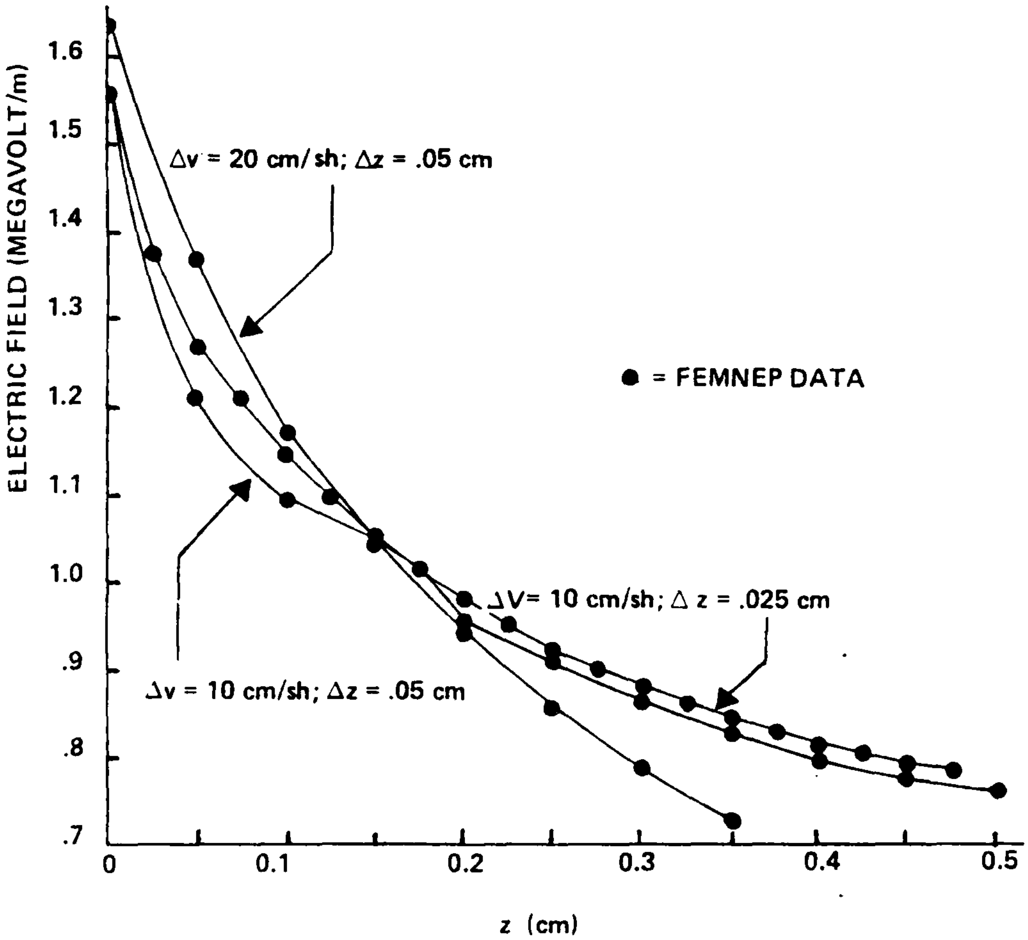

Fig. 20 Electric Field Vs Distance at t = 0.16 sh, Showing Effect of Small Δ v Spacing

leaving (or entering) the mesh from the free boundaries (see Fig. 1). The total number of electrons in the mesh can also be calculated. From this information, particle conservation is checked. The parameters needed are:

NP = total particles in mesh per cm^2

NR = particles returned to surface per cm^2

NL = particles leaving/entering mesh at z_{max} per cm^2

NB = particles leaving/entering mesh at $-v_{max}$ per cm^2

PE = particles emitted into mesh per cm^2 .

Then, PB = particle balance = PE+NR-NL+NB. For perfect conservation, PB would equal NP at all times in the calculation.

These parameters are determined from the following equations:

$$NP = \int_0^{z_{max}} \int_{-v_{max}}^{+v_{max}} f(z,v,t)\ dvdz \qquad (53)$$

$$NR = \int_0^{t} \int_{-v_{max}}^{+v_{max}} vf(0,v,t')\ dvdt' \qquad (54)$$

$$NL = \int_0^{t} \int_0^{+v_{max}} vf(z_{max},v,t')\ dvdt' \qquad (55)$$

$$NB = -\frac{e}{m}\int_0^t\int_0^{z_{max}} E(z,t')f(z,-v_{max},t')\, dzdt' \qquad (56)$$

$$PE = \int_0^t\int_0^{v_{max}} vf(0,v,t')\, dvdt' \qquad (57)$$

The first equation is the definition of the distribution function, and the other equations are expressions for the flow rate of particles across a boundary, integrated over time.

Equation (53) can be expressed as a simple sum over the elements in the rectangular mesh:

$$NP = \sum_{e=1}^{N_e} a^{(e)} b^{(e)} \left[\sum_{i=1}^{4} f_i^{(e)}(t)\right] \qquad (58)$$

where $f_i(t)$, $i=1,\ldots,4$, are the four nodal values of the distribution function for element (e) at time, t. The other equations are in the same form as the integral in Eqn (6). Therefore, Eqns (54) thru (57) are calculated using the procedure described by Eqn (41). For example, Eqn (57) becomes,

$$PE = \sum_{i=1}^{N_t} (\Delta t)_i \Big\{ \sum_{k=k_o}^{k_m} (v_{k+1} - v_k)[2v_k f(0,v_k,t_i) + v_k f(0,v_{k+1},t_i)$$

$$+ v_{k+1} f(0,v_k,t_i) + 2v_{k+1} f(0,v_{k+1},t_i)] \Big\} \qquad (59)$$

where, N_t = number of time steps out to t

k_o = velocity subscript assigned to v = 0

k_m = velocity subscript assigned to $v = v_{max}$

The other equations are computed in a like manner.

Figure 21 shows these parameters for a typical linearly rising pulse. These data correspond to the same output shown in Fig. 13. In the graph, PE = emitted curve, NR = returned curve, NP = total curve, and NB + NL = lost curve. This means that the curve labeled "lost" could actually represent a gain. However, its real meaning is the total number of electrons which either leave the mesh or enter it from a free boundary. This figure is an excellent presentation of the overall behavior of the electrons as a function of time. It shows that at early time, all the particles emitted stay in the mesh. Eventually, the electric field returns so many electrons to the surface that the total number of them levels off. It also shows the number of particles "lost" to the calculation is insignificant with respect to all other particle paramters.

Figure 22 shows the same information for the exponentially rising pulse corresponding to the electric fields of Figs. 14 and 15. In this case, the curves clearly show that equilibrium between the emitted and returned electrons only occurs near the peak of the pulse at t=4.0 shakes. Before this time, and shortly after 5 shakes, the total particles in the mesh is a strong function of time. Also, it is clear that he number of electrons lost to the mesh plays no role whatsoever.

The next two figures present examples of the efficiency of particle

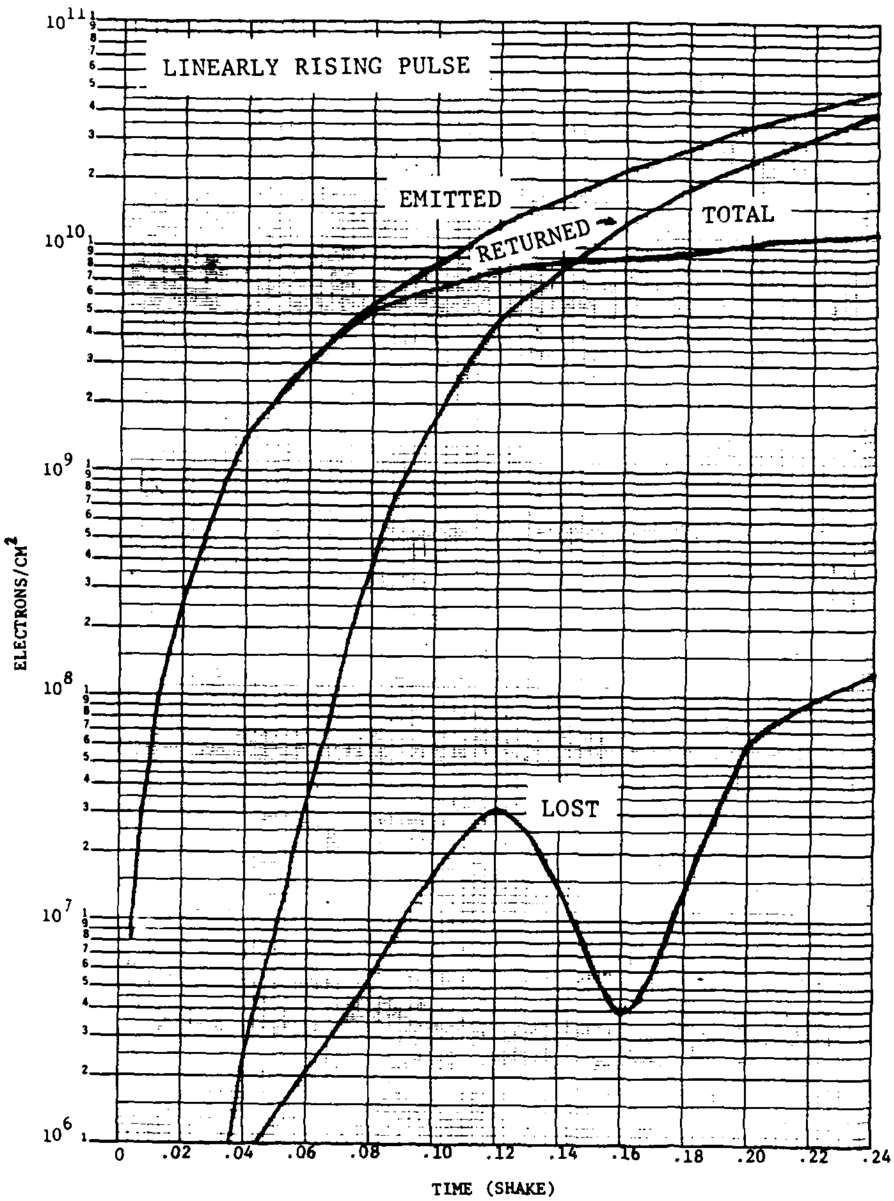

Fig. 21 Particle Conservation Parameters for Linearly Rising Pulse

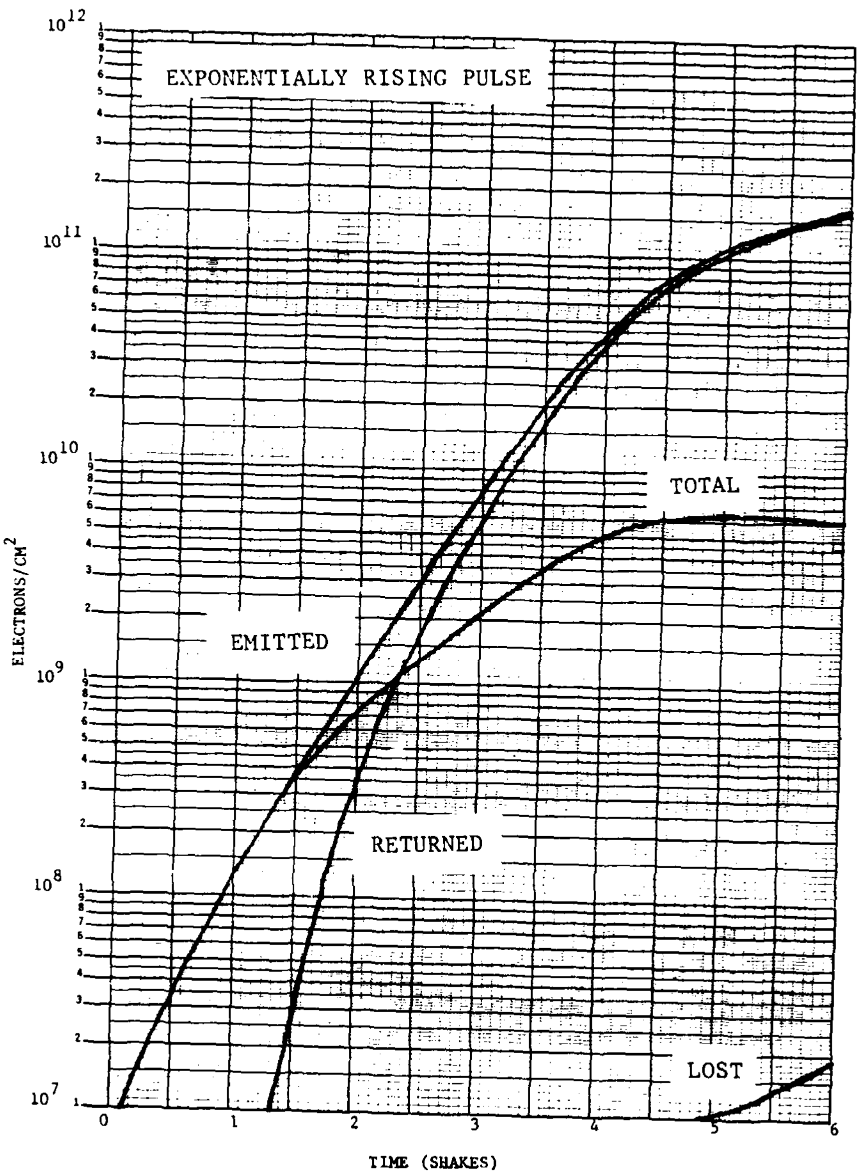

Fig. 22 Particle Conservation Parameters for Exponentially Rising Pulse

conservation for several finite element calculations. Particle conservation, PC, is defined as:

$$PC = \frac{100\ |NP-PB|}{NP} \qquad (60)$$

The smaller this number is, the better the conservation of electrons is preserved. Figure 23 shows PC as a function of time for FEMNEP in the MAD1 comparisons. For this particular calculation, electrons are conserved to an accuracy of better than 90%. It is interesting to note the tracking of this parameter with the source time history.

The final graph in this chapter, Fig. 24, displays the effect of decreasing the time step on particle conservation. The problem used in this example is the linear time history, and results of Figs. 16 and 17. Over most of the time range shown, the electron conservation is better by a factor of 2 to 3 for the smaller t. The anomolous dips in both curves are a curious aspect of this procedure which also shows up in the exponential case of Fig. 24.

CONVERGENCE CRITERIA. The Gauss-Seidel algorithm is used as the algebraic equation solver. An absolute convergence test is applied to determine whether another iteration is required. That is, iterations will continue until,

$$\left| x_i^{(\nu+1)} - x_i^{(\nu)} \right| < \varepsilon \qquad (61)$$

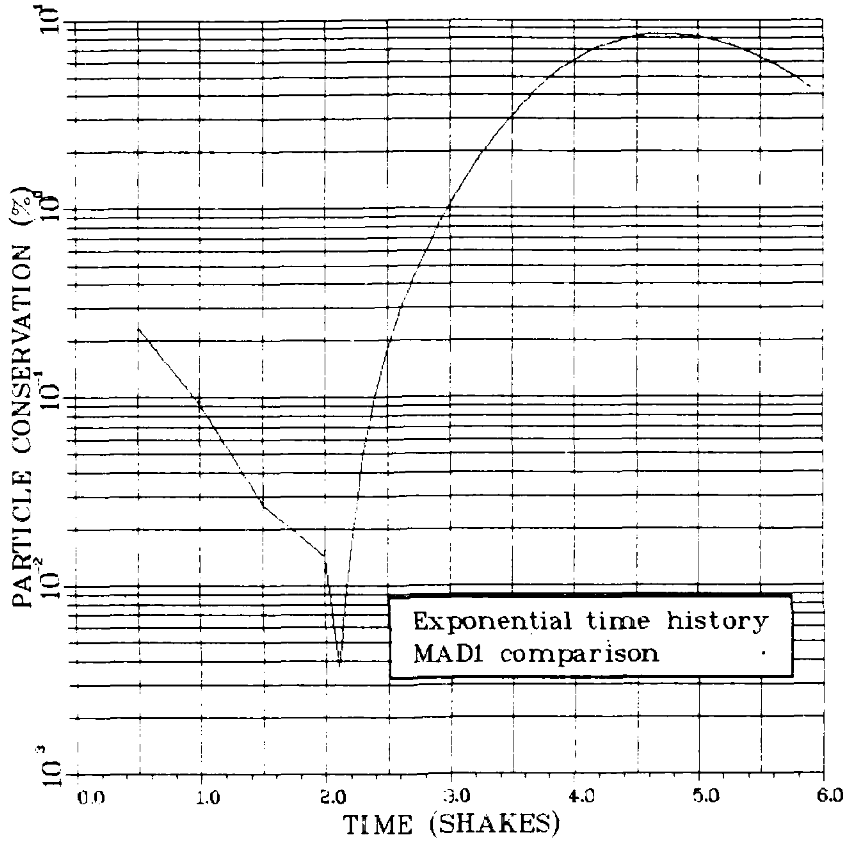

Fig. 23 Particle Conservation for the MADI Comparison

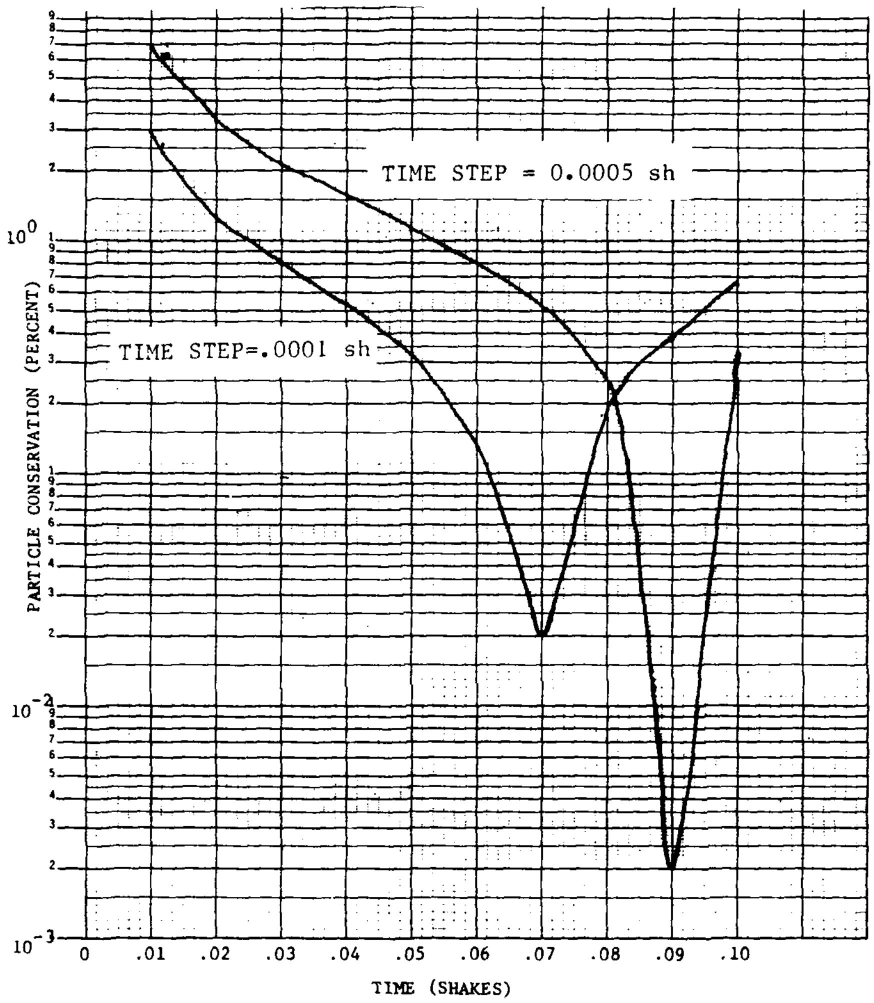

Fig. 24 Particle Conservation for Linearly Rising Pulse at Two Different Time Steps

where, $x_i^{(\nu)}$ = the ith unknown after the νth iteration

ε = absolute convergence criteria

The initial guess for $x_i^{(\nu)}$ is taken to be the last calculated values for x_i at the previous time step, (zero for the first guess). In all of the results presented thus far, $\varepsilon = 0.001$, This is a very stringent test because the unknown function, $f(z,v,t)$, is of the order of 1.0×10^5 for these problems. Table IV shows the effect of relaxing the convergence test on the same problem solution for three different values of ε.

Since program execution time listed in the table includes entire program execution, the percent reduction in running time will increase slightly for longer running jobs (see below). From the data in Table IV, it is obvious that a much less severe convergence test than 0.001 is perfectly acceptable. It is also clear that this factor has an important impact on computer costs. Since no special attempts were made to optimize execution time for the finite element method, comparisons with other techniques to determine the "fastest" method are not possible.

Note that when $|\alpha_i| \neq 2/3$, the execution time increases by 55% compared to the case when $|\alpha_i| = 2/3$, for the same problem. At the same time, the number of iterations remain about the same.

The large ε was used on several different cases in order to determine the reduction of computational time which can be realized without affecting the electric field results significantly (2nd or 3rd significant digit). Table V shows these comparisons for different size jobs.

TABLE IV

Convergence Parameters for a Linearly-Rising

Pulse Problem at t = 0.08 shake

ε	EXECUTION TIME(SEC)	$f(z_o,v_o)$ (sh^2/cm^3)	E(0) MV/M	TOTAL ELECTRONS IN MESH (cm^{-2})	ITERA-TIONS	# NON-ZEROS, [A]	$\lvert\alpha_i\rvert$
0.001	137.3	2496	.9635	5.32643×10^9	30	728	2/3
100	113.3	2496	.9635	5.32643×10^9	22	728	2/3
100000	91.1	2465	.9650	5.32570×10^9	13	728	2/3
100000	141.4	2903	.9646	5.33002×10^9	11	1540	.60

z_o = 7.1 cm, v_o = 90 cm/sh

TABLE V

FEMNEP Execution Time and Memory Requirements

For Several Different Cases (α=2/3)

PROBLEM TYPE	ε	# OF NODES	EXECUTION TIME(SEC)	% REDUCTION IN EXECUTION TIME	MEMORY FOR MATRIX STORAGE	Δt (sh)	# OF TIME STEPS
Steady-State Comparison Fig. 11,	.001	128	8.376	----	8656	.001	125
Δv=30.	100000	128	6.154	27	8656	.001	125
Steady-State Comparsion Fig. 11,	.001	492	111.183	----	35,054	.0005	250
Δv=20	100000	492	76.424	31	35,054	.0005	250
SCAL1D Comparison	.001	192	137.313	----	13,184	.0002	1204
	100000	192	91.108	34	13,184	.0002	1204

Memory requirements listed in the table are for [A], $[A_z]$, and the N_z $[A_v]$ matrices, and their row and column pointer arrays. It does not include other miscellaneous arrays or the remaining program storage. If $|\alpha| \neq 2/3$ for these runs, the storage for matrix [A] would increase by a factor of two, and execution time would suffer, as shown in Table IV. When $|\alpha| = 2/3$ is used, there is a slight increase in the percent savings in execution time, for ε = 100000, as the number of time increments get larger.

The FEMNEP comparison with the MAD1 code, Table II, took 2607 seconds (43.5 minutes) to execute with ε =0.001. However, since 6000 time steps were done in this run, a factor of 34% savings can conservativly be estimated for ε = 100000. This would reduce running time to about 720 seconds (29 minutes). Memory requirement for the matrices in this run was 37,655 decimal words, for $|\alpha|$ =2/3, and 528 nodes.

V. Summary and Conclusions

The overall goal of this study was to investigate the use of the finite element method for the solution to the one-dimensional SGEMP boundary layer problem. This feature of SGEMP plays a significant role in the final amount of current which flows on the surface of the space object. Because of this important effect, the boundary layer has been treated using many different techniques. Numerical approaches are the most prevalent methods currently being used.

SUMMARY. The one-dimensional boundary layer was described by the Boltzmann transport equation for electrons using an analytic source function. This equation is a time-dependent, nonlinear, first-order, partial integro-differential equation in three independent variables: a space variable, z; a velocity variable, v; and time, t. Since this is an initial value problem, a time marching scheme can be used effectively. The temporal behavior of the electrons is treated independent of the space and velocity variables.

The finite element equations were developed for the (z,v) variables using a regular rectangular mesh and linear approximations. The Method of Weighted Residuals was used to derive the integral relationship. The choice of the weight functions was dictated by the dominance of the advective terms in the transport equation, and its nonlinear nature. Weight functions which were identical to the approximating trial functions did not work. Therefore, weights were picked which depend on the electrons' direction of travel through the (z,v) grid. This "upwinding" technique creates a new parameter which determines the amount of bias to be applied to each element. For these equations, a minimum number of non-zeroes occur in the coefficient matrix for the resulting set of algebraic equations if a specified, constant value of 2/3 is used for the magnitude of the upwinding parameter. This value also provides a reasonable compromise between accuracy of pulse propagation and dispersion of the pulse.

With the upwinding scheme, special care was required for the time marching algorithm. Second order, centered, finite difference techniques were not successful. However, a two-step Lax-Wendroff method was found compatible with the finite element portion of the solution.

Boundary conditions on the transport equation in phase space were applied in a manner similar to neutral particle transport techniques in real space. With the upwinding set up in the direction of electron motion through the grid, the distribution of electrons does not get numerically reflected off any of the sides of the mesh.

The algebraic equations were solved twice every time step using an iterative technique. A tightly packed scheme was chosen which only stored non-zero members of the arrays. This method converged for every choice of upwinding parameter, α, used, with the exception of $|\alpha| = 1$.

These methods and procedures were used to generate a new set of results for the electric fields developed near a plane Aluminum surface exposed to X-rays. These finite element solutions were then compared to analytic estimates and particle simulation data. The latter comparisons involved two different sets of data: scaled curves based upon a linearly rising source, and a calculation for an exponentially rising and falling source. Although completely different approaches to the same problem were used for both cases, very good quantitative comparisons were obtained.

Finally, many computations were made to determine the behavior and stablility of the finite element results as a function of the increments used for all three independent variables, z, v, and t. Both physical and numerical limitations were investigated.

CONCLUSIONS. The finite element equations have been developed for application to the SGEMP boundary layer problem. SGEMP is a member of a class of charged particle transport phenomena which are described by time-dependent, nonlinear, partial integro-differential equations. The results of this study indicate that:

(1) Linear trial functions can be used successfully with a weighted residuals approach if the weights are dependent on the direction of particle travel through the mesh.

(2) When linear weight and trial functions are used, a value of 2/3 for the upwinding parameter reduces the storage requirements for the coefficient matrix, [A], when iterative solutions are sought. It also decreases the computational time needed for iterative methods.

(3) The FEM can be implemented for the transport equation and the coupled equation for the electric field in the same calculational mesh when linear trial and weight functions are chosen.

(4) Free surface boundary conditions can be used in the computational mesh, even at the interface where electrons are returning to the surface of the object.

(5) Courant stability conditions are sufficient to ensure that the solutions to the equations do not grow exponentially. This is true for

both the z and v variables. However, v cannot be made indiscriminately small without reducing z as well.

(6) The z increment must be chosen small enough to resolve the plasma Debye length with several mesh steps.

The comparisons of the finite element calculations with other methods show that this technique can be used to analyze the difficult nonlinear SGEMP boundary layer with success. They also provide new results which support particle simulation methods and theory.

BIBLIOGRAPHY

1. Glasstone, S. and Dolan, P.J. The Effects of Nuclear Weapons (3rd ed.). Wash. D.C.: U.S. Department of Defense and Department of Energy, 1977.

2. Evans, R.D. The Atomic Nucleus. New York: McGraw-Hill, 1955.

3. Higgins, D. and Longmire, C. Highly Space Charge Limited SGEMP Calculations. DNA 3885T. Santa Barbara, Cal.: Mission Research Corporation, June 1975.

4. Carron, N. and Longmire, C. On the Structure of the Steady State Space-Charge-Limited Boundary Layer in One Dimension. DNA 3928T. Santa Barbara, Cal.: Mission Research Corporation, Nov 1975.

5. Carron, N. Characteristic Steady-State Electron Emission Properties for Parametric Blackbody X-ray Spectra on Several Materials. DNA 3931T. Santa Barbara, Cal.: Mission Research Corporation, Feb 1976.

6. Longmire, C. and Carron, N. Scaling of the Time Dependent SGEMP Boundary Layer. DNA 3975T. Santa Barbara, Cal.: Mission Research Corporation, April 1976.

7. Carron, N. Description of the Code SCAL1D for Calculating the One Dimensional SGEMP Boundary Layer. DNA 4237T. Santa Barbara, Cal.: Mission Research Corporation, May 1976.

8. Clark, R. and Goplen, B. MAD1 - A Computer Code for Systems Generated Electromagnetic Pulse (SGEMP) in One Dimension. AFWL-TR-76-168. Albuquerque, N.M.: Science Applications, Inc., March 1977.

9. Carron, N. Dynamical Solution of the SGEMP Electron Boundary Layer for Linearly Rising and Constant X-ray Time Histories. DNA 4142T. Santa Barbara, Cal.: Mission Research Corporation, Dec 1976.

10. Goplen, B. and Clark, R.E. MAD3 - A Computer Code for Systems Generated Electromagnetic Pulse (SGEMP) in Three Dimensions. AFWL-TR-76-305. Albuquerque, N.M.: Science Applications, Inc., June 1977.

11. Higgins, D.F., Lee, K.S.H. and Marin, L. "Systems-Generated EMP." IEEE Trans. on Electromagnetic Compatibility, EMC-20: 14-22 (1978).

12. Holland, R. "A Self-Consistent Two-Dimensional EMP Code for Space-Charge Limiting and Secondary Emission." IEEE Trans. on Nuclear Science, NS-23: 1927-1932 (1976).

13. Neal Carron, Mission Research Corportaion, Santa Barbara, Cal., private communication.

14. Cheng, C.Z. and Knorr, G. "The Integration of the Vlasov Equation in Configuration Space." Journal of Computational Physics, 22: 330-351 (1976).

15. Boris, J.P. and Shanny, R.A. (eds.). Proceedings of the Fourth Conference on Numerical Simulation of Plasmas. Wash. D.C.: Naval Research Laboratory, 1970.

16. Huebner, K.H. The Finite Element Method for Engineers. New York: John Wiley & Sons, 1975.

17. Strang, G. and Fix, G. An Analysis of the Finite Element Method. Englewood Cliffs, N.J.: Prentice-Hall, Inc., 1973.

18. Zienkiewicz, O.C. The Finite Element Method in Engineering Science. London: McGraw-Hill, 1971.

19. Gallagher, R.H., Zienkiewicz, O.C., Oden, J.T., et al (eds.). Finite Elements in Fluids, Vol. 3. Chichester, U.K.: John Wiley & Sons, 1978.

20. Demerdash, N.A. and Nehl, T.W. "An Evaluation of the Methods of Finite Elements and Finite Differences in the Solution of Nonlinear Electromagnetic Fields in Electrical Machines." IEEE Trans. on Power Apparatus and Systems, PAS-98: 74-87 (1979).

21. Richards, D.J. and Wexler, A. "Finite-Element Solutions within Curved Boundaries." IEEE Trans. on Microwave Theory and Techniques, MTT-20: 650-657 (1972).

22. Alder, B., Fernbach, S. and Rottenber, M. (eds.). Methods in Computational Physics, Vol. 9, Plasma Physics. New York: Academic Press, 1970.

23. Longmire, C.L. Elementary Plasma Physics. New York: Interscience Publishers, 1963.

24. Marks, J.A. A User's Manual for the Three-Dimensional A3D Electromagnetic Scattering Code. AFWL-TR-77-23. Albuquerque, N.M.: Science Applications, Inc., July 1977.

25. Matthews, J. and Walker, R.L. Mathematical Methods of Physics, 2nd ed. Menlo Park, Cal.: W.A. Benjamin, Inc., 1970.

26. Richtmyer, R.D. and Morton, K.W. Difference Methods for Initial-Value Problems, 2nd ed. New York: Interscience Publishers, 1967.

27. Boris, J.P. and Book, D.L. "Flux-Corrected Transport. I. SHASTA, A Fluid Transport Algorithm That Works." Journal of Comptational Physics, 11: 38-69 (1973).

28. Rose, D.J. and Clark, Jr., M. Plasmas and Controlled Fusion. New York: The M.I.T. Press and John Wiley & Sons, 1961.

29. Bell, G.I. and Glasstone, S. Nuclear Reactor Theory. New York: Van Nostrand Rienhold Company, 1970.

30. Jackson, J.D. Classical Electrodynamics. New York: John Wiley & Sons, Inc. 1962.

31. Dellin, T.A. and MacCallum, C.J. QUICKIE2: A One-Dimensional Code for Calculating Bulk and Vacuum Emitted Photo-Compton Currents. SLA-74-0218. Albuquerque, N.M.: Sandia Laboratories, April 1974.

32. Abramowitz, M. and Stegun, I.A. (eds.). Handbook of Mathematical Functions. New York: Dover Publications, Inc., 1970.

33. Heinrich, J.C., Huyakorn, P.S., Zienkiewicz, O.C. and Mitchell, A.R. "An 'Upwind' Finite Element Scheme for Two-Dimensional Convective Transport Equation." International Journal for Numerical Methods in Engineering, 11: 131-143 (1977).

34. Oden, J.T. and Reddy, J.N. An Introduction to the Mathematical Theory of Finite Elements. New York: John Wiley & Sons, 1976.

35. Jennings, W. First Course in Numerical Methods. London: the MacMillan Company, 1964.

36. Captain Edward Oliver, Applied Physics Division, Air Force Weapons Laboratory, Kirtland AFB, New Mexico, private communication.

APPENDIX A

Derivation of the One-Dimensional Equations

In a fully three dimensional problem, the equations governing the motion of the electron plasma are given by Eqns (1), (2), (3) and (4). When a reduction to one spatial dimension and one velocity direction is desired, the assumption is made that variations of the dependent variables are allowed only in these directions. That is,

$$\begin{aligned} f(\vec{x},\vec{v},t) &= f(z,v_z,t) \\ \vec{a}(\vec{x},\vec{v},t) &= \vec{a}(z,v_z,t) \\ \vec{E}(\vec{x},t) &= \vec{E}(z,t) \\ \vec{B}(\vec{x},t) &= \vec{B}(z,t) \end{aligned}$$

Figure 25 depicts the geometry for the one-dimensional problem. Under these conditions, Eqn (1) immediately becomes:

$$\frac{\partial f}{\partial t}(z,v_z,t) + v_z\frac{\partial f}{\partial z}(z,v_z,t) + a_z\frac{\partial f}{\partial v_z}(z,v_z,t) = S(z,v_z,t) \qquad \text{(A-1)}$$

Thus, only $a_z(z,v_z,t)$ plays a role, and it is now reduced to:

$$a_z(z,v_z,\ t) = -\frac{e}{m}E_z(z,t) \qquad \text{(A-2)}$$

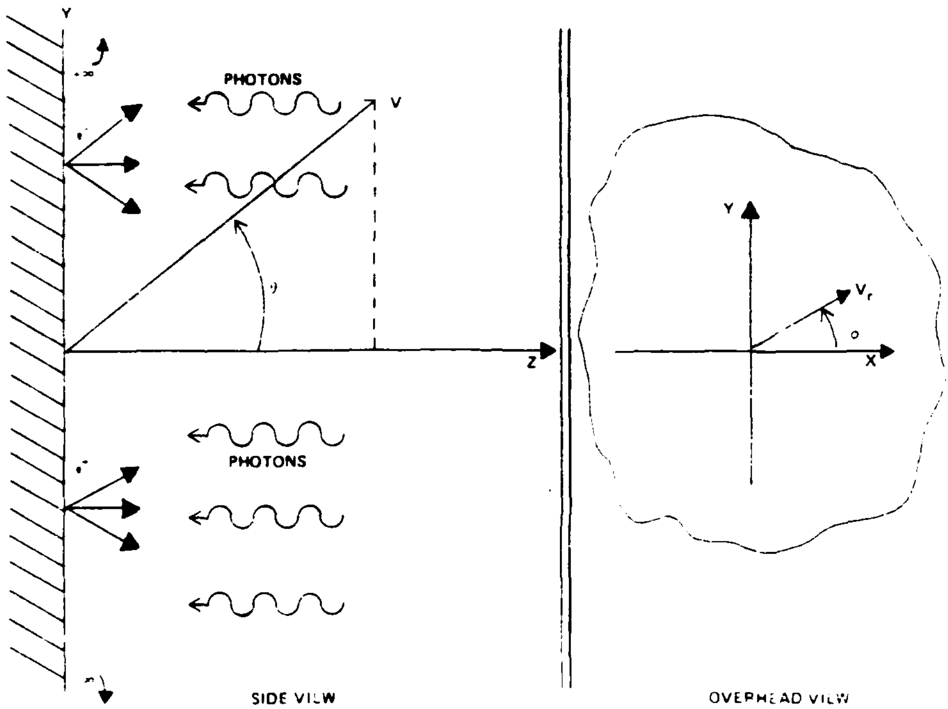

Fig. 25 Geometry for 1D SGEMP

since a_z cannot be a function of v_x or v_y. Also, the two Maxwell's Equations, Eqns (3c) and (3d) become:

$$\frac{\partial E_y}{\partial z}(z,t) = \frac{\partial B_x}{\partial t}(z,t) \qquad \text{(A-3a)}$$

$$\frac{\partial E_x}{\partial z}(z,t) = -\frac{\partial B_y}{\partial t}(z,t) \qquad \text{(A-3b)}$$

$$\frac{\partial B_z}{\partial t}(z,t) = 0 \qquad \text{(A-3c)}$$

And,

$$-\frac{\partial B_y}{\partial z}(z,t) = \mu_o J_x(z,t) + \mu_o \varepsilon_o \frac{\partial E_x}{\partial t}(z,t) \qquad \text{(A-4a)}$$

$$\frac{\partial B_x}{\partial z}(z,t) = \mu_o J_y(z,t) + \mu_o \varepsilon_o \frac{\partial E_y}{\partial t}(z,t) \qquad \text{(A-4b)}$$

$$J_z(z,t) = -\varepsilon_o \frac{\partial E_z}{\partial t}(z,t) \qquad \text{(A-4c)}$$

All but one of these equations can be eliminated from further consideration. For example, the existence of E (z,t) will create an acceleration in the x-direction from Eqn (2), unless,

$$E_x(z,t) = v_z B_y(z,t) - v_y B_z(z,t) \qquad \text{(A-5)}$$

But, if this were the case, Eqn (A-5) can be twice differentiated with respect to time, to give:

$$\frac{\partial^2 E_x}{\partial z^2}(z,t) - \frac{1}{v_z^2}\frac{\partial^2 E_x}{\partial t^2} = 0 \qquad \text{(A-6)}$$

where Eqns (A-3b) and (A-3c) have been used. However, when Eqn (A-4a) is differentiated with respect to t, and Eqn (A-3b) is substituted in, the result is,

$$\frac{\partial^2 E_x}{\partial z^2}(z,t) - \frac{1}{c^2}\frac{\partial^2 E_x}{\partial t^2}(z,t) = 0 \qquad \text{(A-7)}$$

since $\mu_o \varepsilon_o = 1/c^2$.

Comparing Eqns (A-6) and (A-7), the only way both can hold true is if $v_z = c$. Since this is not possible, the only conclusion that can be reached is that $E_x(z,t)=0$. In a similar manner, it is an easy task to show that $E_y(z,t)=0$.

Once E_x and E_y have been identified as zero, Eqns (A-3) require that $\vec{B}(z,t) = 0$, because $\vec{B}(z,0) = 0$. The only remaining Maxwell's Equation is Eqn (A-4c), Ampere's Law. This is one of the two fundamental equations used in this dissertation, the other being Vlasov's Equation, Eqn (A-1) with the source specified by a boundary condition.

APPENDIX B

Derivation of Distribution Function Boundary Condition for an Exponential Energy Dependence

The purpose of this appendix is to derive the expression for the analytic source term, $f_v(v)$, Eqn (17). This expression is valid if the electron energy emission spectrum is assumed to be exponential, which is a good approximation for blackbody photon sources. The derivation given here follows along the reasoning of Carron and Longmire (Ref 4), and uses the angle and direction definitions of Fig. 25.

For an exponential dependence, the electron energy distribution, dF/dW, is related to the X-ray flux, ϕ , via:

$$\frac{dF}{dw}\left[\frac{\#e^-}{m^2\text{-sec-joule}}\right] = \frac{Y\left[\frac{\#e^-}{\text{joule}}\right]\phi(t)\left[\frac{\text{joule}}{m^2\text{-sec}}\right]}{w_1\,[\text{joule}]}\; e^{-w/w_1} \qquad \text{(B-1)}$$

where, Y = material electron yield

w_1 = exponentiation energy.

Note that,

$$\int_0^\infty \frac{dF}{dw}\,dw = Y\phi(t) = F = \text{flux of electrons}$$

Since w = total energy of the electron, the normal component of energy, w_z, is,

$$w_z = \frac{1}{2}mv_z^2 \qquad (B-2)$$

The transformation from (v_x, v_y, v_z) coordinates to ($|\vec{v}|$, θ , ϕ) coordinates is:

$$dv_x dv_y dv_z = |\vec{v}| \sin\theta \; d\theta \; d\phi \; dv \;\; = v^2 d\Omega \; dv \qquad (B-3)$$

where, $v = |\vec{v}|$,

$d\Omega$ = differential solid angle

$= \sin\theta \; d\theta \; d\phi$.

Therefore,

$$\frac{dF}{d\vec{v}} = \frac{d^3 F}{dv_x dv_y dv_z} = \frac{m}{v}\frac{d^2 F}{d\Omega dv} \qquad (B-4)$$

where the identity, dw = mv dv, has been used.

Now, the v_x and v_y directions are integrated out of the velocity distribution, with the help of Eqn (B-4), and

$$v_r^2 = v^2 - v_z^2 = v_x^2 + v_y^2$$

to get:

$$\frac{dF}{dv_z} = \int\!\!\int_{-\infty}^{+\infty} \frac{d^3 F}{dv_x dv_y dv_z} \; dv_x dv_y = m\int_0^{\infty}\!\!\int_0^{2\pi} \frac{d^2 F}{d\Omega dw} \; d\phi dv_r \qquad \text{(B-6)}$$

since, $dv_x dv_y = v_r dv_r d\phi$.

The assumption is now made that the electron emission spectrum can be separated into energy and angle parts, with a $\cos\theta$ angular dependence, and exponential energy history. That is,

$$\frac{d^2 F}{d\Omega dw} = \frac{Y\phi(t)}{\pi w_1} \cos\theta \; e^{-w/w_1} = \frac{Y v_z \phi(t)}{\pi v w_1} \; e^{-w/w_1} \qquad \text{(B-7)}$$

The $1/\pi$ is a normalization factor which is required to give the correct integration over the hemisphere,

$$\int_0^{2\pi} \frac{d^2 F}{d\Omega dw} \; d\Omega = \frac{dF}{dw}$$

Equation (B-7) can be substituted into Eqn (B-6) to give:

$$\frac{dF}{dv_z} = \frac{m^2 Y v_z \phi(t)}{w_1} \int_0^{\infty} \frac{v_r e^{-w/w}}{w} dv_r \qquad \text{(B-8)}$$

But,

$$w = \frac{1}{2}m(v_z^2 + v_r^2)$$

And, $dw = mv_r dv_r$ if v_z is held fixed. As v_r runs from 0 to ∞, w goes from $mv_z^2/2$ to ∞. Thus,

$$\frac{dF}{dv_z} = \frac{mYv_z\phi(t)}{w_1} \int_{\frac{1}{2}mv_z^2}^{\infty} \frac{e^{-w/w_1}}{w} dw \qquad \text{(B-9)}$$

Using the definition of the exponential integral,

$$E_1(x) = \int_x^{\infty} \frac{e^{-t}}{t} dt$$

the differential flux is:

$$\frac{dF}{dv_z} = \frac{mYv_z\phi(t)}{w_1} E_1\left(\frac{1}{2}\,\frac{mv_z^2}{w_1}\right) \quad \text{(B-10)}$$

But, the differential rate for emitting electrons at z=0 is just:

$$\frac{dF}{dv_z} = v_z f(0,v_z,t) \quad \text{(B-11)}$$

That is to say, the flux of electrons at the boundary is equal to the integrated flow rate across the boundary.

$$F(t) = \int_0^{v_{max}} v_z f(0,v_z,t)\, dv_z$$

Comparing Eqn (B-11) to Eqn (B-10),

$$f(0,v_z,t) = \frac{mY\phi(t)}{w_1} E_1\left(\frac{1}{2}\,\frac{mv_z^2}{w_1}\right) \quad \text{(B-12)}$$

Finally, note that

$$\phi(t) = \phi_o\left[\frac{\text{joules}}{m}\right] T(t)\ [\sec^{-1}] \quad \text{(B-13)}$$

When Eqns(B-12) and (B-13) are combined, with the separation of Eqn (46) assumed, the result is:

$$f_v(v_z) = \frac{mY\phi_o}{w_1} E_1\left(\frac{1}{2}\frac{mv_z^2}{w_1}\right) \quad \text{(B-14)}$$

This is the same as Eqn (17), when the z-subscript is dropped.

APPENDIX C

Irregular Meshes and the Use of Non-Rectangular Elements

Rectangular elements were used exculusively throughout this dissertation because of the many simplifications which take place in the finite element equations for one-dimensional SGEMP. However, there are some advantages to using shapes other than rectangles, particularly if more than one spatial dimension is involved. Of course, if this were the case, a two-dimensional problem would require five independent variables, two space coordinates, two velocity coordinates, and time. Then, there is a large combination of elements which could be used; perhaps triangles for the spatial variables, to take advantage of their ability to model odd-shaped surfaces accurately, and rectangles for the velocity variables, to exploit the ease of integration over this type of element (see bel No matter what combination is chosen, the fact that rectangles are not exclusively used will make the analysis more difficult.

In order to see some of the extra analysis which would be required, this appendix will consider the use of triangles in the one-dimensional problem. Figure 26 shows a triangular element in a local area-weighted coordinated system. The primary advantage of triangles over rectangles is that one can cover a region with nodes in any desired location by using large, small, and elongated triangles. A mesh showing this type of covering is given in Fig. 27. The very nature of the arbitrary location of the nodes when using triangles is the cause for the more dif-

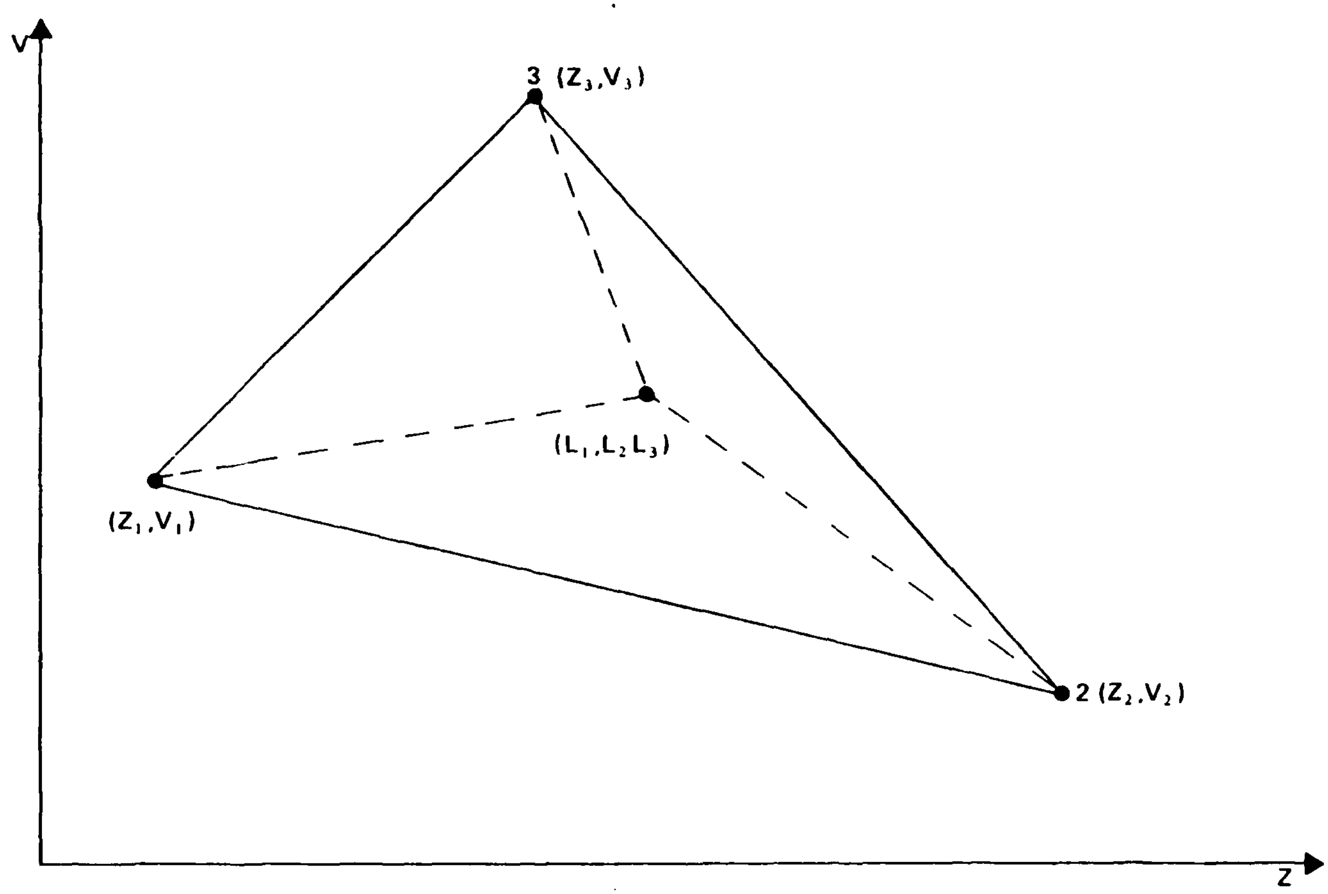

Fig. 26 Triangular Element in Area-Weighted Coordinate System

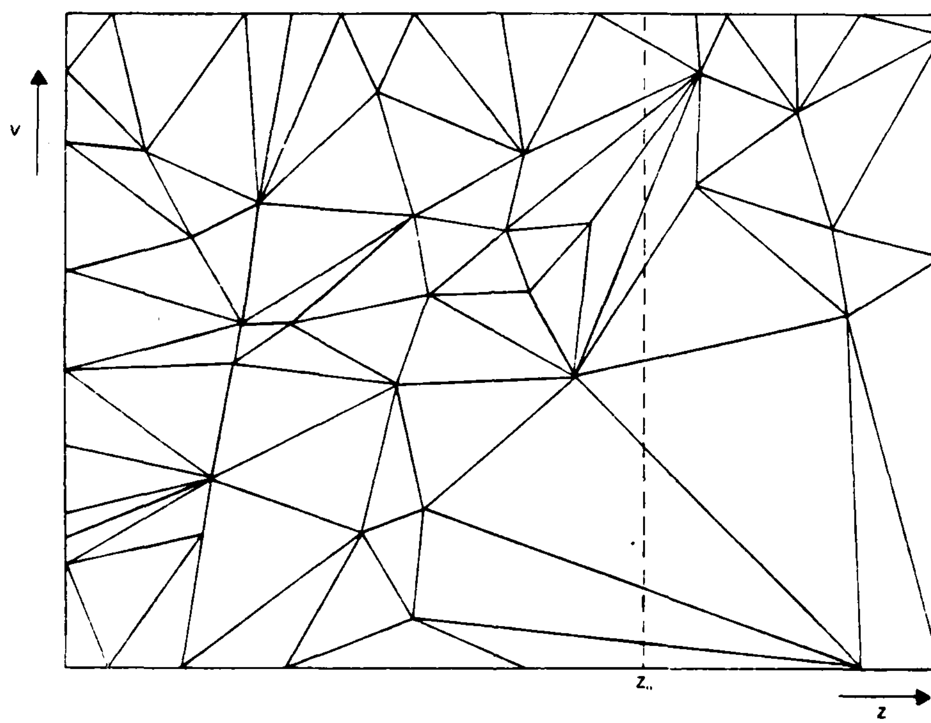

Fig. 27 Irregular Triangular Mesh

ficult analysis.

The linear trial functions used to approximate the unknowns, E(z,t) and f(z,v,t), for the element of Fig. 26 are:

$$T_i = (a_i + b_i z + c_i v)/2\Delta \qquad \text{(C-1)}$$

Δ = area of triangle 123

$$= \begin{vmatrix} 1 & x_1 & y_1 \\ 1 & x_2 & y_2 \\ 1 & x_3 & y_3 \end{vmatrix} \qquad \text{(C-2)}$$

And,

$$a_i = z_{i+1} v_{i+2} - z_{i+2} v_{i+1} \qquad \text{(C-3a)}$$

$$b_i = v_{i+1} - v_{i+2} \qquad \text{(C-3b)}$$

$$c_i = z_{i+2} - z_{i+1} \qquad \text{(C-3c)}$$

where the subscripts, i, are cyclic; that is, i=1231231...

The area-weighted coordinates for the triangle, (T_1, T_2, T_3) are obviously a dependent set, with $T_1 + T_2 + T_3 = 1$. The transformation back to the (z,v) global coordinates is accomplished by:

$$z = T_1 z_1 + T_2 z_2 + T_3 z_3 \qquad \text{(C-4a)}$$

$$v = T_1 v_1 + T_2 v_2 + T_3 v_3 \qquad \text{(C-4b)}$$

In this local system, the linear trial functions, N_i, i=1,2,3 are equal to the coordinates themselves. That is, $N_i = T_i$, i = 1,2,3. These trial functions are excellent candidates to approximate f(z,v,t) using Eqn (22). However, unlike the rectangular trial functions of Eqn

(29), the triangular functions cannot be written as a product of two functions, each only dependent on one of the global coordinates, like Eqns (32). This causes "coupling" of the z and v directions in the triangle elements (or any other non-rectangular element). For example, in Fig. 26, $E(z_o,t)$ is calculated by integrating the product of v times $f(z_o,v,t)$ along the dotted line, which intersects several triangles. The upper and lower limits of each of these triangles are, in general, functions of z. Therefore, a large amount of computer coding would be required to calculate this line integral on an element-by-element basis. Search routines would be necessary to determine which triangles are being crossed, and, the functional dependence of each upper and lower limit must be evaluated. This probably would result in numerical integrations for all element matrices, requiring more computational logic. For rectangular elements, on the other hand, the upper and lower limits of the element are never functions of z. Furthermore, the regular pattern of the rectangular elements allows the FEM to be applied to Eqn (6) without having to use the Method of Weighted Residuals.

This is related to the question of separate meshes for the Vlasov Equation and Ampere's Law raised in Chapter III. Consider Ampere's Law, with the trial functions, $M_J(z)$, $J=1,\ldots,N_z$, and $N_i(z,v)$, $i=1,\ldots,N$, for $f(z,v,t)$. The N can be taken as the same functions used in Vlasov's Equation for this regular mesh scheme. The projection of the N_i's on the one-dimensional z-space produces the same nodal placement as would be picked for a solely one-dimensional problem. Thus, Eqn (6) can be expressed as:

$$\sum_{J=1}^{N_z} M_J(z)\dot{E}_J \;\frac{e}{\varepsilon_o}\sum_{i=1}^{N}\int_{\substack{\text{all}\\ v}} vN_i(z,v)\;dv\;f_i(t) \qquad \text{(C-5)}$$

But, since any piecewise linear polynomial will do for the finite element approximation for E, the $M_J(z)$ can be taken as the one-dimenional projection of the bilinear functions, $N_i(z,v)$ onto z. Therefore, only the nodal values of E are needed. They can be evaluated at the k-th node using the fact that $M_J(z_k) = \delta_{Jk}$.

$$\dot{E}_k = \frac{e}{\varepsilon_o}\sum_{i=1}^{N} \int v N_i(z_k,v)\, dv\, f_i(t) \qquad \text{(C-6)}$$

Therefore, in order to calculate the electric field at a node of z, only the integral on the right-hand-side needs to be evaluated, not Eqn (27). However, if $N_i(z,v)$ did not have a z-node at z_k, the integral on the right-hand-side of Eqn (C-6) would be a function of z_k. Thus, simplification of this integral only takes place is for the rectangular elements. Then, Simpson's rule can be applied directly to Eqn (C-6), as is done in Chapter III.

APPENDIX D

The Assembly Process

The purpose of this appendix is to fully describe the meaning of Eqns (36) and (38) which symbolically indicate the relationship between the local element matrix and the global matrix. The following concepts have been taken from Oden and Reddy (Ref 34, Chapter 6), and applied to the matrix assembly needed for the one-dimensional SGEMP equations.

Let $\{x_i\}$, i=1,...,N, represent the set of N global nodal points, and, $\{x_i^{(e)}\}$, $i=1,\ldots,N^{(e)}$, e=1,...,N , represent the set of $N^{(e)}$ local nodal points for each element, e. Then, the transformation which takes the local nodal points into the global nodes is:

$$x_i = \sum_{j=1}^{N^{(e)}} \Lambda_{ij}^{(e)} x_j^{(e)} \qquad \text{(D-1)}$$

where,

$$\Lambda_{ij}^{(e)} = \begin{cases} 1, & \text{if node } j \text{ of element (e) coincides} \\ & \text{with node } i \text{ of the global set;} \\ 0, & \text{otherwise.} \end{cases}$$

The $[\Lambda^{(e)}]$ is a Boolean rectangular $(N \times N^{(e)})$ matrix which maps the numbering system of the local nodes in element, (e), into the global numbering of the nodes. The set $\{[\Lambda^{(e)}]\}$, $e = 1,\ldots,N_e$, is a collection of all mappings, which puts the nodes of all the elements into their proper location in the global model.

Consider Fig. 28, which shows a set of three elements, one rectangle and two triangles. The local and global numbering chosen for the nodes are also shown. In this case, $N = 6$, $N_e = 3$, $N^{(1)} = 3$, $N^{(2)} = 4$, and $N^{(3)} = 3$. Thus, for element 1,

$$\begin{bmatrix} x_1 \\ x_2 \\ x_3 \\ x_4 \\ x_5 \\ x_6 \end{bmatrix} \quad \begin{bmatrix} 1 & 0 & 0 \\ 0 & 1 & 0 \\ 0 & 0 & 0 \\ 0 & 0 & 0 \\ 0 & 0 & 0 \\ 0 & 0 & 1 \end{bmatrix} \begin{bmatrix} x_1^{(1)} \\ x_2^{(1)} \\ x_3^{(1)} \end{bmatrix} = \begin{bmatrix} x_1^{(1)} \\ x_2^{(1)} \\ 0 \\ 0 \\ 0 \\ x_3^{(1)} \end{bmatrix} \qquad \text{(D-3)}$$

The above 6 x 3 matrix is $[\Lambda^{(1)}]$. The other two Boolean matrices, $[\Lambda^{(2)}]$ and $[\Lambda^{(3)}]$, can be written in a similar fashion. The set, $[\Lambda^{(1)}]$, $[\Lambda^{(2)}]$, $[\Lambda^{(3)}]$ fully describes the process of transforming from the local nodes to the global nodes.

Using these Boolean matrices, it is now possible to express in more detail the meaning of Eqn (36):

$$(A)_{ij} = \sum_{(e)=1}^{N_e} \sum_{k=1}^{4} \sum_{\ell=1}^{4} \Lambda_{ik}^{(e)} \Lambda_{j\ell}^{(e)} \; a^{(e)} b^{(e)} \int_{-1}^{+1}\int_{-1}^{+1} W_k^{(e)}(\xi,\eta) N_\ell^{(e)}(\xi,\eta)\; d\xi d\eta$$

$$= \sum_{(e)=1}^{N_e} \sum_{k=1}^{4} \sum_{\ell=1}^{4} \Lambda_{ik}^{(e)} \Lambda_{j\ell}^{(e)} a_{k\ell}^{(e)} \;, \quad i,j = 1,\ldots,N \qquad \text{(D-4)}$$

The sums over ℓ and k run from 1 to 4 because $N^{(e)} = 4$. The matrices

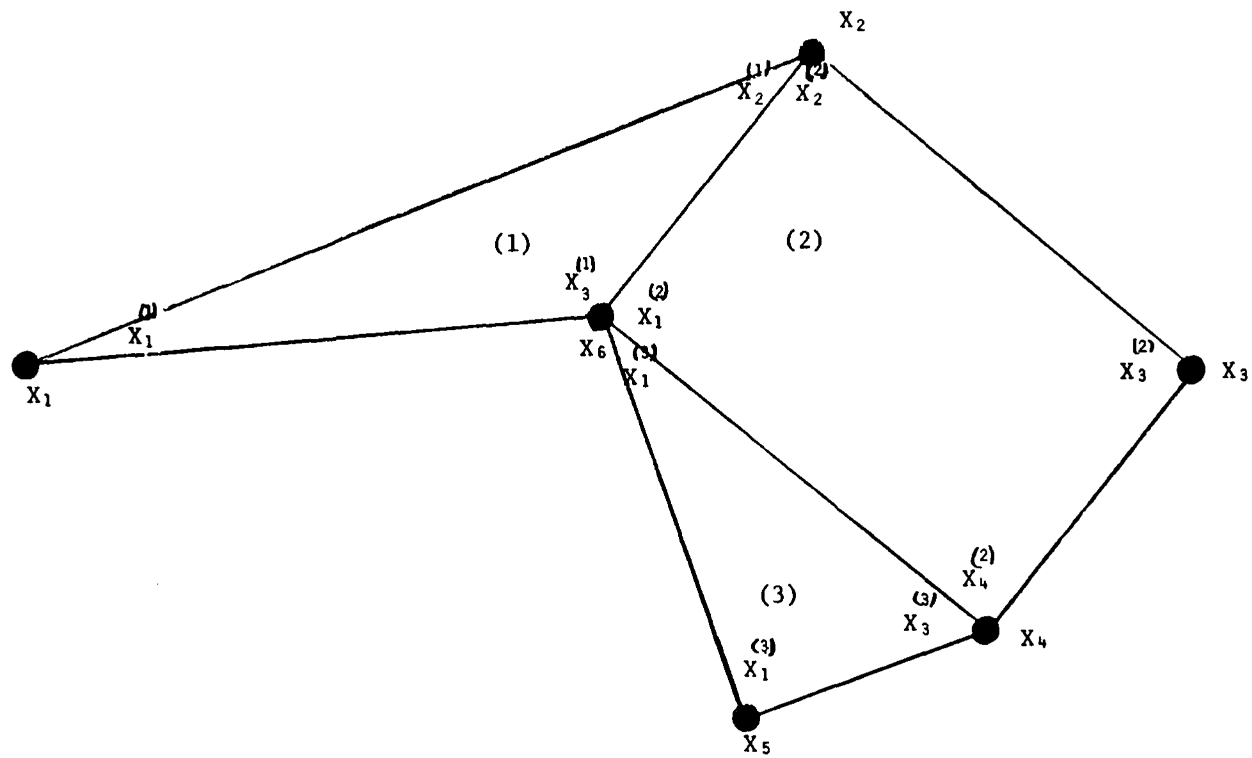

Fig. 28 Three Element Mesh Showing Local and Global Numbering

$[\Lambda^{(e)}]$ are dimensioned N x 4, and there are N_e of them. The expression for $[A_z]$ is similar:

$$(A_z)_{ij} = \sum_{(e)=1}^{N_e} \sum_{k=1}^{4} \sum_{\ell=1}^{4} \Lambda_{ik}^{(e)} \Lambda_{j\ell}^{(e)} \, b^{(e)} \int_{-1}^{+1}\int_{-1}^{+1} (b^{(e)}\eta + v_c^{(e)}) \cdot W_k^{(e)}(\xi,\eta) \frac{\partial N_\ell^{(e)}}{\partial \xi} (\xi,\eta) \, d\xi d\eta$$

$$= \sum_{(e)=1}^{N_e} \sum_{k=1}^{4} \sum_{\ell=1}^{4} \Lambda_{ik}^{(e)} \Lambda_{j\ell}^{(e)} (a_z^{(e)})_k , \quad i,j = 1,\ldots,N \qquad \text{(D-5)}$$

The method for transforming $[A_v]_J$ is governed by a different rule, Eqn (38). Like [A] and $[A_z]$, $[A_v]_J$ can be written:

$$[(A_v)_J]_{ij} = \frac{e}{m} \sum_{(e)=1}^{N_e} \sum_{k=1}^{4} \sum_{\ell=1}^{4} \Lambda_{ik}^{(e)} \Lambda_{j\ell}^{(e)} \, a^{(e)} \int_{-1}^{+1}\int_{-1}^{+1} M_J(z) W_k^{(e)}(\xi,\eta) \frac{\partial N_\ell^{(e)}}{\partial \eta} (\xi,\eta) \, d\xi d\eta$$

(D-6)

But Eqn (D-6) can be further reduced by expressing $M_J(z)$ as a function of only the local coordinates. In order to do this, a one-dimensional z-mesh must be defined which is coincident with the z-portion of the rectangular (z,v) grid. Then, the functions, $L_1(\xi)$ and $L_2(\xi)$, Eqns (31), can be used, and $M_J(z)$ can be formally written:

$$M_J(z) = \sum_{(e_z)=1}^{N_z-1} \sum_{n=1}^{2} \Lambda_{Jn}^{\prime(e_z)} L_n^{(e_z)}(\xi) \qquad \text{(D-7)}$$

The (e_z) elements are the linear segments between two nodes at constant v in the (z,v) mesh. The Boolean matrix, $[\Lambda'^{(e_z)}]$, dimensioned $2x(N_z-1)$, must be constructed to project the two nodes for each z-segment onto the global nodes of the rectangular mesh. For example, consider the two rectangles in Fig. 29. Here, $N_z = 2$, $N = 6$, $N_e = 2$, so that:

$$\Lambda^{(1)} = \begin{bmatrix} 1 & 0 & 0 & 0 \\ 0 & 1 & 0 & 0 \\ 0 & 0 & 1 & 0 \\ 0 & 0 & 0 & 0 \\ 0 & 0 & 0 & 0 \\ 0 & 0 & 0 & 1 \end{bmatrix}, \quad \Lambda^{(2)} = \begin{bmatrix} 0 & 0 & 0 & 0 \\ 0 & 0 & 0 & 0 \\ 0 & 1 & 0 & 0 \\ 0 & 0 & 1 & 0 \\ 0 & 0 & 0 & 1 \\ 1 & 0 & 0 & 0 \end{bmatrix}, \quad \Lambda'^{(1)} = \begin{bmatrix} 1 & 0 \\ 0 & 1 \\ 0 & 1 \\ 0 & 1 \\ 1 & 0 \\ 1 & 0 \end{bmatrix}$$

Now, Eqn (D-6) may be written as,

$$[(A_v)_J]_{ij} = \frac{e}{m} \sum_{(e)=1}^{N_e} \sum_{(e_z)=1}^{N_z-1} \sum_{k=1}^{4} \sum_{\ell=1}^{4} \sum_{n=1}^{2} \Lambda_{ik}^{(e)} \Lambda_{j\ell}^{(e)} \Lambda'^{(e_z)}_{Jn} (a_{vn}^{(e)})_{k\ell}$$

where,

$$(a_{vn}^{(e)})_{k\ell} \quad a^{(e)} \int_{-1}^{+1} \int_{-1}^{+1} L_n^{(e_z)}(\xi) W_k^{(e)}(\xi,\eta) \frac{\partial N_\ell^{(e)}}{\partial \eta}(\xi,\eta)\, d\xi\, d\eta \qquad \text{(D-8)}$$

This equation is the precise definition of what is meant by Eqn (38).

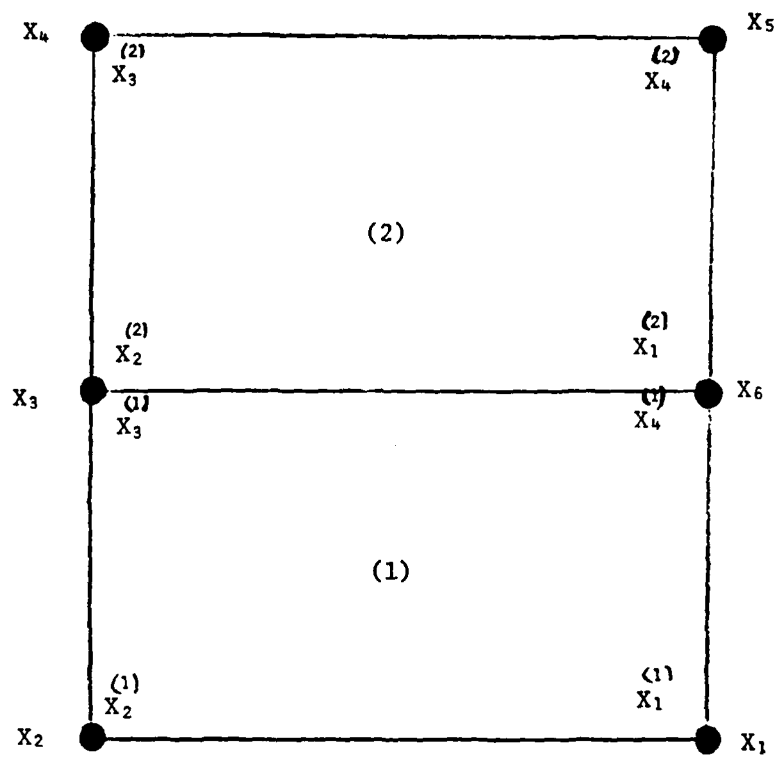

Fig. 29 Two Rectangular Elements With Global and Local Labels

APPENDIX E

Derivation of Element Matrices

Equations (40) show the end product of performing the integrations in Eqns (37) and (39), which define the 4 x 4 element matrices, [a], $[a_z]$, $[a_{v1}]$, and $[a_{v2}]$. Since all 16 members of each matrix has been derived separately, it is not practical to include them all here. However, for purposes of illustration, one member of each of these matrices will be derived to illustrate how the final expressions for them are obtained.

All of the integrations over the element rectangle are reduced to integrations over the linear functions, $L_1(x)$ and $L_2(x)$, defined by Eqns (31). The identities given in Table VI are useful in these derivations.

First, consider Eqn (47a). Using the definition given by Eqns (33d) and (32b),

$$a_{42} = ab\int_{-1}^{+1}\int_{-1}^{+1}[L_1(\xi) + \alpha_3F(\xi)][L_2(\eta) - \alpha_4F(\eta)]L_2(\xi)L_1(\eta)\, d\xi d\eta$$

$$= ab\int_{-1}^{+1}[L_1(\xi)L_2(\xi) - 3\alpha_3L_1(\xi)L_2^2(\xi)]\, d\xi \cdot \int_{-1}^{+1}[L_1(\eta)L_2(\eta) + 3\alpha_4L_1^2(\eta)L_2(\eta)]d\eta \qquad \text{(E-1)}$$

where the meaning of $F(\xi)$ and $F(\eta)$ have been used, Eqn (34). Table VI gives the values for the integrals in Eqn (E-1), which now can be

TABLE VI

Useful Integrals of $L_1(x)$ and $L_2(x)$

$$\int_{-1}^{+1} L_i(x)\,dx = 1 \qquad \int_{-1}^{+1} L_i^2(x)\,dx = \frac{2}{3}$$

$$\int_{-1}^{+1} L_i(x)L_j(x)\,dx = \frac{1}{3} \qquad \int_{-1}^{+1} L_i^3(x)\,dx = \frac{1}{2}$$

$$\int_{-1}^{+1} L_i^2(x)L_j(x)\,dx = \frac{1}{6} \qquad \int_{-1}^{+1} L_i^2(x)L_j^2(x)\,dx = \frac{1}{15}$$

$$\int_{-1}^{+1} L_i^3(x)L_j(x)\,dx = \frac{1}{10}$$

$$i,j = 1,2 \qquad i \neq j$$

expressed:

$$a_{42} = ab[(\tfrac{1}{3} - \tfrac{1}{2}\alpha_3)(\tfrac{1}{3} + \tfrac{1}{2}\alpha_4)] = \frac{ab}{36}(2 - 3\alpha_3)(2 + 3\alpha_4) \qquad \text{(E-2)}$$

Figure 3 shows that for $i=4$, $j=2$, $\xi = -1$, $\xi = +1$, $\eta = +1$, and $\eta = -1$. Therefore, Eqn (40a) becomes,

$$a_{42} = \frac{ab}{36}(\tfrac{2}{3} + \alpha_4)(\tfrac{2}{3} - \alpha_3) = \frac{ab}{36}(2 - 3\alpha_4)(2 - 3\alpha_3) \qquad \text{(E-3)}$$

identical to Eqn (E-2).

Now, recall the definition of $[a_z]$ given by Eqn (37b). In order to calculate $(a_z)_{23}$, the following derivative is needed:

$$\frac{\partial N_3}{\partial \xi}(\xi,\eta) = \frac{1}{2}L_2(\eta)$$

Thus,

$$(a_z)_{23} = \frac{b}{2}\int_{-1}^{+1}\int_{-1}^{+1}(b\eta + v_c)[L_2(\xi) - \alpha_1 F(\xi)][L_1(\eta) + \alpha_2 F(\eta)]L_2(\eta)\ d\xi d\eta$$

$$= \frac{b}{2}\int_{-1}^{+1}[(2bL_2(\eta) - b + v_c)\{L_1(\eta)L_2(\eta) - 3\alpha_2 L_1(\eta)L_2(\eta)\}]d\eta\ \cdot$$

$$\cdot \int_{-1}^{+1}[L_2(\xi) + 3\alpha_1 L_1(\xi)L_2(\xi)]\ d\xi \quad , \qquad \text{(E-4)}$$

since $\eta = 2L_2(\eta) - 1$. Carrying out these integrations yields:

$$(a_z)_{23} = (1 + \alpha_1)[v_c - b)(\frac{1}{6} - \frac{3}{10}\alpha_2) + 2b(\frac{1}{3} - \frac{1}{2}\alpha_2)]$$

$$= -\frac{b}{6}(1 + \alpha_1)[\frac{3}{10}b\alpha_2 - v_c(1 - \frac{3}{2}\alpha_2)] \qquad \text{(E-5)}$$

With i=2, j=3, which implies that k=1, p=2, ξ =+1, ξ =+1, η =-1, η =+1, Eqn (40b) gives,

$$(a_z)_{23} = \frac{b}{12}(1 + \alpha_1)[(2 - 3\alpha_2)v_c - \frac{3}{5}\alpha_2 b)] \qquad \text{(E-6)}$$

which is the same as Eqn (E-5).

Now, for $(a_{v1})_{12}$:

$$\frac{\partial N}{\partial \eta}2(\xi,\eta) = -\frac{1}{2}L_2(\xi)$$

Therefore,

$$(a_{v1})_{12} = -\frac{a}{2}\int_{-1}^{+1}\int_{-1}^{+1} L_1(\xi)[L_1(\xi) + \alpha_1 F(\xi)][L_1(\eta) + \alpha_4 F(\eta)]L_2(\xi)\, d\xi d\eta$$

$$= -\frac{a}{2}\int_{-1}^{+1}[L_1^2(\xi)L_2(\xi) - 3\alpha_1 L_1^2(\xi)L_2^2(\xi)]\, d\xi \cdot \int_{-1}^{+1}[L_1(\eta) - 3\alpha_4 L_1(\eta)L_2(\eta)]\, d\eta \qquad \text{(E-7)}$$

The above equation yields upon integration:

$$(a_{v1})_{12} = -\frac{a}{2}(\frac{1}{6} - \frac{1}{5}\alpha_1)(1 - \alpha_4) = -\frac{a}{60}(1 - \alpha_4)(5 - 6\alpha_1) \qquad \text{(E-8)}$$

Again, by definition, with i=1, j=2, p=4, k=1, ξ_i=-1, ξ_j=+1, η_i=-1, η_j=-1, Eqn (40c) is,

$$(a_{v1})_{12} = -\frac{a}{20}\frac{(1-\alpha_4)}{3}[5-\frac{1}{2}(9+3)\alpha_1] = -\frac{a}{60}(1-\alpha_4)(5-6\alpha_1) \qquad \text{(E-9)}$$

identical to Eqn (E-8).

Finally, consider the evaluation of $(a_{v2})_{33}$. Since,

$$\frac{\partial N}{\partial \eta}3(\xi,\eta) = \frac{1}{2}L_2(\xi)$$

then,

$$(a_{v2})_{33} = \frac{a}{2}\int_{-1}^{+1}\int_{-1}^{+1} L_2^2(\xi)[L_2(\xi) - \alpha_3 F(\xi)][L_2(\eta) - \alpha_2 F(\eta)]\, d\xi d\eta$$

$$= \frac{a}{2}\int_{-1}^{+1}[L_2^3(\xi) + 3\alpha_3 L_2^3(\xi)L_1(\xi)]\, d\xi \cdot \int_{-1}^{+1}[L_2(\eta) + 3\alpha_2 L_1(\eta)L_2(\eta)]\, d\eta \qquad \text{(E-10)}$$

Integration gives:

$$(a_{v2})_{33} = \frac{a}{2}(\frac{1}{2} + \frac{3}{10}\alpha_3)(1+\alpha_2) = \frac{a}{20}(5+3\alpha_3)(1+\alpha_2) \qquad \text{(E-11)}$$

With, i=3, j=3, k=3, p=2, ξ_i=+1, ξ_j=+1, η_i=+1, η_j=+1, and ξ_5= ξ_1=-1, Eqn (40d) yields,

$$(a_{v2})_{33} = \frac{a}{20}\,\frac{(1+\alpha_2)}{(2-1)}\left[5 + \frac{1}{2}(9-3)\alpha_3\right] = \frac{\ }{20}(1+\alpha_2)(5+3\alpha_3) \qquad \text{(E-12)}$$

which is correct.

All of the other members of [a], $[a_z]$, $[a_{v1}]$, and $[a_{v2}]$ are obtained similarly, to give the expressions shown by Eqns (40).

VITA

John A. Gaudet was born on 4 April 1947 in Fitchburg, Massachusetts. He graduated from high school in his home town in 1965. He then attended the College of the Holy Cross in Worcester, Massachusetts from which he was awarded the Bachelor of Arts degree in June 1969. Upon graduation, he received a commission in the USAF through the ROTC program. Before entering active duty, he attended the University of Notre Dame in South Bend, Indiana. In May 1971, he was awarded the Master of Science degree. He entered active service in the Air Force in August 1971 as a Weapons Controller for the 73rd Tactical Control Flight at Myrtle Beach AFB, South Carolina. Then he became the Operations Training Officer at Kotzebue AFS, Alaska. In October 1973, he entered the Air Force Institute of Technology's School of Engineering.

Permanent Address: 4811 Splitrail Dr
Colorado Springs, Colorado 80917

ATE

LMED

8